Basic Biological Models

The ocean is inhabited by innumerable individuals of many different genera and species, each having its own developmental/ physiological state and each being immersed in its own environment. The organisms move, both because of water flow and because of their own swimming or buoyancy, and interact with their environment by gathering resources which they need and by excreting waste products. The assimilated material can be used for maintenance, growth, or reproduction. Finally, the organisms can die either from natural causes or because of attacks by another organism.

Furthermore, the processes just described must generally be regarded as stochastic. For example, the probability of a predator capturing a prey item will depend on multiple factors, each with its own probability:

- finding a prey item in range
- the choice to attack (presumably depending on the level of satiation of the predator and the perceived nature of the prey)
- success in the attack (a function of the condition of the predator and of the prey)
- competition against others

Such a description suggests an "agent-based" or IBM with each agent carrying information about its position, its species, its physiological state, etc. Organisms can grow, reproduce, and die. Certainly, we can build small versions of such models, but the number of individuals is necessarily limited (compared to nearly 20,000 copepods per cubic meter observed during Globec [Incze, 19xx], or to phytoplankton densities on the order of 10^8 per cubic meter). However, such experiments may indeed give insight into the way in which the local, stochastic interactions translate into terms representing, for example, grazing rates in terms of average densities.

Once again, we could take the alternative view of attempting to predict the probability distribution for biomass in a continuous space, in this case using something like weight and "species" as our variables. The latter is, of course, discrete, yet different organisms can be genetically or, more importantly, functionally quite close to others. If we choose a species ordering such that the maximum growth rate varies smoothly, we may expect that other terms entering the dynamics such as the losses by predation will also fall on a fairly smooth curve. Certainly on any diagram such as figure 3.1 the gaps will be so small as to be negligible, and viewing the ordinate as a continuous variable is not unreasonable. We can then consider the ways that the processes described above alter the biomass distribution in this space.

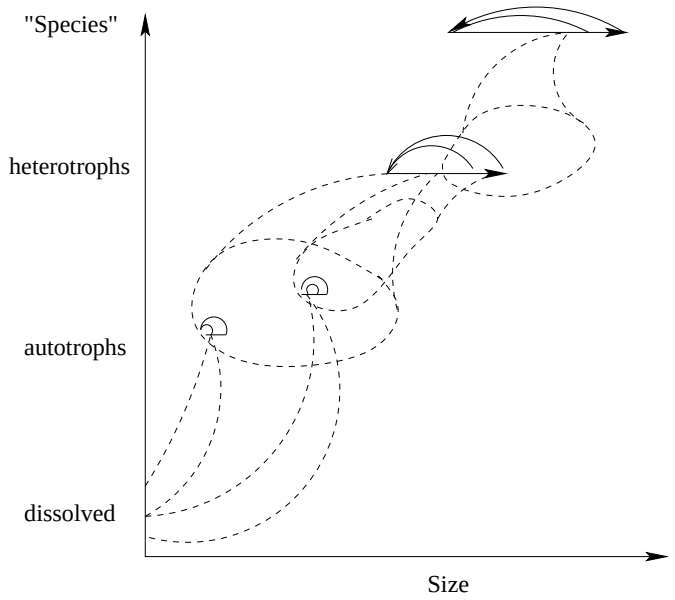

Figure 3.1: Sketch of a few elements in a size-"species" system; biomass moves along the size direction (purely horizontally) by growth (transferring b to larger sizes) or by reproduction (the arcs shifting it from large to small sizes). Biomass moves in both size and "species" by predation.

As in the individual-based model, the number of variables we would have to consider is still unmanageably large. Furthermore, for each (w, sp), we need to specify the sources, the sink, and the transfer rates, including possible nonlinear dependence on the local biomass $b(w, s|\mathbf{x}, t)$ and the density at the source/ sink $b(w', s'|\mathbf{x}, t)$.

Any attempt to construct such a model or the IBM version will inevitably point out how little we know about most of the species inhabiting the ocean. But we may be able to use general rules such as allometric scaling (properties proportional to some power of the weight or some factor times the log of the weight; c.f., xxx, 19xx) to simplify the interactions, recognizing that there will be many exceptions. We shall return to some of these approaches in chapters xx and xx, but focus now on the basic structure to help us understand the meaning and limitations of conventional models.

3.0.1 — Trait-based models

We can build a potentially more complex version of fig. 3.xx by considering each type of organism as specified by the values of a set of trait variables $\mathbf{s} = (s_1, s_2, \ldots, s_N)$; we can think of these as a simplified genetic code. The value of $\mathbf{s}$ determines the phenotype, which, for the modeller, means the vital rates for uptake of resources, reproduction, vulnerability to various predators, etc. Sensitivity to external factors such as temperature would also depend on $\mathbf{s}$. For example, we could specify nutrient uptake rates as

$$\frac{1}{P}\frac{\partial}{\partial t}P = \mu_0 \frac{4L_0 L}{(L + L_0)^2}\frac{N}{N + N_h} + \ldots$$

where μ_0 gives the maximum growth rate at the optimal light level L_0 and abundant nutrient, while N_h sets the properties of the nutrient uptake curve: both $\frac{\partial \mu}{\partial N}$ at low resource levels and how large N has to be for the uptake to begin to saturate. Such forms will be discussed in more detail below, but here we just want to consider the relationship of such formulae to trait space. We might be tempted to take μ_0, L_0, N_h as the traits; however, we suspect that they are not independent. Species which prefer low light may need higher nutrients, for example. In that case, we can think of L_0 and N_h as varying parametrically with a single trait variable so that the trait space would have dimension two or lower rather than three.

Once we've define the trait space and the dependence of vital rates (as well as what parts of the space serve as food sources or predators for organisms with trait $\mathbf{s}$), we can construct the dynamical equations. If the interactions are all of the quadratic/ Lotka-Volterra kind, we will have

$$\frac{\partial}{\partial t} b(\mathbf{s}) = \int d\mathbf{s}' L(\mathbf{s}, \mathbf{s}') b(\mathbf{s}') + \int d\mathbf{s}' d\mathbf{s}'' N(\mathbf{s}, \mathbf{s}', \mathbf{s}'') b(\mathbf{s}') b(\mathbf{s}'') \tag{3.1}$$

Biotic variables respond on a per-capita basis, so that we can simplify this using

$$L(\mathbf{s}, \mathbf{s}') = L'(\mathbf{s}) \delta(\mathbf{s} - \mathbf{s}') \quad , \quad N(\mathbf{s}, \mathbf{s}', \mathbf{s}'') = N'(\mathbf{s}, \mathbf{s}') \delta(\mathbf{s} - \mathbf{s}'')$$

giving

$$\frac{\partial}{\partial t} b(\mathbf{s}) = b(\mathbf{s}) \Big[L'(\mathbf{s}) + \int d\mathbf{s}' N'(\mathbf{s}, \mathbf{s}') b(\mathbf{s}') \Big] \tag{3.2}$$

The choice of an integral rather than just a term like $n(\mathbf{s}, \mathbf{s}')b(\mathbf{s}')$ is an important step in gerneralizing trait-based models. Such forms are known as **functionals**, and they map a function like $b(\mathbf{s})$ into a real number. Since the term in square brackets in 3.xx has to be a real number (with dimensions of $1/T$), but $b(\mathbf{s})$ is a function, functionals are the appropriate mathematical operators. Another way to see this is consideration of the dimensions: $\mathbf{b}$ has units of concentration (mass per unit physical volume per unit phase space volume). The integral takes care of the extra phase space volume in the quadratic term.

Another way of viewing the issue is to consider the discrete form: suppose we want to know the biomass of a particular phytoplankton type $\mathbf{s}_1$. If we have a value when this is the only only active type, but then add another nearby one at $\mathbf{s}_2$, we expect b_1 to get smaller; e.g., we might be balancing $\sum g_i b_i$ with d_Z/a in the grazer equation. As more and more nearby types are added, making a denser coverage of trait space and assuming that they all survive somehow, b_1 will decrease in inverse proportion to the number of types. In contrast, the function $b(\mathbf{s})$ will have a well-defined limit as the discretization gets finer and finer. This discussion indicates the difficulty of defining "species" in this type of model: it really represents a small but finite volume in trait space. Offspring do vary somewhat in the finer details of their phenotype, so that the biomass in particular species is best thought of as an integral measure of a peaked distribution. The biotic form 3.xx presumes offspring have exactly the same $\mathbf{s}$ as the parents; at very high resolution of trait space, we would want to use 3.xx with reproduction occuring with a kernel which

spreads the new $\mathbf{s}$ values slightly. (Mutation will also cause spreading in trait space.) And, when considering interactions with other types, we must assume that predators will not distinguish among organisms which are very close in trait space, again making an integral formulation appropriate.

Finally, we note that some traits, such as weight, are fungible and may change significantly over a lifetime with noticable impact on properties such as swimming, feeding, reproduction, etc. In figure 3.xx, this appears as the horizontal arrows; we shall discuss adding this to models in chapter xx.

NPZ MODELS

Having laid out a fairly general framework, let us now examine the relationship to models like the one in chapter 1 and then discuss common elaborations used in these discrete, low-dimensional systems. We can view conventional NPZ type models as singular solutions with

$$b(\mathbf{x}, t, \mathbf{s}) = \sum b_i(\mathbf{x}, t)\delta(\mathbf{s} - \mathbf{s}_i)$$

This form still has finite biomass $\mathbf{b}_i$ when integrated over a volume around $\mathbf{s}_i$. With this form, the dynamical equations 3.xx or 3.xx reduce to algebraic form

$$\frac{\partial}{\partial t} b_i = L_{ij} b_j + N_{ijk} b_j b_k \tag{3.3}$$

or

$$\frac{\partial}{\partial t} b_i = b_i [L'_i + N'_{ij} b_j] \quad \text{(biotic)}$$

with terms such as N'_{ij} equal to $N'(\mathbf{s}_i, \mathbf{s}_j)$.

Alternatively, we can regard the b_i as representing a collection of different types occupying some volume in trait space. In essence, we are making an approximate separation of variables

$$b(\mathbf{x}, t, \mathbf{s}) \simeq \sum b_i(\mathbf{x}, t) f_i(\mathbf{s})$$

and we take f_i to be nonzero in a finite part of trait space, with unit integral. The approximate dynamics follows from integrating 3.xx over the i^{th} subvolume to give 3.xx, but with $L_{ij} = \int_{V_i} d\mathbf{s} \int d\mathbf{s}' L(\mathbf{s}, \mathbf{s}') f_j(\mathbf{s}')$. Thus terms like a death rate for P are attempting to sum up the death rates of each type weighted by its abundance.

For the rest of this chapter, then, we shall retreat to dealing with variables such as P viewed either as the integral over some range of traits or as a single point in the space – in either case fixing the shape of the distribution in trait space. We can then presume that transfers into and out of the resulting "black-boxes" can be represented as functions just of the integrated values and attempt to parameterize those. In the following sections, we shall examine stochasitic effects, the ways in which transfers are parameterized, and various box models. In the next one, weight-structured models are considered and then we work back towards the kind of system represented in figure 3.1.

3.1 — Deterministic/ stochastic dynamics

We shall mostly use differential equations to describe the changes in biomass or other properties for each species or class modelled. But, at a more fundamental level, we are really attempting to calculate the **expected value** of the property. Even if we could simulate each organism, we would need to represent its actions stochastically; we are forced at some level to deal with processes which are not predictable although we may have some handle on mean rates (and perhaps variances). In addition, when we compare a model to data, we would ideally like to know the variance not only of the data but also of the model in order to decide whether the inevitable disagreement is significant or not.

In this section, therefore, we shall consider some simple problems, using not only the conventional, deterministic equations but also equations for the probability distributions, so that we can understand

- how the variability alters the equations for the means
- how large the variances might be

To consider an example, a biomass field b really represents the mean from a probability distribution of numbers and weights:

$$b(t) = \sum_{n=0}^{\infty} \int_{w_0}^{w_{max}} nw\mathcal{P}(n, w, t)\, dw$$

where $\mathcal{P}(n, w, t)dw$ gives the probability that there are n organisms with weights between w and $w + dw$. The deterministic model will predict b, while the stochastic model will examine the whole probability distribution $\mathcal{P}$. Intermediate models may attempt other moments of $\mathcal{P}$ such as the mean weight and variances in numbers, weights, and biomass. Monte-Carlo simulations of a reasonable number of realizations provide another approach to estimating the statistics, although such calculations can be time-consuming and difficult to meld with physical models.

3.1.1 — Exponential growth

For our first example, we begin with constant growth, using phytoplankton as the target organism. If there are no limitations on resources, each cell would divide in a time of about τ. In the absence of any synchronization, this implies a constant probability of division per unit time and

$$b(t + \delta t) = [1 + g\, \delta t]b(t)$$

so that

$$\frac{\partial}{\partial t} b = gb \qquad \Rightarrow \qquad b(t) = b_0 \exp(gt) \quad .$$

To achieve doubling over time τ, we need $g = \ln 2/\tau$. The population grows exponentially; clearly such a model is of limited validity. As we shall see, exponential growth (or decay) is characteristic of linear models. Some terms which are nonlinear in the biological variables are required to limit the population growth.

3.1.2 — Stochastic dynamics

Now, let us take into account the stochastic nature of birth and death processes, so that $g\,\delta t$ and $d\,\delta t$ represent the probability a cell will divide or will die during time interval dt. Does the expected population satisfy the same exponential law? If we start with a set of isolated seed populations, how much variation would we expect to find among them at some later time? What is the probability the population will become extinct? (For reference, see Barucha-Reid, 1960, *Elements of the Theory of Markov Processes and their Applications*, McGraw Hill, NY.)

For the linear model (no density dependence), we can answer such questions exactly. Consider a vector $\mathcal{P}_n(t)$ giving the probability that there are n organisms at time t; we would like to predict $\mathcal{P}_n(t+dt)$ or, in the limit as $dt \to 0$, $\frac{\partial}{\partial t}\mathcal{P}$. Assuming that a given organism can double, can die, or can survive during time dt leads to

$$\mathcal{P}_n(t+dt) = \mathcal{P}_{n-1}(n-1)\delta t + \mathcal{P}_{n+1}(n+1)d\delta t + \mathcal{P}_n(t)(1 - ng\delta t - nd\delta t) + \mathcal{O}(\delta t^2) \quad .$$

I.e., we can move from having $n-1$ organisms to n if one of the $n-1$ individuals divides (the probability of two dividing in time δt is another factor of δt smaller and will be neglected.) From this, we derive the "master equation":

$$\frac{\partial}{\partial t}\mathcal{P}_n = (n-1)g_{n-1}\mathcal{P}_{n-1} + (n+1)d_{n+1}\mathcal{P}_{n+1} - n(g_n + d_n)\mathcal{P}_n \tag{3.4}$$

where we have allowed for the possibility that the *per capita* birth and death rates may be density dependent; if not, they are simply given by g and d, respectively.

The first few equations help us gain insight into the character of the solutions

$$\begin{aligned}
\frac{\partial}{\partial t}\mathcal{P}_0(t) &= d_1\mathcal{P}_1(t) \\
\frac{\partial}{\partial t}\mathcal{P}_1(t) &= -(d_1+g_1)\mathcal{P}_1(t) + 2d_2\mathcal{P}_2(t) \\
\frac{\partial}{\partial t}\mathcal{P}_2(t) &= -2(d_2+g_2)\mathcal{P}_2(t) + g_1\mathcal{P}_1(t) + 3d_3\mathcal{P}_3(t) \\
\frac{\partial}{\partial t}\mathcal{P}_3(t) &= -3(d_3+g_3)\mathcal{P}_3(t) + 2g_2\mathcal{P}_2(t) + 4d_4\mathcal{P}_4(t) \quad .
\end{aligned}$$

The probability of extinction, $\mathcal{P}_0$, increases monotonically; whether it is bounded by some value less than one will depend on how rapidly $\mathcal{P}_1$ decreases with time. Thus, we cannot expect to find a truly steady solution to the master equation.† Populations either grow indefinitely or become extinct; however, as we shall see, the extinction time for large populations can be so long that we find a quasi-steady solution. We shall return to this issue when we discuss density-dependent dynamics.

† Unless a single individual is immortal ($d_1 = 0$)!

In general, we are less concerned with the detailed probability distribution than with its moments

$$\langle n^m \rangle = \sum_n n^m \mathcal{P}_n$$

in particular, the mean $\langle n \rangle$ and the variance $\sigma^2 = \langle n^2 \rangle - \langle n \rangle^2$; these are quantities which may be measurable and which can be related to the deterministic density b.

From the form of (3.1), we can show that

$$\frac{\partial}{\partial t} \sum \mathcal{P}_n = -\sum n g_n \mathcal{P}_n - \sum n d_n \mathcal{P}_n + \sum (n-1) g_{n-1} \mathcal{P}_{n-1} + \sum (n+1) d_{n+1} \mathcal{P}_{n+1}$$

so that

$$\frac{\partial}{\partial t} \sum_n \mathcal{P}_n(t) = 0$$

implying that $\langle n^0 \rangle$ is preserved at its initial value 1 — as required for a probability distribution. The first moment equation is

$$\frac{\partial}{\partial t} \langle n \rangle = \sum n (g_n - d_n) \mathcal{P}_n \quad .$$

When the birth and death rates are constant, this reduces to

$$\frac{\partial}{\partial t} \langle n \rangle = (g-d) \langle n \rangle \quad ,$$

and the mean satisfies the same exponential rule $\langle n \rangle = \langle n \rangle_0 \exp([g-d]t)$ as the deterministic case.

The second moment (with constant rates) satisfies

$$\frac{\partial}{\partial t} \langle n^2 \rangle = 2(g-d) \langle n^2 \rangle + (g+d) \langle n \rangle \quad ;$$

substituting $\langle n^2 \rangle = \sigma^2 + \langle n \rangle^2$ and using the dynamical equation for $\langle n \rangle$ results in the same equation for the variance. The solution is

$$\sigma^2(t) = \left(\sigma^2(0) + \langle n \rangle_0 \frac{g+d}{g-d} \right) e^{2(g-d)t} - \langle n \rangle_0 \frac{g+d}{g-d} e^{(g-d)t} \quad .$$

For large times and a growing population, the first term dominates, and the ratio of the standard deviation to the mean becomes constant

$$\lim_{t \to \infty} \left(\frac{\sigma}{\langle n \rangle} \right) = \sqrt{\frac{\sigma^2(0) + \langle n \rangle_0 \frac{g+d}{g-d}}{\langle n \rangle_0^2}}$$

implying that the error bars on a plot of $\log \langle n \rangle$ versus t would be uniform.

What about the extinction probability? For the case with constant birth and death rates ($g_n = g,\ d_n = d$), an exact solution can be obtained. Since the derivation is not very general, we refer the reader to Barucha-Reid for details and simply give the result: the extinction probability becomes constant

$$\lim_{t\to\infty} p(0,t) = \sum_n \mathcal{P}_n(0) \left(\frac{d}{g}\right)^n \quad . \tag{3.5}$$

(When $d > g$, the mean decays exponentially, and the extinction probability limits to 1.) If we start with exactly N organisms, the extinction probability will be $(d/g)^N$. Even if the birth rate is only 1% higher than the death rate, the extinction probability beginning with 1000 organisms, 5×10^{-5}, corresponds to a 50/50 survival chance after 15,000 generations.

3.1.3 — Logistic equation

The simplest form of limitation arises from competition for scarce resources, leading to a decrease in the growth rate g as b increases. Let us consider a general form

$$\frac{\partial}{\partial t} b = g(b) b$$

and take the first two terms in a Taylor expansion of b

$$g(b) = g_0 \left(1 - \frac{b}{b_0}\right)$$

where g_0 is the "intrinsic growth rate" and b_0 is the "carrying capacity." The logistic equation

$$\frac{\partial}{\partial t} b = g_0 b \left(1 - \frac{b}{b_0}\right)$$

has an analytical solution, which can be found by looking at the equation for the inverse $s = 1/b$.

$$\frac{\partial}{\partial t} s = -s^2 g_0 \frac{1}{s} \left(1 - \frac{1}{s b_0}\right) = -g_0 s + \frac{g_0}{b_0}$$

so that

$$s = \frac{1}{b_0} + \left(\frac{1}{b(0)} - \frac{1}{b_0}\right) \exp(-g_0 t)$$

thus

$$b = \frac{b_0}{1 + \left(\frac{b_0 - b(0)}{b(0)}\right) \exp(-g_0 t)} \quad . \tag{3.6}$$

The solution has a sigmoid shape. For $b(0) \ll b_0$ and short times, we have

$$b = b(0) \exp(g_0 t) \quad .$$

For long times b limits to b_0, the carrying capacity, whether b starts above or below b_0. The latter holds under the assumption that we can carry the Taylor expansion beyond $b = b_0$, which may or may not be the case.

Note that the inverse trick also holds for the advection operator

$$\frac{D}{Dt} \equiv \frac{\partial}{\partial t} + \mathbf{u} \cdot \nabla$$

but not for diffusion.

More formal justification...

We can justify the logistic form to some degree using the following argument:

- The nutrient available per organism is inversely proportional to the population density — $Avail = N_0/b$.
- The cells require a minimum amount of nutrient to offset respiration — $Avail > Resp$. This sets the carrying capacity $b_0 = N_0/Resp$. The division rate increases as the available nutrient increases.
- The division rate has a maximum value.

These suggest a division rate vs. available nutrient like

$$\begin{aligned} Division\ rate &= Max\ rate \frac{Avail - Resp}{Avail} \\ &= D_{max} \frac{1/b - 1/b_0}{1/b} \\ &= \begin{cases} D_{max}\left(1 - \frac{b}{b_0}\right) & b < b_0 \\ 0 & b > b_0 \end{cases} \end{aligned} .$$

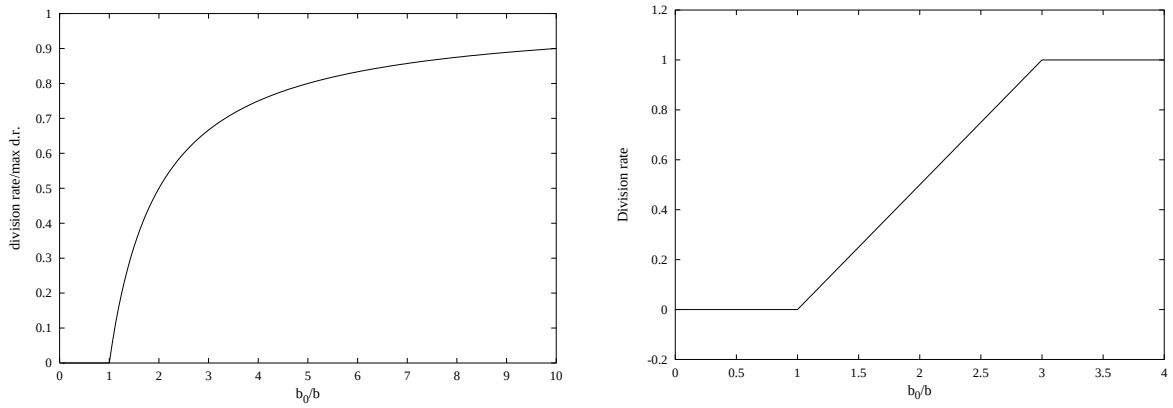

Figure 3.2: Examples of division rates vs. nutrient available per organism.

When we set $D_{max} = \ln 2/\tau$, we recover the logistic equation, except that the growth rate remains zero, rather than going negative, when the population exceeds the carrying capacity. The resulting growth rate, $\frac{\partial}{\partial t}b$, is a truncated quadratic function of b.

We will encounter formulae like the one above where the value changes if some condition is satisfied or not. Mathematically, this can be handled with a Heaviside function; we will use a programming notation with the function $(b < b_0)$ being 1 when true and 0 when false. So we can write

$$Division\ rate = D_{max}\left(1 - \frac{b}{b_0}\right)(b < b_0) \quad .$$

Since we also often want only positive branches, with zero when the argument is negative, we will introduce another notation

$$Division\ rate = D_{max}\left(1 - \frac{b}{b_0}\right)_+$$

which means it is zero when the quantity in the parentheses is negative.

Of course, we can think of many other functions which satisfy the conditions, such as a ramp function which makes $\frac{\partial}{\partial t}b$ a tent map of b instead of a quadratic. But the time-dependent solution is very similar – in this case, a growing exponential joined to an exponential which approaches b_0.

Adding a death rate, d (which we shall associate with predation by herbivores, although it could also include cell senescence) gives

$$\frac{\partial}{\partial t}b = g(b)b - db \quad .$$

For constant g, we still have exponential growth

$$b(t) = b(0)\exp[(g-d)t] \quad .$$

The quasi-logistic form

$$\frac{\partial}{\partial t}b = g_0 b\left(1 - \frac{b}{b_0}\right)_+ - db \tag{3.7}$$

is again solvable; if we start with a small b value, the population grows as $\exp([g_0 - d]t)$ and then slows and approaches the asymptote $b_0(g_0 - d)/g_0$. The solution is the same as (3.3), except for the different growth rate and asymptote:

$$b = \frac{b(0)b_0(g_0 - d)}{g_0 b(0) + (b_0[g_0 - d] - g_0 b(0))\exp(-[g_0 - d]t)} \quad .$$

If we start with a population larger than $b_0(g_0 - d)/g_0$, it will decay to this value. But the decay may occur in two stages: if $b(0) > b_0$, we have $b = b(0)\exp(-dt)$ until the time when $b = b_0$, after which the solution above takes over.

3.1.4 — Stochastic logistic dynamics

If the birth/death processes are stochastic, the master equation (3.1) applies; however, we now assume that the probability of reproducing decreases with increasing n (based on the same food availability arguments) $g_n = g(1 - n/n_0)$ [or zero for $n > n_0$], $d_n = d$. We still have

$$\frac{\partial}{\partial t} \sum_n \mathcal{P}_n(t) = 0$$

but now

$$\frac{\partial}{\partial t}\langle n \rangle = (g-d)\langle n \rangle - \frac{g}{n_0}\langle n^2 \rangle = (g-d)\langle n \rangle - \frac{g}{n_0}\langle n \rangle^2 - \frac{g}{n_0}\sigma^2 \quad . \tag{3.8}$$

If the variance $\sigma = \sqrt{\langle n^2 \rangle - \langle n \rangle^2} << \langle n \rangle$, then $\langle n^2 \rangle \simeq \langle n \rangle^2$ and we recover the logistic form; in general, they will not agree, since the variance is not negligible.

We carried out simulations of the master equation for $g = 0.2$, $d = 0.15$, and a range of (rather small) n_0 values from 100 to 1000, for which the logistic equations would estimate $\langle n \rangle = 25$ to 250. The initial conditions were $\mathcal{P}(n_0/5, 0) = 1$, and the simulations ran for 1000 time units. The final probability distributions shown in figure 3.3 indicate that they narrow as n_0 increases, and that the values near $n = 0$ decrease precipitously so that the extinction probability drops.

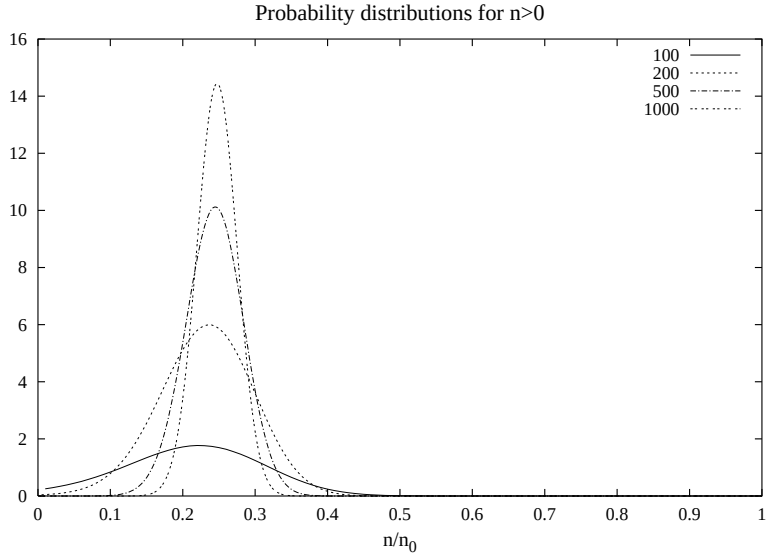

Figure 3.3: Probability distributions $n_0\mathcal{P}_n$ plotted versus n/n_0. (The normalization preserves the integral, but, for $n_0 = 100$ and 200, substantial extinction — 58% and 3%, respectively — has occurred so that the areas under the curves are smaller.)

As shown in figure 3.4a, the mean values approach the logistic estimate $\hat{n} = n_0(g - d)/g$, but remain significantly below it. The variance (calculated below) increases in the same way, $\langle n \rangle^{1/2}$, as in simple sampling problems (see figure 3.4b). For very large n_0, then, the last term in (3.5) will be order one compared to the others which are order n_0,

so that the use of the simple logistic equation for $\langle n \rangle$ is indeed justified; a simulation with n_0=5000 produced $\langle n \rangle / n_0 = 0.2494$ compared to the 0.25 predicted by $\hat{n}/n_0$.

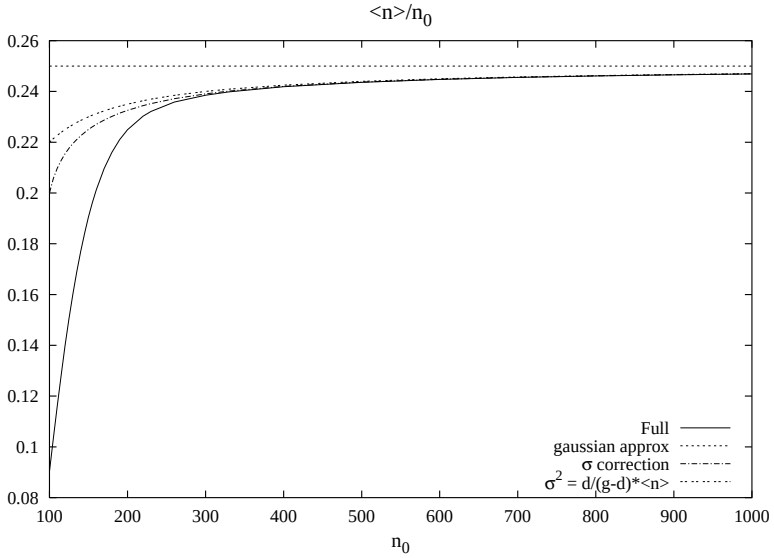

Figure 3.4a: Mean populations (as a fraction of n_0). The solutions to the master equation are indicated by "Full"; the others are discussed below.

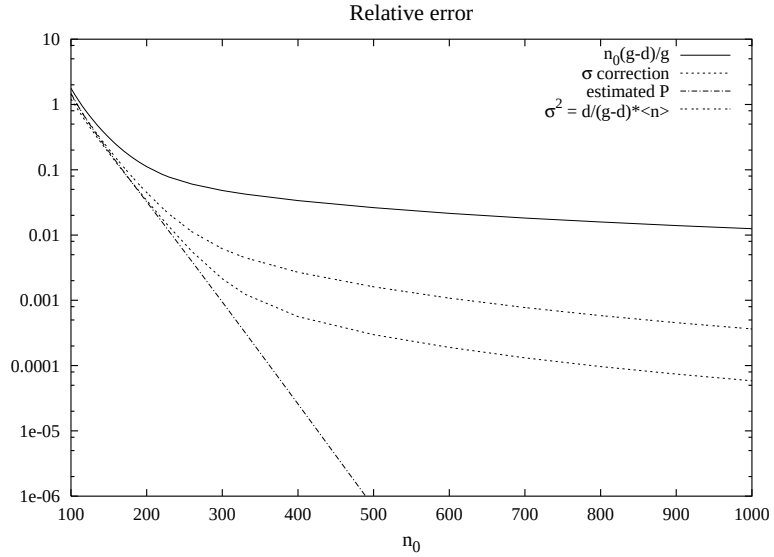

Figure 3.4b: Relative error for approximations to the mean.

For this model, the extinction probability eventually approaches 1, rather than limiting to a smaller value as in the exponential growth model (3.2). Instead, the extinction rate becomes nearly constant. We can estimate the extinction rate by assuming that the shape of the probability distribution $\mathcal{P}_1, \mathcal{P}_2, \mathcal{P}_3, \ldots$ remains unchanged but the amplitude varies:

$$\mathcal{P}_n = \begin{cases} 1 - A(t) & n = 0 \\ A(t) f_n & n > 0 \end{cases}$$

with $\sum f_n = 1$. We find f_n by starting with $f_0 = 0$, $f_1 = 1$, and stepping the steady version of (3.1) forward to find f_2, f_3, f_4, etc. stopping when one becomes zero (or negative). We then renormalize the positive values so that the sum of the f_n's is one. The behavior of $A(t)$ is found from the equation for the extinction state:

$$\frac{\partial}{\partial t}(1 - A) = dAf_1 \quad \Rightarrow \quad A = \exp(-df_1 t) \quad .$$

Thus the mean population will decay in a characteristic time $1/df_1$; as shown in figure 3.4c, this gives an excellent estimate of the rates.

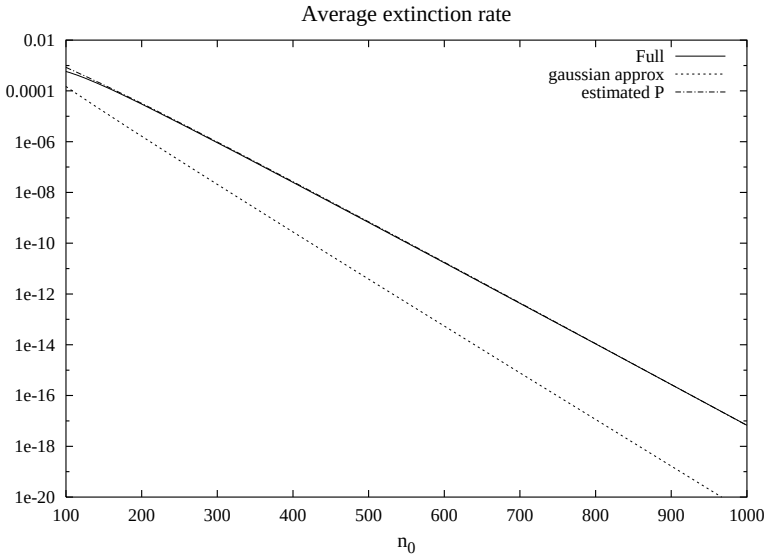

Figure 3.4c: Extinction rates

We can see the connection between the stochastic and deterministic equations by Taylor-expanding (3.1), assuming that n is large and treating it as a continuous variable:

$$\frac{\partial}{\partial t}\mathcal{P}(n) \simeq -\frac{\partial}{\partial n}\left[ng(n)\mathcal{P}(n) - nd(n)\mathcal{P}(n)\right] + \frac{\partial^2}{\partial n^2}\left[\frac{ng(n) + nd(n)}{2}\mathcal{P}(n)\right] \qquad (3.9) \quad .$$

By analogy to the Boltzman equation, the first term on the right corresponds to the deterministic dynamics

$$\frac{\partial}{\partial t}N = Ng(N) - Nd(N)$$

which is just our logistic equation, while the second term causes a spreading of the probability distribution, giving a non-zero variance. For large n_0, we can examine equation (3.6) in the vicinity of $\hat{n}$ for which $g(\hat{n}) = d(\hat{n})$ — i.e., $\hat{n} = n_0(g - d)/d$ for the logistic case we have been treating. Then the equation simplifies to

$$\frac{\partial}{\partial t}\mathcal{P}(n) \simeq -\frac{\partial}{\partial n}\left[D(n - \hat{n})\mathcal{P}(n)\right] + \frac{\partial^2}{\partial n^2}\left[K\mathcal{P}(n)\right] \qquad (3.10)$$

with $D = \hat{n}g'(\hat{n}) - \hat{n}d'(\hat{n}) < 0$ and $K = \hat{n}d(\hat{n})$. This equation appears in other problems: tracer behavior in a region of converging flow, intensification of vorticity gradients in 2D turbulence, and the concentration of depth-keeping animals near a front (c.f., Olson and Backus, 19xx). The steady state distribution is Gaussian

$$\mathcal{P} = \frac{1}{\sqrt{2\pi\sigma}} \exp[-(n-\hat{n})^2/2\sigma^2]$$

with the standard deviation given by $\sigma^2 = K/|D|$ which is dn_0/g in the logistic problem. Although we can estimate $\mathcal{P}_1$ from this form, the probability distribution is closer to exponential for small n so that the Gaussian understimates the extinction rate significantly (figure 3.4c).

Given that the use of the logistic equation for the mean seems to have very small errors when n_0 (or $\langle n \rangle$) is large, why should we be concerned any further? The problem lies in the presumption, inherent in this model, that the biota and their resources are all well-mixed; otherwise, extinction can occur in small subregions (which can, by themselves, support fewer organisms) and replenishment by mixing may overcome such losses.

Various studies (xxx, xxx, xxx) have examined this issue with individual-based models and theories. We follow a procedure like that of Hernández-Garcia and López: for each organism, we calculate an estimate of neighbor density R (using xx.xx) and then adjust the birth probability to be $g(1-R/\rho_0)\delta t$; the probability of dying remains $d\delta t$. Births occur at the location of the parent; in between time steps the organisms move with random flights characterized by the parameters κ and r. Figure 3.5 shows the densities compared to the logistic value $\rho_0(g-d)/g$. For large diffusivities the competition is essentially global; for small densities, it is local, and we find small clumps of organisms which die out while new ones form as individuals move out of the competitive range and begin to reproduce more effectively. forming a new clump.†

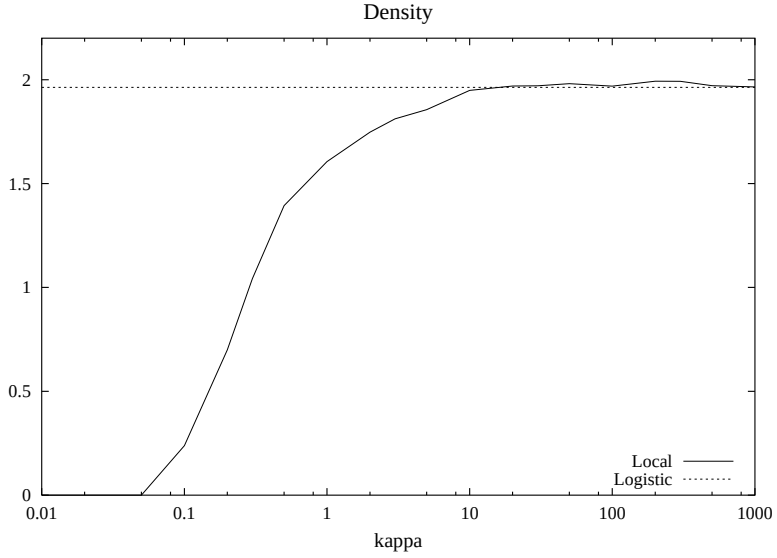

† Unlike Hernández-Garcia and López (20xx), but consistent with the results of Birch and Young (20xx), we do not find regular patterns for the parameters used.

Figure 3.5: Mean density in a 20×20 domain for various κ parameters controlling the random flight.

The localized nature of competition for resources (or other biological interactions) thus provides some justification for understanding the stochastic model for modest numbers of organisms a bit further. Let us first try to predict the value of σ^2. We can construct the equation for the second moment

$$\frac{\partial}{\partial t}\langle n^2 \rangle = 2(g-d)\langle n^2 \rangle - 2\frac{g}{n_0}\langle n^3 \rangle + (g+d)\langle n \rangle - \frac{g}{n_0}\langle n^2 \rangle \quad .$$

We now run into a closure problem: to calculate $\langle n \rangle$, we need $\langle n^2 \rangle$; to calculate $\langle n^2 \rangle$ we need $\langle n^3 \rangle$; etc. If we assume the first and second moment equations reach a steady state and write $n = \langle n \rangle + n'$, we have

$$\left[2(g-d) - 4\frac{g}{n_0}\langle n \rangle\right]\sigma^2 = -2d\langle n \rangle + 2\frac{g}{n_0}\langle n'^3 \rangle \simeq -2d\langle n \rangle \quad . \tag{3.11}$$

If we neglect the skewness in the final state, $\langle n'^3 \rangle = 0$, we can solve the approximate equation (3.8) together with (3.5) to find the steady state mean and variance. These results are labelled "σ correction" in figures 3.4a-b. But 3.6 also indicates clearly that $\sigma^2 \sim \langle n \rangle$, so that (3.5) predicts $\langle n \rangle \simeq (g-d)n_0/g$ and therefore $\sigma^2 \simeq d\langle n \rangle/(g-d)$ in the large $\langle n \rangle$ limit (labelled $\sigma^2 = d/(g-d) * \langle n \rangle$ in the figures).

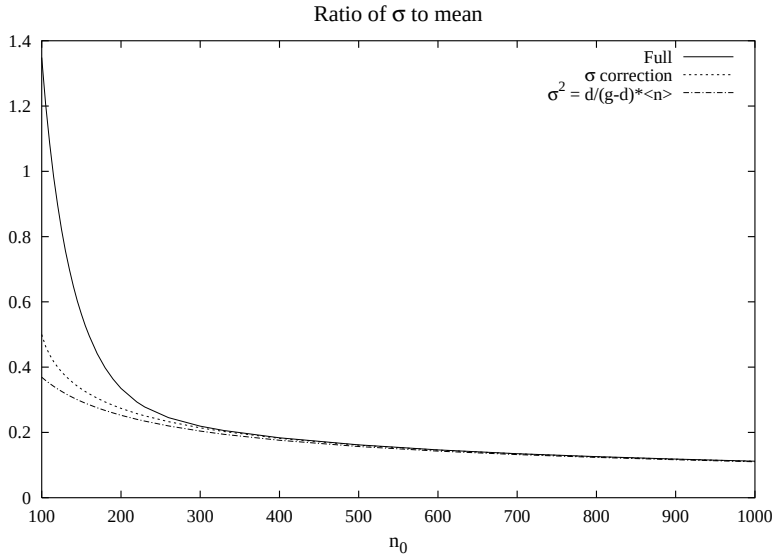

Figure 3.6: Ratio $\sigma/\langle n \rangle$.

3.1.5 — Lotka-Volterra and QNPZ dynamics

To complete our discussion of stochastic models, let us consider predator-prey models of the classic Lotka-Volterra

$$\frac{\partial}{\partial t}P = \hat{\mu}P - gPZ$$
$$\frac{\partial}{\partial t}Z = gPZ - d_z Z$$

or the quadratic NPZ model (chapter 1) which replaces $\hat{\mu}$ by $\mu N = \mu(N_T - P - Z)$. The master equation for the probability $\mathcal{P}(P, Z, t)$ of having biomasses P and Z (in nitrogen units) becomes

$$\begin{aligned} m_P \frac{\partial}{\partial t}\mathcal{P}(P,Z,t) = {} & \mu(P - m_P)N^-\mathcal{P}(P - m_P, Z, t) - \mu PN\mathcal{P}(P,Z,t) + \\ & g(P + m_P)(Z - am_P)\mathcal{P}(P + m_P, Z - am_P, t) - gPZ\,\mathcal{P}(P,Z,t) + \\ & d_p(P + m_P)\mathcal{P}(P + m_P, Z, t) - d_p P\,\mathcal{P}(P,Z,t) + \\ & \frac{d_z}{a}(Z + am_P)\mathcal{P}(P, Z + am_P, t) - \frac{d_z}{a}Z\,\mathcal{P}(P,Z,t) \end{aligned} \tag{3.12}$$

with m_P being the biomass of an individual. The a factors account for the fact that a loss m_P from the P biomass increases the Z biomass by am_P.

Solving equation (3.9) in the Lotka-Volterra version ($N^- = N = \text{const.}$) runs into difficulties: as $\mathcal{P}$ diffuses, it reaches the trajectories that take long excursions and pass close to the origin or the $Z = 0$ axis. As a result, there will be a flux of $\mathcal{P}$ into the largest P values (indeed to infinity along the line where the herbivores have become extinct). Preventing reproduction out of the maximum P grid points allows $\mathcal{P}$ to move up in Z and eventually return into the domain moving diagonally towards larger Z and smaller P; however, it then returns near the $P = 0$ axis, moves own towards the origin, and feeds more $\mathcal{P}$ into the extinct zooplankton line. It appears likely that the zooplankton will all become extinct and the phytoplankton population will grow exponentially thereafter.

In the QNPZ case ($N^- = N_T - P - m_P - Z$, $N = N_T - P - Z$), however, the probability function settles quickly when $\mu = 0.6$, giving mean values very close to those predicted by the deterministic model. Even for $\mu = 0.05$, the deterministic and probabilistic models track quite well (figure 3.7). The standard deviation again grows as $\sqrt{N}$ where $N = PV/m_p$ is the number of organisms in the volume considered to be well-mixed; therefore, the expected error bars in the densities P and Z decrease as V/m_p increases.

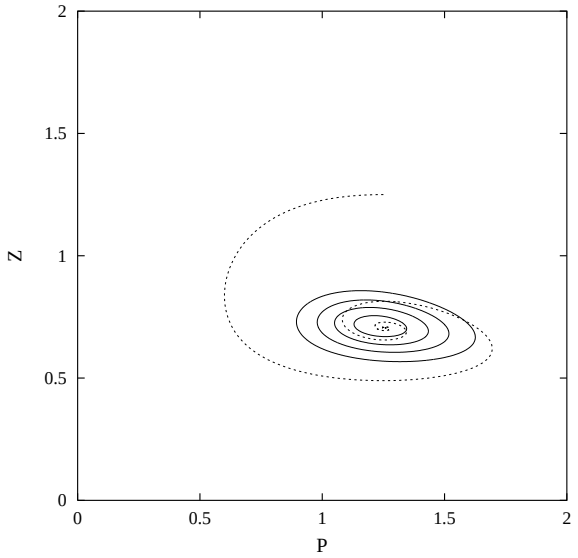

Figure 3.7: Probablilistic QNPZ model with $m_P = 0.0078125$ showing the final probability distribution (contour interval 5×10^{-5}) and the trajectory of the mean.

3.2 — Functional forms

In the QNPZ model, we used the simplest Lotka-Volterra form of interaction between the consumers and their resources: the growth rate of the consumer $\frac{1}{Z}\frac{\partial Z}{\partial t}$ was presumed to be proportional to the density of the resource P. Such a form is unlikely to be realistic for two reasons: first, competition among the consumers, as discussed above, limits the consumer populations and, second, organisms have limits on the rates at which they can assimilate their resource(s). Therefore, in constructing reaction terms for

$$\frac{1}{b_i}\frac{\partial}{\partial t}b_i = \mathcal{R}_i(\mathbf{b}, \mathbf{x}, t)$$

we generally expect $\mathcal{R}_i$ to be a nonlinear function of its arguments, reaching a finite limit or decreasing as the relevant **b**'s increase. Holling (19xx) discussed a number of possible forms for $\frac{1}{b}\frac{\partial b}{\partial t}$ (figure 3.8); for each group being modelled, we need to assess which type of response is appropriate. Here, we shall give arguments for common forms.

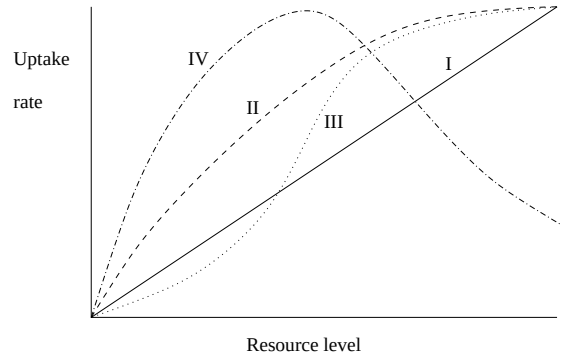

Figure 3.8: Response curves $\mathcal{R}_i(resource)$, showing Holling type I-IV behavior. Type I, rather than remaining linear, may switch to a constant saturation level at some point.

3.2.1 — Grazing model

To represent foraging for prey, consider the following scenario: an individual zooplankter searches over a volume μ in a time τ. If it finds prey in this volume, it eats it; otherwise it tries again the next time period. Assume that the prey are randomly distributed at each time with an average number density P/m_P (where P is the phytoplankton biomass in nitrogen units and m_P is the biomass in nitrogen units of an individual). Then the probability the zooplankter will feed is equal to the probability that there is at least one prey item in volume μ,

$$\mathcal{P}_{feed} = \sum_{n=1}^{\infty} \mathcal{P}(n)$$

which is also equal to $1 - \mathcal{P}(0)$. For the Poisson distribution, appropriate for randomly distributed prey, we have

$$\mathcal{P}_{feed} = 1 - \exp(-\mu P/m_P)$$

and the expected rate of feeding of an individual zooplankter is

$$\frac{1}{\tau}\left[1 - \exp(-\mu P/m_P)\right] \quad .$$

The predator incorporates a fraction a of the prey mass into its own biomass, so the rate of assimilation of mass will be am_P times the above. Finally, we must also multiply by the number of individual zooplankton, Z/m_Z, to find the overall rate of growth of Z:

$$\frac{D}{Dt}Z = a\,\frac{m_P}{\tau m_Z}\,Z\left[1 - \exp(-\frac{\mu}{m_P}P)\right]$$

If we define $g \equiv \mu/\tau m_Z$ and $\nu = \mu/m_P$, we end up with Ivlev grazing formulation

$$\frac{D}{Dt}Z = agZ\frac{1}{\nu}\left[1 - \exp(-\nu P)\right] + \ldots$$

which has a typical saturating shape.

Davis, et al. (19xx) studied a physiologically more detailed model of zooplankton encountering a stochastic sequence of prey items and processing them or not, depending on its gut-fullness; the net uptake rate as a function of food concentration follows the Ivlev model fairly well.

3.2.2 — Nutrient uptake

Nutrients are a bit different, since they are present in solution rather than as discrete prey items. The uptake of nitrogen by phytoplankton is usually represented by a biochemically-based form, Michaelis-Menten kinetics. (See Michaelis, L. and M.L. Menten, 1913. Die kinetic der invertinwirkung. *Biochemische Zeitschrift* **49**:333-369. Laidler, K.J., 1950. *Chemical Kinetics*. McGraw-Hill Book Company, Inc., New York, 408pp). The conversion of nitrogen from the substrate within the cell into protein products occurs via enzymatic reactions

$$E + N \underset{k_{-1}}{\overset{k_1}{\rightleftarrows}} C \xrightarrow{k_2} E + R \quad .$$

C represents the enzyme-substrate complex and R the product used to make more tissue. The rates of change of the concentrations satisfy

$$\begin{aligned}
\frac{\partial}{\partial t}[C] &= k_1[N][E] - k_{-1}[C] - k_2[C] \\
\frac{\partial}{\partial t}[N] &= -k_1[N][E] + k_{-1}[C] + N_s \\
\frac{\partial}{\partial t}[E] &= -k_1[N][E] + k_{-1}[C] + k_2[C] + E_s \\
\frac{\partial}{\partial t}[R] &= k_2[C] + R_s
\end{aligned}$$

where the N_s, E_s, and R_s represent other reactions which serve as sources or sinks.

Murray (19xx) analyzes this kind of equation in detail (although without the additional source-sink terms) and shows that the concentrations change on two time scales (see figure 3.9a). In the rapid phase, the source terms play no role and the enyzme and complex concentrations come into equilibrium: from the first and third equations $[C] + [E] \equiv E_0$ is constant over this period so that $[C]$ satisfies

$$\frac{\partial}{\partial t}[C] = k_1[N]E_0 - (k_1[N] + k_{-1} + k_2)[C]$$

and relaxes rapidly to

$$[C] \simeq \frac{k_1[N]E_0}{(k_1[N] + k_{-1} + k_2)} \quad .$$

Using this in the $[N]$ equation gives

$$\frac{\partial}{\partial t}[N] = -k_1[N]E_0 + (k_1[n] + k_{-1})[C] + N_s = -\frac{k_2E_0[N]}{[N] + (k_{-1} + k_2)/k_1} + N_s \quad .$$

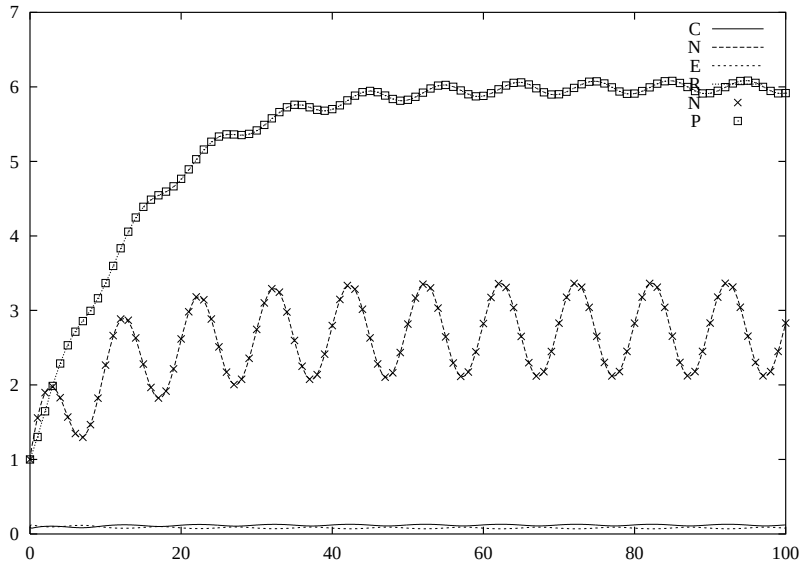

Figure 3.9a: Solutions of the full equation set and the approximations for $[N]$ and $[P]$ using sinusoidally varying N_s.

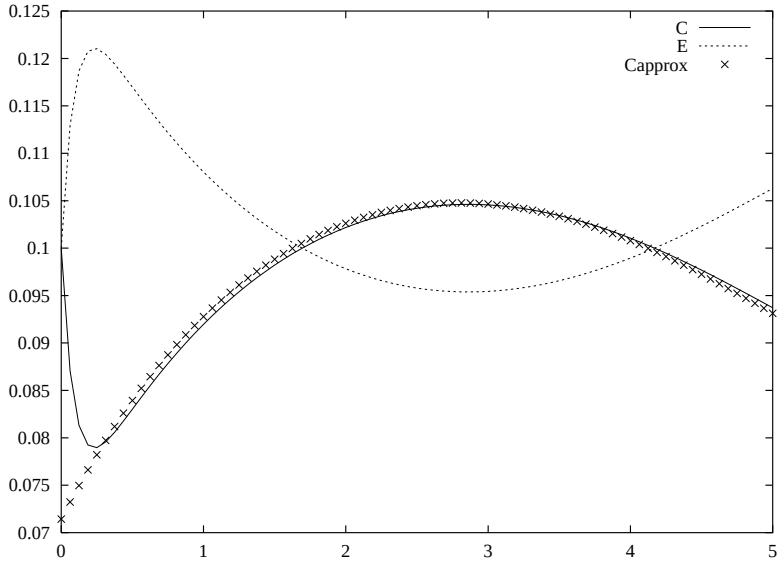

Figure 3.9b: Detail of the initial adjustment.

To convert to an uptake rate for dissolved nitrogen from the whole assemblage of phytoplankton, we assume the internal store $[N]$ is proportional to the dissolved nitrogen in the water column $[N] = \alpha N$ and multiply by the number of organisms present P/m_P; this gives us the Michaelis-Menten (abbreviated as MM) form:

$$\frac{\partial}{\partial t}N = -\mu\frac{NP}{N+N_h} + \text{other terms} \quad .$$

The half-saturation constant N_h (often written k_s) gives the value of N such that the uptake rate is half the maximum. In principle, $\mu = \alpha k_2 E_0/m_P$ and $N_h = (k_{-1}+k_2)/(\alpha k_1)$, but in practice, these parameters are found by fitting to lab or field data. Such a disconnect between the simple theory and practice should not be that surprising since many processes have been glossed over or ignored:

- Phytoplankton do store nutrients internally and use the internal stock, when it is abundant enough, in their biochemical processes. How does the nutrient cross the cell boundary and how is it modified into the internal form?
- Primary production and growth in cell numbers and biomass involve many complex reactions, and cells may use different biochemical pathways under different conditions.
- Cells undergo a cycle, incorporating nutrients and growing and then dividing; cells which have just divided cannot immediately do so again. Pascual and Caswell (19xx) show that this kind of delay can lead to oscillations in a system with a constant nutrient supply or chaotic variability in cell numbers when the nutrient supply fluctuates.
- Building new cells requires more than nitrogen. If the supplies of carbon, phosphorus, or trace elements such as iron are not sufficient, phytoplankton biomass cannot increase. We shall discuss this further below.

For such reasons, we cannot predict from basic biochemistry how rapidly a cell will grow and divide given the composition of the surrounding water and the light level. Certainly, models more complex than the $\mu NP/(N + N_h)$ form can be built (e.g., Flynn, *et al.*20xx) and even incorporated into nutrient-phytoplankton-zooplankton models (Collins, 20xx). But we need to be sure of the goals: do we wish to understand phytoplankton better or to be able to predict some phenomenon such as red tide which may depend on both circulation and ecosystem dynamics? Building a model always requires thinking about the complexities of each sub-piece and attempting to balance how much we include or exclude: a phytoplankton model with lots of detail may not be helpful in a large-scale ecosystem model if other parts (e.g., grazing) are treated much more crudely.

We mentioned light above, and it is, of course, important since it provides the basic energy source for primary production and the subsequent secondary production in ocean ecosystems (with the exception of vent communities). But the distribution and absorption of light can also be a complex problem (c.f., Jerlov, 19xx) requiring treating different wavelengths separately. And the response of phytoplankton to light can depend on their history (photo-adaptation). In addition, ocean biology can feed-back upon the ocean physics by altering the amount of absorption and its distribution with depth, thereby affecting the heating in the upper waters. However, assuming an exponential depth distribution of light (constant absorption) and that μ depends on the light (perhaps with photo-inhibition at high intensities) is usually sufficient (again considering the issue of balance).

3.2.3 — Ratio-dependent

The previous forms have assumed that the specific growth rates $\frac{1}{b_i}\frac{\partial b_i}{\partial t}$ depend upon the resource concentration, either linearly in the Lotka-Volterra case, or nonlinearly. Thus, the more general form we might take in, for example, the zooplankton equation

$$\frac{1}{Z}\frac{\partial}{\partial t}Z = g(P, Z)$$

became

$$\frac{1}{Z}\frac{\partial}{\partial t}Z = g(P) \quad .$$

Arditi and Ginzburg (1989) have argued that, on the longer time scales appropriate for population reproduction and growth, limitations like those producing the logistic equation should apply: g should depend on the amount of resource available *per individual*

$$g = g(P/Z)$$

Examples include the logistic form

$$g(P, Z) = g_{max}\left(\frac{P/Z - r_0}{P/Z}\right)_+ = g_{max}\left(\frac{P - r_0 Z}{P}\right)_+$$

[with $F_+ = max(F, 0)$], a modified Ivlev form

$$g(P, Z) = \frac{g_{max}}{\nu}\left[1 - \exp(-\nu P/Z)\right]$$

or a hyperbolic or Michaelis-Menten form

$$g(P, Z) = g_{max}\frac{P/Z}{R_h + P/Z} = g_{max}\frac{P}{R_h Z + P} \text{ `.}$$

In general, we might expect some mixture of forms: when the zooplankton density is small so that they are not competing with each other directly, the standard Ivlev form $g(P)$ seems appropriate. As the animals begin to compete for resources, the ratio of the resource density to that of the animals becomes more relevant. One simple model for the interplay between these two effects considers randomly distributing N_P prey and N_Z predators in a volume. Each predator can forage a volume ν_0 in the time period t to $t + \delta t$. If the closest predator-prey pair is within the predator's foraging volume, the predator eats the prey and is satiated for that time period. After eliminating both of these organisms, the next closest pair is selected and tested. We repeat this until either all the prey are gone, all the predators have fed, or all remaining pairs are too far apart. We use the results from 100 random realizations to find the average number of prey consumed per unit time and per predator – an estimate of $g(P, Z)$. Figure 3.10 shows the Ivlev model, a ratio-dependent form, results from a 2D version of the simulation just described, and a mixed form

$$g(P, Z) = g_{max}\left[1 - e^{-\nu(Z)P}\right] \quad , \quad \nu(Z) = \frac{1}{Z}[1 - \exp(-\nu_0 Z)] \quad .$$

We construct the latter by computing the expected volume which is outside the range of all the randomly distributed predators. Just as $\exp(-\nu_0 P)$ gives the probability all prey are outside a foraging volume, $\exp(-\nu_0 Z)$ represents the probability that all predators are more than a foraging volume away from a randomly chosen point.† Thus the volume covered by all the predators is $\mathcal{V}[1-\exp(-\nu_0 Z)]$, and, when we partition this among the $Z\mathcal{V}$ predators, the expected volume each can cover (allowing for interference by others) is the $\nu(Z)$ above. Note that $\nu(Z)$ becomes $1/Z$ with less than 5% error for $\nu_0 Z > 2$, so the ratio form indeed applies at large densities (each zooplankton tending to have at least one competitor within its foraging volume).

The simulation at $Z = 2$ (in rather arbitrary units) shows noticeable deviation from the Ivlev form $1-\exp(-\nu(Z)P)$ no matter what choice is made for the value of $\nu(2)$. The feeding process described implies the grazing events are not independent; a P may be accessible to one Z but be grabbed by another, and having two P in one grazer's volume does not ensure both are safe, since the second one may be picked off by a different Z.

3.2.4 — Effects of using different forms

Different functional forms can give very different results. If, for example, we modify the QNPZ model (chapter 1) to have saturating responses

$$\begin{aligned}\frac{\partial}{\partial t}P &= \mu\frac{(N_T-P-Z)P}{N_h+N_T-P-Z} - \frac{g}{\nu}[1-\exp(-\nu P)]Z - d_p P \\ \frac{\partial}{\partial t}Z &= \frac{ag}{\nu}[1-\exp(-\nu P)]Z - d_z Z\end{aligned} \qquad MM/Iv$$

or ratio-dependent forms (in this example only in the predator equation; ratio dependence could also be applied in the nutrient equation)

$$\begin{aligned}\frac{\partial}{\partial t}P &= \mu\frac{(N_T-P-Z)P}{N_h+N_T-P-Z} - gZ[1-\exp(-P/Z)] - d_p P \\ \frac{\partial}{\partial t}Z &= \frac{ag}{\nu}Z[1-\exp(-\nu P/Z)] - d_z Z\end{aligned} \qquad MM/ratio$$

the equilibria and/or their stability properties can be quite different. Figures 3.11a-c show the equilibria and their stability as N_T varies. The phytoplankton and zooplankton biomass both increase as the total nitrogen increases for the ratio-dependent forms, whereas P becomes constant in the other two. For the MM/Iv form, Z also approaches a limit, and addition of nutrients only increases the pool of dissolved N. If we vary depth instead of N_T, we see similar pictures, with QNPZ and MM/Iv having fixed P values until nearly the bottom of the biotic region, while P/Z is fixed in the MM/ratio system, both decreasing to zero (see figure 3.12). The MM/Iv form has instabilitites for large N_T (or at intermediate depths) and develops a limit cycle. The MM/ratio system permits phytoplankton to grow deeper than the cutoff, but if any zooplankton are present, they will graze P down, and

† Thanks to Andrew Solow, WHOI, for clarifying this argument.

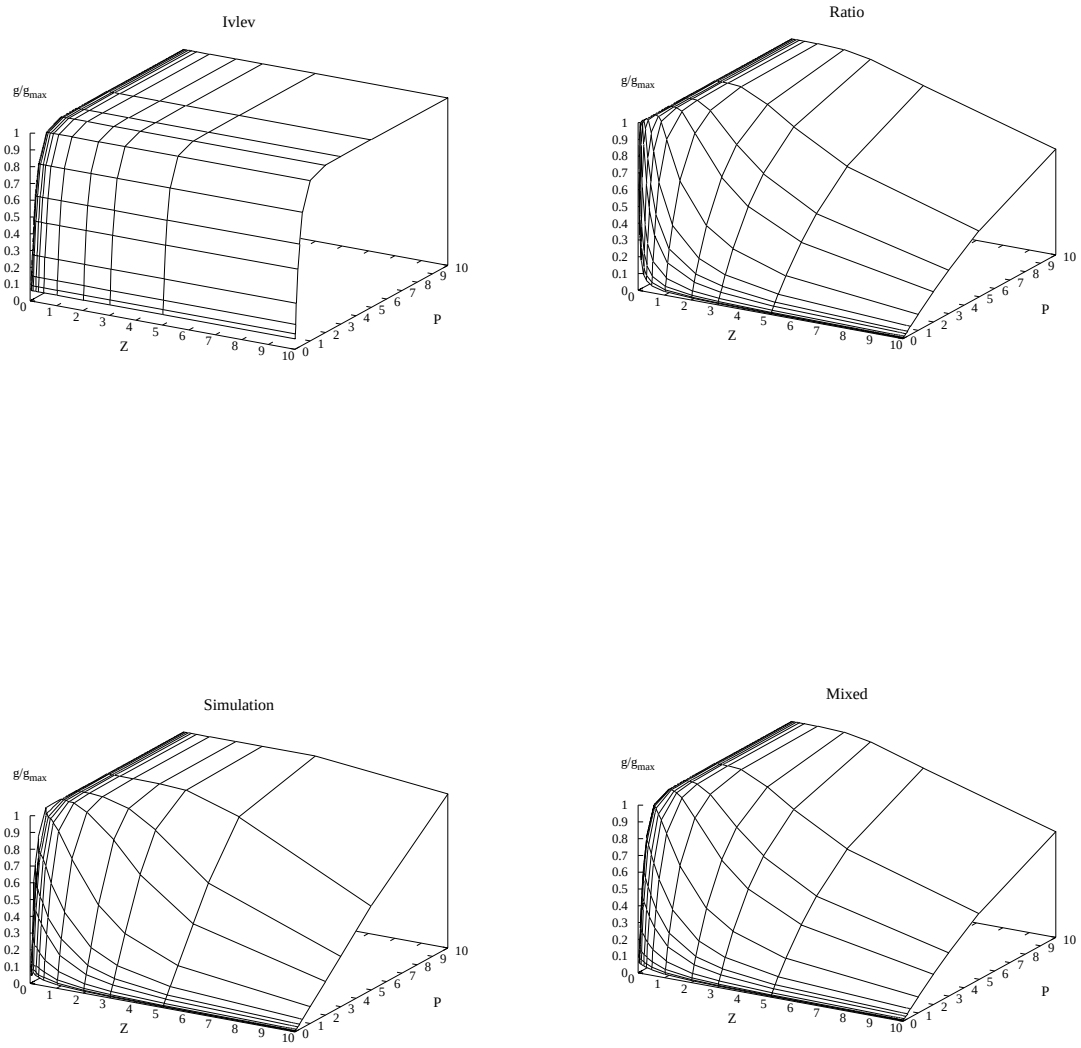

Figure 3.10: Examples of grazing rates vs. P and Z. Upper left shows $1 - \exp(-\pi P)$, upper right $1 - \exp(-P/Z)$, Lower left the simulation, and lower right $1 - \exp[-\nu(Z)P]$ with $\nu(Z) = \frac{1}{Z}[1 - \exp(-\pi Z)]$.

both will die out. In the P, Z plane, this corresponds to the origin being unstable along the $Z = 0$ axis and stable along a $P/Z = const.$ attracting line.

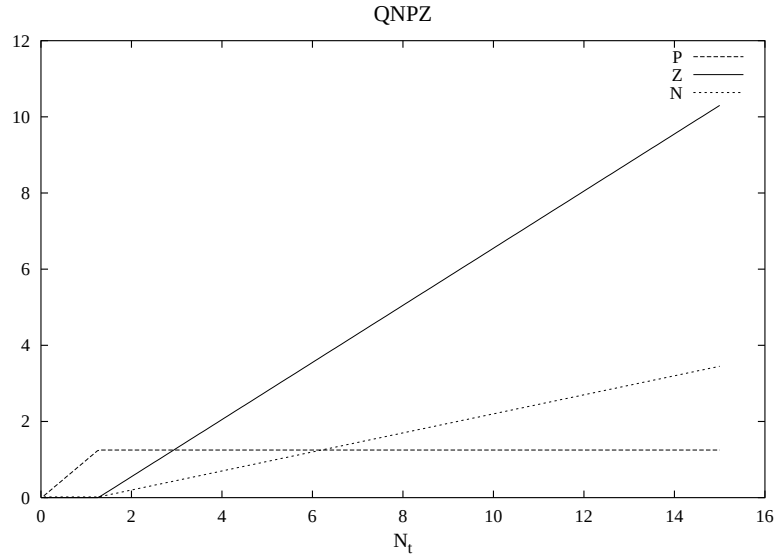

Figure 3.11a: Steady states for the QNPZ model. The growth rates for perturbations are always negative.

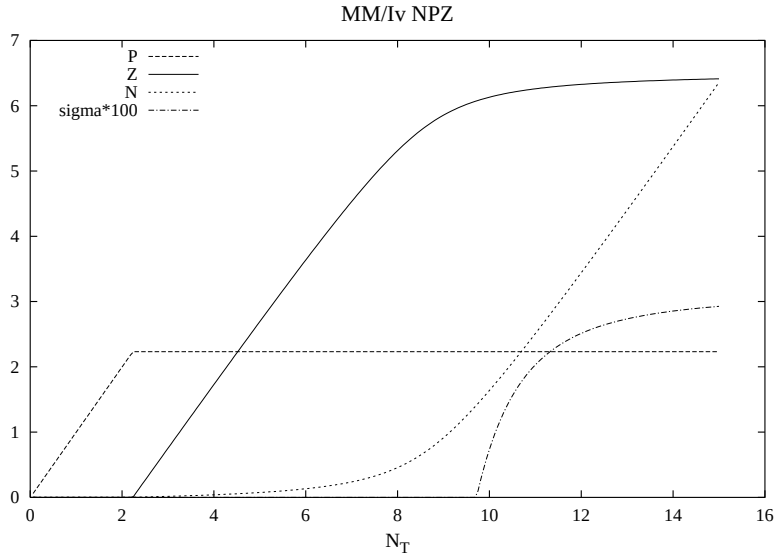

Figure 3.11b: Steady states for the NPZ model with MM/Iv functional forms. At high enough values of N_T, the equilibrium is unstable, and a limit cycle develops.

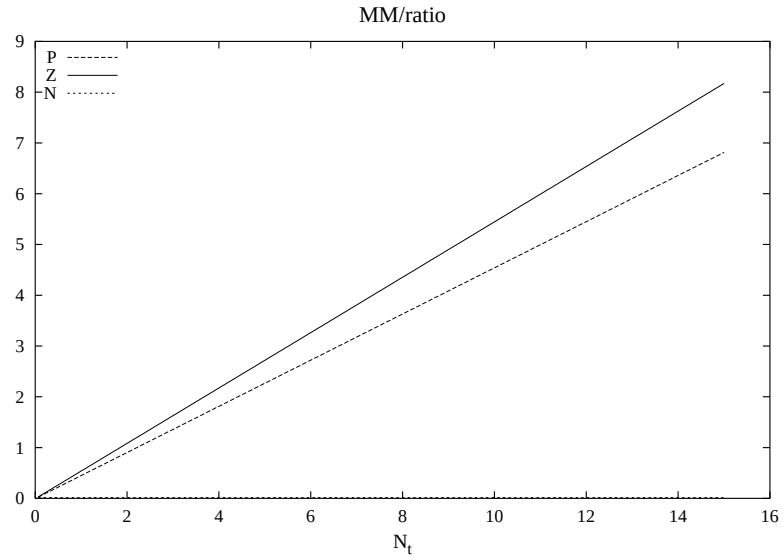

Figure 3.11c: Steady states for the MM/ratio model. The growth rates for perturbations are always negative.

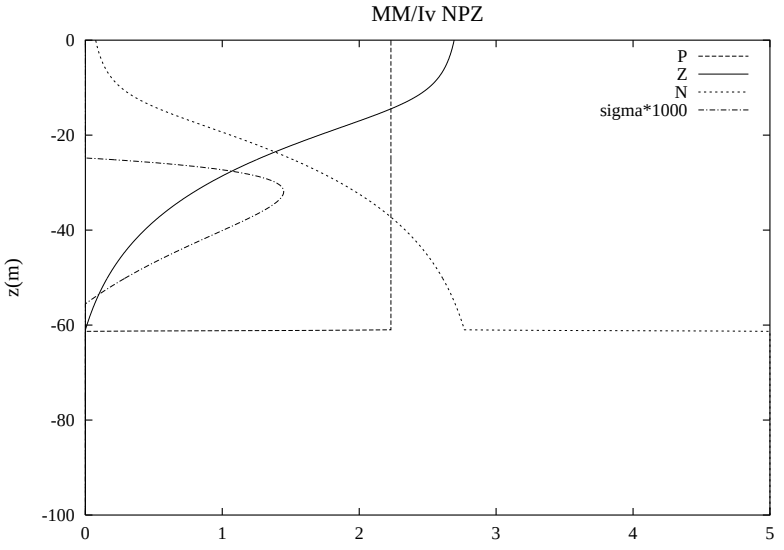

Figure 3.12a: Steady states for the NPZ model with MM/Iv functional forms. At intermediate depths, the equilibrium is unstable, and a limit cycle develops.

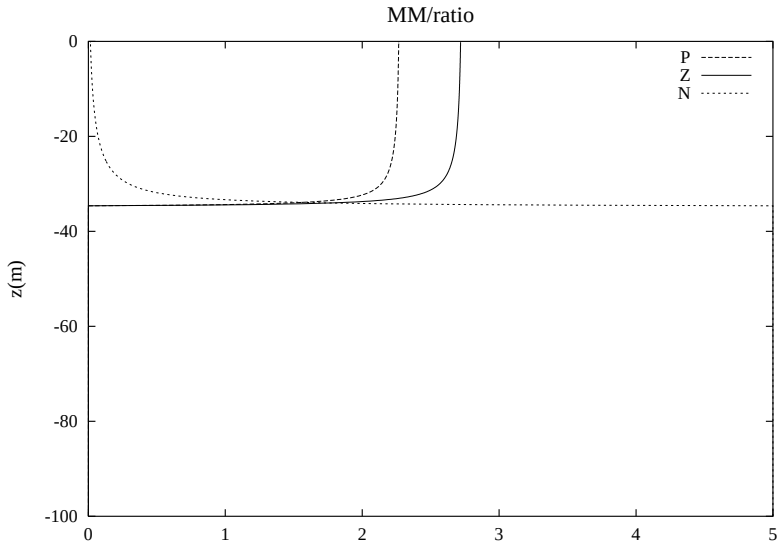

Figure 3.12b: Steady states for the MM/ratio model. These are stable.

For all the models above, except the MM/ratio form, P is constant when zooplankton can survive; such a result will hold whenever $\frac{1}{Z}\frac{\partial Z}{\partial t}$ depends only on P, not on Z. Conversely, introducing a nonlinear term in the Z equation, such as Henderson and Steele's (19xx) quadratic death rate $d_z Z^2$, will lead to P varying with N_T or μ. Indeed, with Lotka-Volterra grazing, the ratio $P/Z = d_z/ag$ becomes constant.

3.3 — Multiple components

Many models are built by linking different "compartments" usually using saturating forms like the ones above for the transfers. Conceptually, we are defining areas in size-species space and attempting to calculate the integrated biomass within the area. Transfers across the boundary are defined in terms of the net biomasses in different compartments; therein lies the simplication but also the difficulty: in general, we would expect grazing rates and uptake rates to depend on the distribution of biomass among the different types of organisms which have been lumped together in one compartment. The physical analogue — the box models used to study the overturning circulation (e.g., Stommel, 19xx) or climate (Marotzke, 19xx) — likewise try to determine the average temperature (or other properties) over a large volume of water. The averages $\langle T \rangle_i$ over different volumes are well-defined and change according to the fluxes through the boundaries of each volume; however, to obtain a closed set of equations for the averages, we again are forced to parameterize the fluxes as functions of these global properties despite the fact that the transport really depends on the local gradients and flow at the boundaries. Despite the caveats, compartment models are and will remain a reasonable compromise between complexity and inclusion of significant aspects of ecosystem dynamics.

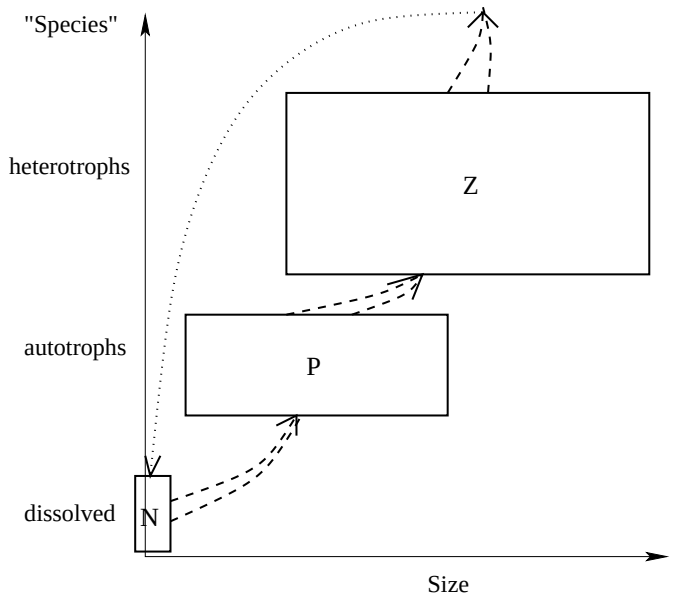

Figure 3.13: Sketch of the simplification involved in a compartment model.

As we learn more about particular groups, we may split compartments into, for example, $P_{diatoms}$, $P_{cyanobacteria}$, and $P_{dinoflagellates}$; furthermore, we can modify the functional forms to represent their preference for nitrate vs. ammonium, their need for silica, etc. We can often characterize this kind of model by a flow diagram such as those in figure 3.14 with arrows between the compartments showing the flow of nitrogen.

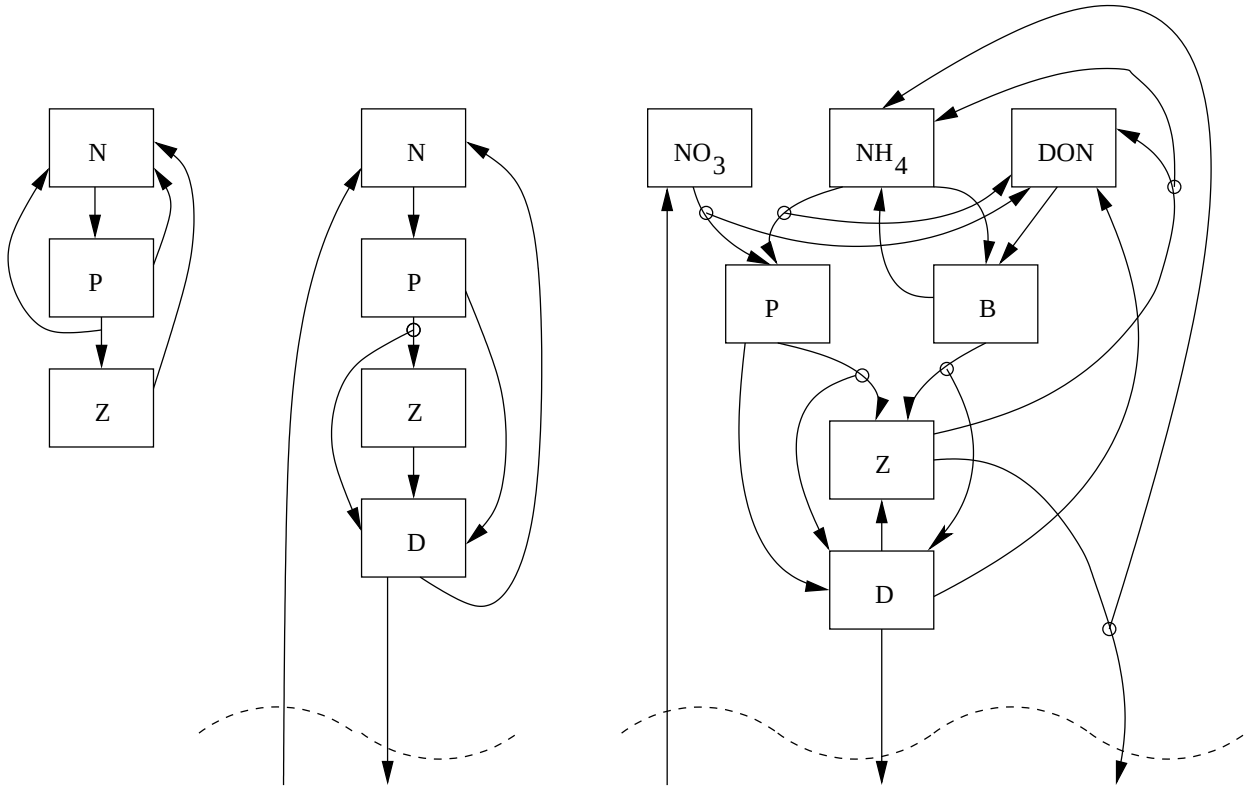

Figure 3.14: Diagrams of biological models. On the left is the Nutrient-Phytoplankton-Zooplankton model like that in Chapter 1. In the middle case we add a Detritus compartment. The arrows crossing the dashed, wavy line indicate the system is *open* and loses/ gains nitrogen from the deep water. On the right is the Fasham, Ducklow, McKelvie model for three kinds of nitrogen, phytoplankton, bacteria, zooplankton, and detritus. The arrows beginning from small circles indicate a fraction of the flux is diverted (e.g., by excretion or failure to assimilate) to another compartment.

Model complexity grows both as the number of compartments increases and as the functions used to describe the interactions have more parameters controlling their shape. Boxes can be added or removed and different connections or functional forms can be tried, depending on the kinds of information and measurements available and the modeller's goals. Some features can be qualitatively robust to changes in the model; for example, all three of these may exhibit a spring bloom given light and mixed-layer depth changes.

Figure 3.14 illustrates another aspect of biological models: many are **open** in the sense that the currency is presumed to leave the region being considered (e.g., the surface ocean) and to be supplied externally. The overall level – the sum total in all the compartments – is set eventually by these import/export processes. Models can also be **closed** (such as the NPZ model in the diagram) so that the totals are set *ab initio*. The distinction carries over when flow, mixing, and movement are included, but in the sense of integrated over the domain. Open systems have exchanges with the atmosphere or the sediments.

Given the choice of compartments b_1, b_2, b_3 ...(which we collect into a biological "vector" $\mathbf{b}$), the functional forms for the exchanges, and the values of the parameters required, we have a fully-specified set of biological equations

$$\frac{\partial}{\partial t} b_i = \mathcal{B}_i(\mathbf{b}, \mathbf{x}, t) \quad . \tag{3.13}$$

Adding the physics and biological movements gives

$$\frac{\partial}{\partial t} b_i + \nabla \cdot (\mathbf{u} b_i + \mathbf{u}_{bio\,i} b_i) - \nabla \kappa \nabla b_i - \nabla \kappa_{bio\,i} \nabla b_i = \mathcal{B}_i(\mathbf{b}, \mathbf{x}, t) \quad . \tag{3.14}$$

3.3.1 — Mathematical Analysis of Biological Models

All too often, once a model has been put together, the builders try to get "realistic" behavior by:

- Adjusting the parameters which are not well known. As discussed above the rates in patchy enviroments and stochastic conditions may differ from those measured in a well-mixed container on shipboard or in the lab. In addition, of course, variables like P collect many disparate species so that the rates of uptake can be very different depending on which species is dominant. Other properties, such as grazing, are very difficult to quantify directly. Given these kinds of concerns, use of empirical values rather than attempting to derive them from first principles seems justified.
- Sensitivity experiments may be conducted to determine how solutions are altered when some of the parameters are altered.

However, after specifying a model, we can gain a great deal of insight into its behavior by studying various mathematical properties of the dynamical system:

- What do the steady states (or equilibria – values of $\mathbf{b}$ such that $\frac{d}{dt}\mathbf{b} = 0$) look like? For the dynamical system
$$\frac{\partial}{\partial t} b_i = \mathcal{B}_i(\mathbf{b}, \mathbf{x}, t)$$
we can have steady solutions if the reaction terms do not have explicit time-dependence. In that case, all of the $\mathcal{B}_i(\mathbf{b}, \mathbf{x})$ can vanish for one or more sets of values of the fields, $\mathbf{b} = \overline{\mathbf{b}}(\mathbf{x})$.
- Are the equilibrium points stable or unstable? As shown in chapter 1, small amplitude perturbations evolve according to
$$\frac{\partial}{\partial t} b'_i = \left(\frac{\partial \mathcal{B}_i}{\partial b_j} \right) \Big|_{\overline{b}} b'_j \equiv \mathcal{B}_{ij} b'_j \quad .$$
If $\mathcal{B}_{ij}$ has any eigenvalues with a positive real part, the equilibrium will be unstable. if all eigenvalues have negative real parts, it will be stable.
- Even if stable, does the system respond to perturbations by making large excursions before settling back to the equilibrium? Neubert and Caswell(1987) discuss a number of measures for this property, of which
$$\max \frac{|\mathbf{b}'(t)|}{|\mathbf{b}'(0)|}$$
is perhaps the best measure, but the most difficult to evaluate. The time at which the maximum excursion appears is also significant relative to the time scales of the forcing. For the linear problem, this becomes
$$\text{amp} = \max_t \, || \exp(\mathcal{B}_{ij} t) || \tag{3.15}$$
(using the matrix exponential and the matrix norm). These ideas carry over to nonlinear dynamics, but the amplification factor will generally be computed by simulations and will depend on the size of the initial perturbation.

- Are there cyclic solutions (known as limit cycles), and do solutions approach these or diverge from them?
- Is there an "attractor," meaning that the solution resides mostly in a subspace of the full region? For example, the seven-dimensional system in figure 3.14, if closed, can be reduced by one order using conservation of N_T but may, in fact, occupy either a zero-dimensional point or a one-dimensional curve. The last statement does not mean that only one of the variables changes with time; rather, it means that many solutions started in a four-dimensional region end up on a curve $\mathbf{b}_{lc}(s)$ parameterized by a single along-curve distance (or time) s. See figure 3.18 below.

NPZ

As an example, we consider a refined NPZ model (figure 3.14) using Michaelis-Menten uptake of nutrients and Ivlev grazing, but also including the kinds of sources and sinks that can arise from transfer across the base of the mixed layer (making it an open model):

$$\frac{\partial}{\partial t}\begin{pmatrix} N \\ P \\ Z \end{pmatrix} = \begin{pmatrix} -\text{uptake by P} + \text{unassimilated grazing} + \text{dead P\&Z} + \text{mixing gain/loss} \\ \text{uptake by P} - \text{grazing by Z} - \text{death} - \text{mixing loss} \\ \text{grazing/assimilation} - \text{death} - \text{mixing loss} \end{pmatrix}$$

or, expressed mathematically,

$$\begin{aligned} \frac{\partial}{\partial t}N &= -\overline{\mu}\frac{NP}{N+N_h} + \frac{e_Z(1-a)g}{\nu}Z[1-e^{-\nu P}] + r_P d_p P + r_Z d_z Z + k(N_{deep}-N) \\ \frac{\partial}{\partial t}P &= \overline{\mu}\frac{NP}{N+N_h} - \frac{g}{\nu}Z[1-e^{-\nu P}] - d_p P - kP \qquad (NPZ) \\ \frac{\partial}{\partial t}Z &= \frac{ag}{\nu}Z[1-e^{-\nu P}] - d_z Z - kZ \quad . \end{aligned}$$

We have used the common approach of assuming the fields are well-mixed and averaging over the mixed-layer depth h, so that $\overline{\mu} = \frac{1}{h}\int_{-h}^{0}\mu(z)$ (see Appendix 3.xx for a simple physical model). In this form, the r_P and r_Z give the regenerated fraction of the dead phytoplankton and zooplankton (although one could also consider the d_z term as including excretion of nitrogen in the form of ammonium). The constant e_Z is the fraction of unassimilated phytoplankton which goes back to nutrients rather than being lost as sinking fragments. The parameter k gives the rate at which the mixed layer values are restored to the deep values (assuming no organisms live below the layer). As pointed out in Appendix 3.xx, such a representation may be adequate when the mixed-layer is deepening, but is more questionable otherwise. Some models assume that the mixing acts differently on the phytoplankton and the more active zooplankton.

ANALYSIS:

The results from the closed system $r_P = r_Z = e_Z = 1$, $k = 0$ were presented above in figures 3.11b and 3.12a. If $k \neq 0$, we can still sum the equations to find

$$\frac{\partial}{\partial t}(N + P + Z) = kN_{deep} - k(N + P + Z) \quad .$$

Thus, the total nitrogen in the mixed layer becomes the same as the deep value, and the system again has two degrees of freedom. The k simply serves to increase the effective death rates to $d_p + k$ and $d_z + k$.

Although we recover the QNPZ model in the limit $N << N_h$, $\nu P << 1$, the closed model can display qualitatively different behavior. A model with two degrees of freeom can only have fixed points and/or limit cycles. This result follows from the fact that trajectories in the (P, Z) plane cannot cross since the "velocity" vector ($\frac{\partial P}{\partial t}$, $\frac{\partial Z}{\partial t}$) has a unique value at each point in the phase plane (given $N = N_T - P_Z$).

Stability of an equilibrium is determined by the eigenvalues of

$$\mathcal{B}_{ij} = \begin{pmatrix} \frac{\partial \mathcal{P}}{\partial P} - \frac{\partial \mathcal{P}}{\partial N} & \frac{\partial \mathcal{P}}{\partial Z} - \frac{\partial \mathcal{P}}{\partial N} \\ \frac{\partial \mathcal{Z}}{\partial P} & \frac{\partial \mathcal{Z}}{\partial Z} \end{pmatrix}$$

$$= \begin{pmatrix} \overline{\mu}\frac{N}{N+N_h} - \overline{\mu}\frac{N_h P}{(N+N_h)^2} - gZe^{-\nu P} - d_p - k & -\frac{g}{\nu}[1 - e^{-\nu P}] - \overline{\mu}\frac{N_h P}{(N+N_h)^2} \\ agZe^{-\nu P} & \frac{ag}{\nu}[1 - e^{-\nu P}] - d_z - k \end{pmatrix} \quad .$$

The 2×2 case is particularly simple: the eigenvalues are given by

$$\sigma^2 - \sigma \mathrm{Tr}(\mathcal{B}_{ij}) + \mathrm{Det}(\mathcal{B}_{ij}) = 0$$

where the trace, $\mathrm{Tr}(\mathcal{B}_{ij}) = \mathcal{B}_{ii}$ is the sum of the diagonal elements and $\mathrm{Det}(\mathcal{B}_{ij})$ is the determinant $\mathcal{B}_{11}\mathcal{B}_{22} - \mathcal{B}_{12}\mathcal{B}_{21}$. The growth rate $\Re(\sigma)$ will be positive if the trace is positive or the determinant is negative.

We now list the three potential equilibrium states and their properties.

Equilibrium	$\mathcal{B}_{ij}$	Stability condition
$P = Z = 0,\ N = N_T$	$\begin{pmatrix} \overline{\mu}\frac{N}{N+N_h} - d_p - k & 0 \\ 0 & -d_z - k \end{pmatrix}$	Det< 0
' $Z = 0,\ P > 0$	$\begin{pmatrix} -\overline{\mu}\frac{N_h P}{(N+N_h)^2} & -\frac{g}{\nu}[1 - e^{-\nu P}] - \overline{\mu}\frac{N_h P}{(N+N_h)^2} \\ 0 & \frac{ag}{\nu}[1 - e^{-\nu P}] - d_z - k \end{pmatrix}$	Det< 0
$P > 0,\ Z > 0$	$\begin{pmatrix} \frac{d_z+k}{a}\frac{Z}{P} - \overline{\mu}\frac{N_h P}{(N+N_h)^2} - gZe^{-\nu P} & -\frac{d_z+k}{a} - \overline{\mu}\frac{N_h P}{(N+N_h)^2} \\ agZe^{-\nu P} & 0 \end{pmatrix}$	Tr> 0

As in the QNPZ case, increasing N_T or $\overline{\mu}$ leads to succesive bifurcations, first to a state with finite phytoplankton biomass (when $\overline{\mu}\frac{N}{N+N_h} > d_p + k$) and then to states where

zooplankton can survive ($\frac{ag}{\nu}[1 - e^{-\nu P}] > d_z + k$). Here, however, we can have a third bifurcation to predator-prey oscillations when $\mathcal{B}_{11} > 0$.

Note that $\mathcal{B}_{22} = 0$ when the equilibrium has non-zero Z; such a result applies for many models: when

$$\frac{\partial}{\partial t} b_i = b_i B_i(\mathbf{b}, \mathbf{x}, t)$$

and B_i depends only on the other variables in the system – the per-capita biological rates for these organisms are independent of their density – then $\mathcal{B}_{ii}$ will be zero. Intuitions drawn from tracers for which perturbations decay directly (meaning diagonally dominant $\mathcal{B}_{ij}$) will not work. For example, consider perturbations of the equilibrium by physical flows (as discussed in Chapter 1)

$$\frac{\partial}{\partial t} b_i' = \mathcal{B}_i(\overline{\mathbf{b}} + \mathbf{b}') - \mathcal{B}_i(\overline{\mathbf{b}}) - \mathbf{u} \cdot \nabla(\overline{b}_i + b_i') \simeq \mathcal{B}_{ij} b_j' - \mathbf{u} \cdot \nabla \overline{b}_i \quad .$$

Advection of high $b_2 = Z$ into a region (e.g., $-\mathbf{u} \cdot \nabla \overline{Z} > 0$) will not be offset directly by increasing zooplankton population (as would occur for the logistic model), but must be balanced by changes in the other fields (reduced phytoplankton concentration $P' < 0$ in the NPZ example).

The amplification factor (eqn. 3.12) shows an increase from around 1.4 as the depth increases (interrupted by the unstable range) and peaks where Z drops out, with amplifications of about 330. It drops back to 1 (meaning purely decaying solutions) below the biotic zone. Thus the region near the base of the biotic zone is the most sensitive to perturbations, and, in addition, the time scales for the growth and decay are order years, so that anomalies can be very persistent. The QNPZ model has a similar response (especially noticeable when we squeeze the vertical scale by a factor of 1.5), without the gap for an unstable equilibrium and with much less sensitivity in the deep water. The ratio-dependent model, however, is much less sensitive to perturbations (except for a spike below the biotic zone), and the sensitivity decreases rather than increases with depth. Again, we see that changes in the functional forms can significantly alter the dynamics.

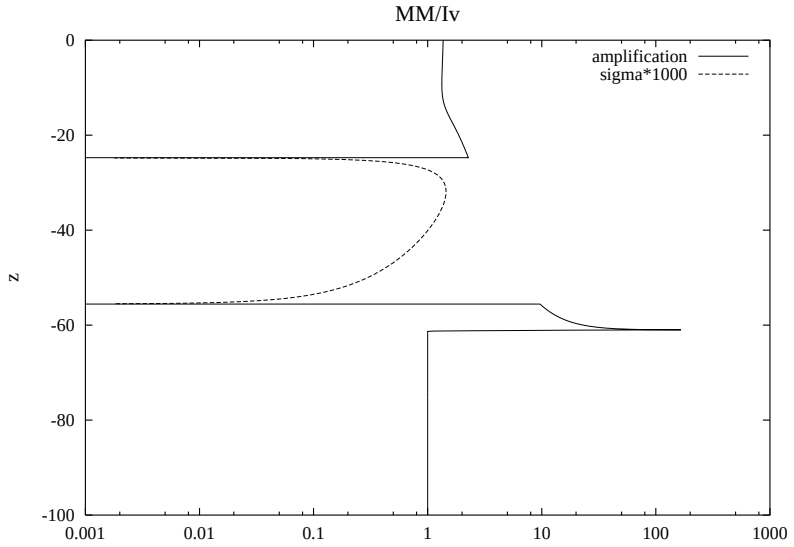

Figure 3.15a: Amplification factors and growth rates for the NPZ model with MM/Iv functional forms.

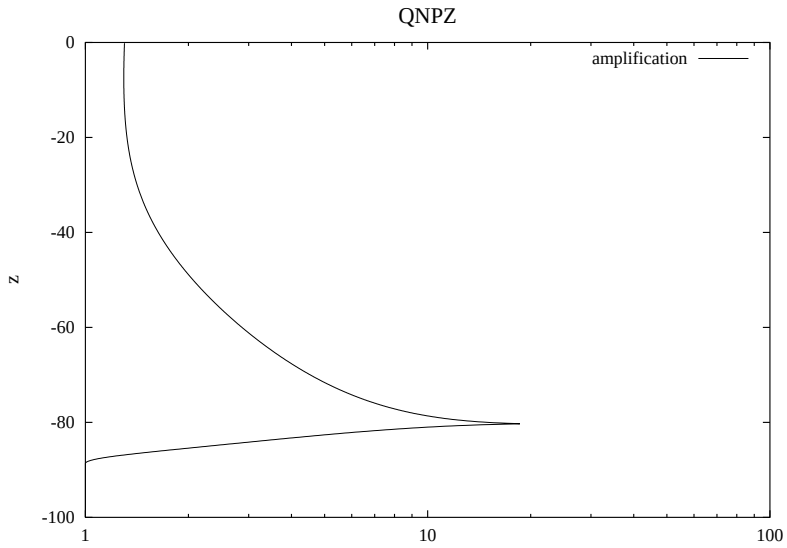

Figure 3.15b: Amplification factors for the QNPZ model vs. depth.

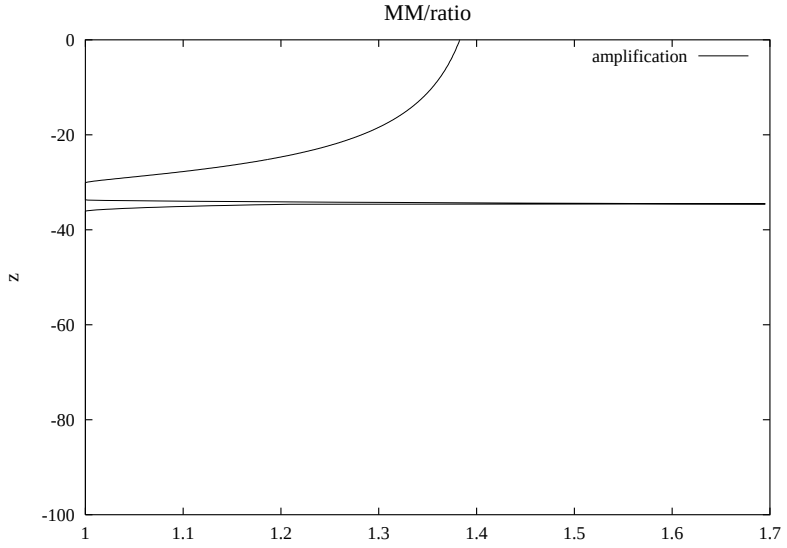

Figure 3.15c: Amplification factors for the MM/ratio model. Note the linear scale here.

The open system is more difficult to analyze, since it has more parameters. If a fraction of dead or unassimilated grazing is directly lost from the mixed layer, the response is similar to the model including detritus discussed next.

NPZD

If we add a detrital box which collects dead plankton and unassimilated grazing (figure 3.14), our model becomes

$$\begin{aligned}
\frac{\partial}{\partial t}N &= -\overline{\mu}\frac{NP}{N+N_h} + \frac{e_Z(1-a)g}{\nu}Z[1-e^{-\nu P}] + rD + k(N_{deep}-N) \\
\frac{\partial}{\partial t}P &= \overline{\mu}\frac{NP}{N+N_h} - \frac{g}{\nu}Z[1-e^{-\nu P}] - d_pP - kP \qquad (NPZD) \\
\frac{\partial}{\partial t}Z &= \frac{ag}{\nu}Z[1-e^{-\nu P}] - d_zZ - kZ \\
\frac{\partial}{\partial t}D &= d_pP + d_zZ + \frac{(1-e_Z)(1-a)g}{\nu}Z[1-e^{-\nu P}] - rD - kD - \frac{w_D}{h}D
\end{aligned}$$

with r giving the rate at which usable nutrient is regenerated from detrital material and w_D the sinking rate.

The number of parameters is becoming large enough that exploration of the full parameter regime is difficult. We show one example, altering the sinking rate, in figure 3.16; this strongly suggests that there are two regimes, one for slow sinking (having limit cycles) and a second (having steady solutions) which applies for rapid sinking. We can analyze both limits fairly easily.

With slow sinking, the mixing makes the total nitrogen value in the upper layer equal to N_{deep}; we can find the equilibrium state for $w_D = 0$ easily. We find the value of P from $\frac{1}{Z}\frac{\partial Z}{\partial t} = 0$, use $D = N_{deep} - P - Z - N$ in $\frac{\partial D}{\partial t} = 0$ to get a linear relation between Z and N, and substitute these into the $\frac{\partial P}{\partial z} = 0$ to derive a quadratic expression for N. Then, we can show that this equilibrium (as well as the trivial ones with $Z = 0$ or $Z = P = 0$) is unstable. A truncated model in the spirit of Hopf bifurcation analysis (Appendix 3.xx) can give an estimate of the amplitude and structure of the limit cycle; however, solving numerically is straightforward.

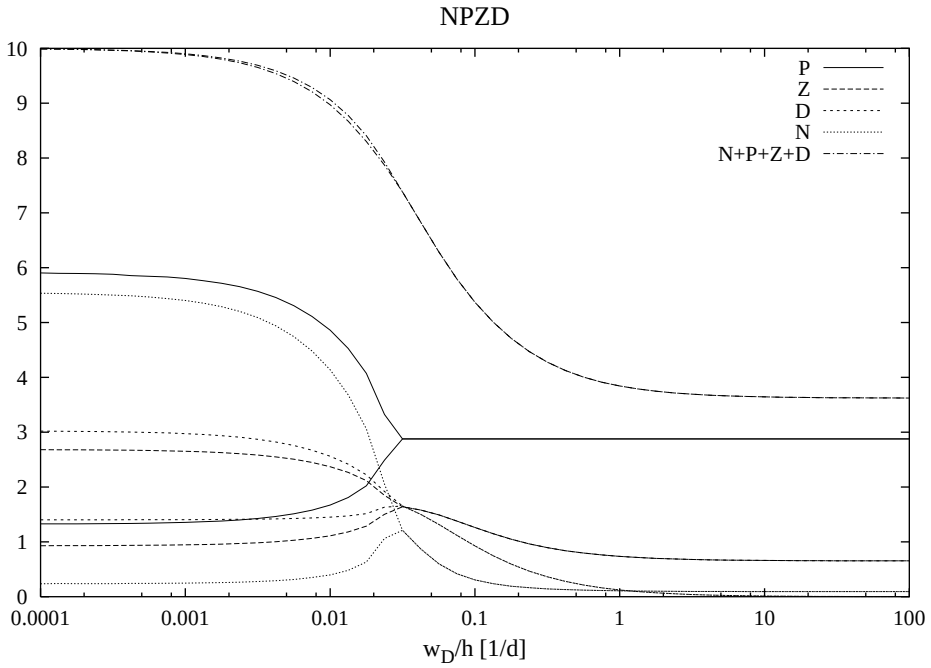

Figure 3.16: Effects of varying the sinking velocity in the NPZD model. The maximim and minimum values of the variables over times 4800-5000 d are plotted; when these are the same the system has settled to a steady state. Parameter values are in table 3.xx

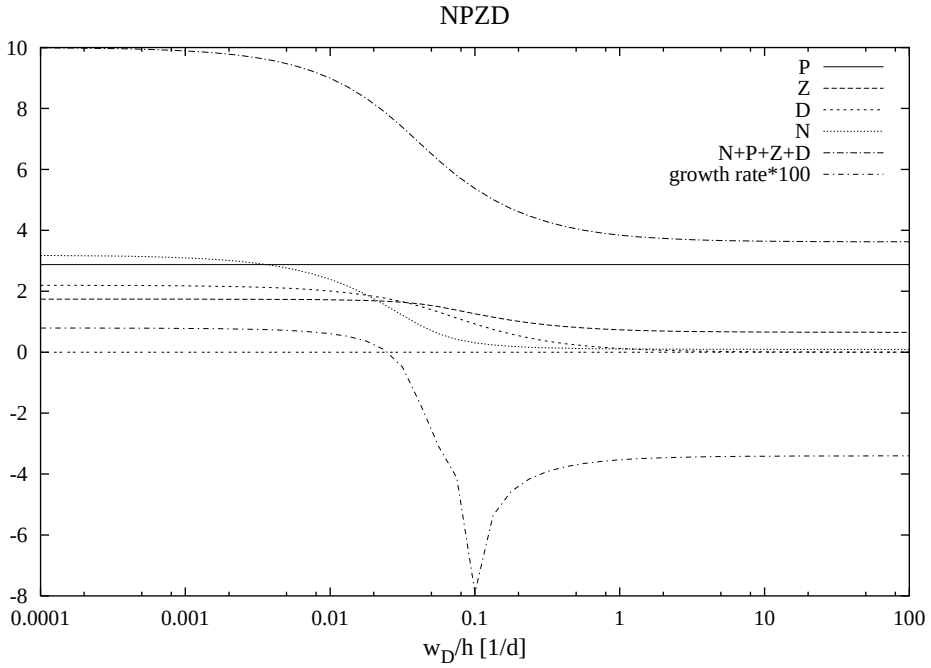

Figure 3.17: Steady equilibrium states and growth rates $[1/d]$ of perturbations.

The case of rapid sinking is easier to analyze: the detritus sinks out so quickly that $D \simeq 0$ in the mixed layer. The NPZD system reduces to the open NPZ system with

$r_P = r_Z = 0$. For $w_D/h = 100\ d^{-1}$, the steady state solutions agree to better than 0.2%. Thus the four-dimensional model behaves like a lower order system. Indeed, we can see a similar reduction in order even in the small sinking rate case: if we look at the trajectories, we see that a cloud of initial conditions rapidly condenses onto a two-dimensional surface and then moves to a 1-D manifold, the limit cycle (Figure 3.18). Even if we allow the parameters to vary slowly, the system may reside in a lower-dimensional space. Later, we shall come back to ways to exploit this kind of behavior and simplify a model.

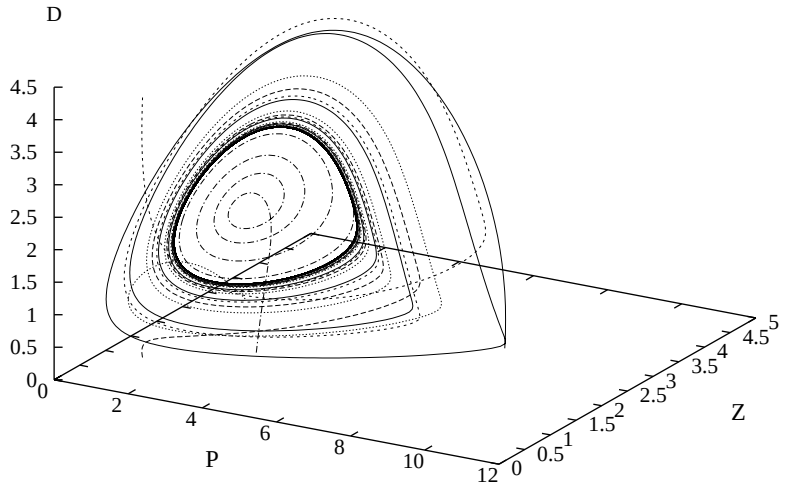

Figure 3.18: Trajectories in P, Z, D space, showing a rapid movement onto a 2-D surface and then slower spiraling towards a 1-D limit cycle. $w_D/h = 0.001\ d^{-1}$

3.4 — Multiple resources

In the next examples, we consider cases in which the organisms deal with multiple resources. A required nutrient may be obtained from several different sources and/or the biochemical processes may need various elements in differing proportions (and substitutions may or may not be allowed). For example, the phytoplankton growth equation may look more like

$$\frac{1}{P}\frac{\partial}{\partial t}P = \sum_j g_j(N_1, N_2, N_3, \ldots) - grazing - cell\ senescence$$

with the j^{th} nutrient being depleted at a rate $g_j P$. Example forms for g_j include:

1) independent: $g_j = \mu_j N_j/(N_{h,j} + N_j)$. Each nutrient is incorporated according to its own MM law and the sum of the intake provides the growth.
2) indiscriminate: $g_j = \mu a_j N_j/(N_h + \sum a_j N_j)$. The organism simply regards the usable nutrient as a weighted sum of that in all the possible sources and takes them up in proportion. The a_j factors give the preference for each particular nutrient, but do not

represent switching behavior. The ratio of the uptake of N_1 to N_2 is proportional to the ratio of the concentrations.

3) preferred: $g_j = a_j N_j^2/(N_h \sum a_k N_k + \sum a_k N_k^2)$. When the second nutrient is low, the organism uses the first with a normal MM form. When the second nutrient has a larger value, the uptake of the first is significantly reduced. In this case the ratio of the uptake rates grows as N_1^2/N_2^2, dominated by the one which is more available.
4) switching: $g = max(\mu_j N_j/[N_{h,j} + N_j])$. A more extreme form of preference, in which the uptake of the first will stop completely when the second gives more benefit.
5) inhibiting: $g_1 = \mu_1 N_1 \exp(-a_1 N_2)/(N_{h,1} + N_1)$. This case applies to nitrogen utilization by phytoplankton: the organisms can use nitrate (N_1) much more easily than ammonium (N_2), but the presence of the latter decreases their ability to take up nitrate (xx, 19xx). The uptake of ammonium proceeds according to the standard MM form.
6) limiting: $g = \mu\ min(N_j/[N_{h,j} + N_j])$. With this form, two nutrients or resources are simultaneously limiting when $N_1/N_2 = N_{h,1}/N_{h,2}$; in the case of nitrogen and phosphorus, for example, we can regard this as the Redfield ratio R_{NO_3/PO_4}. We would expect the nutrients to be removed in the same ratio, so that the optimal uptake rates μ_j in

$$\frac{\partial}{\partial t} N_i = -\mu_i\ min \frac{N_j}{N_j + N_{h,j}} + \ldots$$

would satisfy $\mu_1/\mu_2 = N_{h,1}/N_{h,2}$. When N_1 is limiting, the uptake of N_2 will be that required to maintain the Redfield ratio and will be less than that predicted by the MM form $\mu_2 N_2/(N_2 + N_{h,2})$. Recent models which explicitly include the internal stores of nutrients (discussed below) give a more detailed picture of nutrient limitation and Redfield ratios.

Figure 3.19 shows the partitioning of the resource utilization between two resources as a function of the ratio of N_1 to the total $N_1 + N_2$ according to the schemes outlined above. We've assumed a_1, μ_1 are 0.25 and a_2, μ_2 are 0.75.

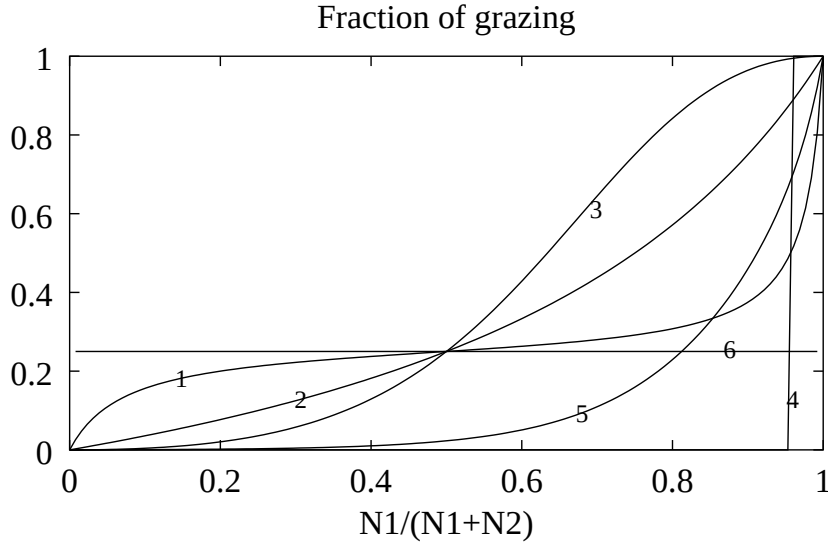

Figure 3.19: Ratio of the uptake rate of N_1 versus the total uptake rate as a function of the ratio of resource density

NNPZ

For nitrogen-based models, we should incorporate the fact that nitrogen within the water appears in a number of forms: "fixed nitrogen" (nitrite, nitrate, ammonium) which phytoplankton can use, dissolved gas which must be converted by nitrogen fixers, and particulate or dissolved organic nitrogen which can be processed by bacteria.

McGillicuddy *et al.*(19xx) dealt with nitrate and ammonium, with the former being supplied from below by physical processes, while the latter increases by excretion and regeneration of dead microzooplankton (the organisms represented by Z).

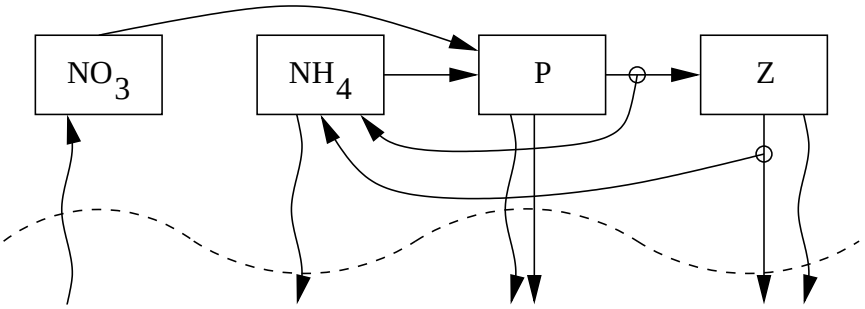

Figure 3.20: NNPZ model. The solid arrows descending from the P and Z compartments indicate sinking of particulate organic nitrogen.

Phytoplankton prefer nitrate, but the presence of ammonium inhibits their ability to use nitrate. The resulting form for nutrient uptake

$$\frac{D}{Dt}P = \mu_{max}\left(1 - e^{-I/I_1}\right)e^{-I/I_2}\left[\frac{NO_3\, e^{-k_n NH_4}}{NO_{3,h} + NO_3} + \frac{NH_4}{NH_{4,h} + NH_4}\right] - \dots$$

includes a sensitivity to light intensity I such that the uptake rate approaches a saturation value μ_{max} and then falls off again when the light becomes too strong. (However, McGillicuddy *et al.*, 19xx, conclude that light inhibition is not a factor in the JGOFS region they are simulating.)

NNNPBZD

The Fasham, Ducklow, and McKelvie (19xx) model (figure 3.14) adds dissolved organic nitrogen and detritus (PON) and includes explicitly the bacterial component.

NPZFe

More Complex Models

4.1 — Size-spectrum models

The models so far have split the species-size space by collecting species into functional groups (plants, herbivores, predators,...) and ignoring size information. Various researchers have treated small and large zooplankton separately (e.g., xxx); rather than explore that route here, we shall now look at models which treat a full spectrum of sizes. Moloney and Fields(19xx) developed a PZ model based on logarithmic size classes, and Armstrong(19zxx) analyzed the steady state behavior in more detail. Like the ratio-dependent forms, his model allows both the phytoplankton and zooplankton biomasses to increase as the total nitrogen increases; however, the net population growth arises because the food chains of larger and larger sized organisms come into play. We shall discuss both discrete and continuum versions of size-spectrum models here.

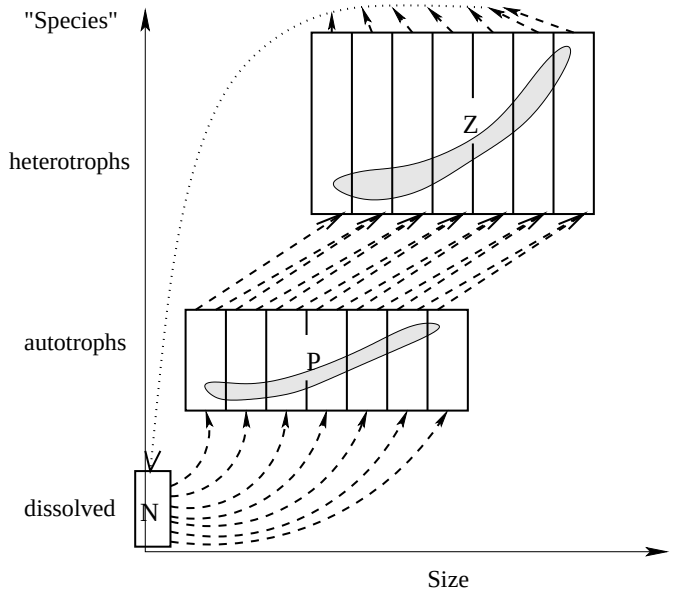

Figure 4.1: Sketch of the a size-spectrum model. Multiple arrows indicate heterotrophs in one size class may feed on several classes of autotrophs.

4.1.1 — Model formulation

Logarithmic size classes are commonly used to allow spanning a wide range of lengths or weights. If we take the weight W (in nitrogen units) as our underlying variable, then $\omega = \ln(W/W_0)$ will be our coordinate, with W_0 the size of the smallest autotroph. At times, we shall discuss the "length" L taken to be the equivalent spherical radius $\rho_0 \frac{4\pi}{3} L^3 = W$. The variable P_j measures the biomass in the log-size class $\omega = j\Delta$ to $\omega = (j+1)\Delta$ where Δ is the logarithmic width of each class. The center of the j^{th} class is at $\omega = (j + \frac{1}{2})\Delta$. For the heterotrophs, the smallest class will be ω_Z, and Z_j represents the biomass with log-size centered at $\omega_Z + (j + \frac{1}{2})\Delta$. The smallest classes of P and Z may be photosynthesizing bacteria (e.g., *prochlorococcus*) and protozoans, repectively; however,

we shall use "phytoplankton" ("PP") and "zooplankton" ("ZP") as shorthand names for the two groups.

Let us begin by defining the food available for the ZP in size class i:

$$F_i = p_{ij} P_j \tag{4.1}$$

where p_{ij} expresses the range of PP which will be grazed (non-zero values) and the preference or ability to forage for different-sized prey. We shall make a number of assumptions about the structure of the matrix p_{ij}: (1) the entries represent relative preferences so that $\sum_j p_{ij} = 1$, (2) the ZP of size $\omega_Z + j\Delta$ can only ingest prey of size $j\Delta$ and smaller ($p_{ij} = 0$ for $j > i$), and (3) the preferences or foraging abilities are fixed, independent of whether there is prey in a particular size class or not. For example, if the food available for Z_2 is $(P_0 + P_1 + P_2)/3$, it will remain so even if $P_1 = 0$, not switch to $(P_0 + P_2)/2$. These assumptions interact with the presumption that there is a minimum weight, W_0, in subtle ways; alterations in them may have unexpected effects on the system.

The grazing rate will be taken to be a saturating function of the available food

$$g_i \frac{F_i}{1 + F_i/C_i}$$

so that the rate of removal of PP in class j by ZP in size i is

$$g_i \frac{F_i}{1 + F_i/C_i} \frac{P_j}{F_i} = g_i \frac{P_j}{1 + F_i/C_i} \quad .$$

We choose the Monod form, rather than the Ivlev version, because it makes the equation above slightly simpler. Of the grazed food, a fraction a_i is assimilated (although we could use a_{ij} if the ZP assimilate different prey differently). Our equation for Z_i becomes

$$\frac{\partial}{\partial t} Z_i = Z_i \left[a_i g_i \frac{F_i}{1 + F_i/C_i} - d_{Zi} \right] \tag{4.2}$$

and the PP equation is

$$\frac{\partial}{\partial t} P_i = P_i \left[\mu_i \frac{N}{N_{h,i} + N} - \frac{g_j p_{ji} Z_j}{1 + F_j/C_j} - d_{Pi} \right] \quad . \tag{4.3}$$

The continuum equations follow by replacing sums with integrals

$$F(\omega) = \int d\omega' p(\omega, \omega') P(\omega') \tag{4.4}$$

$$\frac{\partial}{\partial t} P(\omega) = P(\omega) \left[\frac{\mu(\omega) N}{N_h(\omega) + N} - \int d\omega' \, \frac{g(\omega') p(\omega', \omega) Z(\omega')}{1 + F(\omega')/C(\omega')} - d_p(\omega) \right] \tag{4.5}$$

$$\frac{\partial}{\partial t} Z(\omega) = Z(\omega) \left[\frac{a(\omega) g(\omega) F(\omega)}{1 + F(\omega)/C(\omega)} - d_z(\omega) \right] \quad . \tag{4.6}$$

Equations 4.1-3 or 4.4-6 constitute the size-spectrum model.

The number of parameters seems now to be unmanageably large: for each PP class, we must specify μ_i, $N_{h,i}$, d_{Pi}, and for each ZP class g_i, a_i, d_{Zi}, C_i, and a preference matrix p_{ij}.

For functions such as $\mu_i = \mu(\omega_i)$ or $g(\omega_i)$, we invoke allometric relations

$$\mu(\omega_i) = \mu_0 \left(\frac{W}{W_0}\right)^{\beta_\mu} = \mu_0 \exp(\beta_\mu \omega)$$

where μ_0 and β_μ are the constants which define the shape of the curve. Allometric relationships make a lot of sense: many biological characteristics scale with the length, surface area, or weight. For example, nutrient transport into a cell would depend on the surface area, the net metabolic loss would vary with the weight, and properties such as foraging volumes would generally increase as the size increases. Various authors have explored physiological mechanisms for allometric scaling; *e.g.*, West, *et al.*(1997) argue that constraints on the transport of fluid through branching networks (such as circulatory or vascular systems) give metabolic rates proportional to $L^{1/4}$ and that the fractal nature of subsystems implies most properties will scale as quarter powers ($L^{n/4}$). Empirically, such relationships seem to hold fairly well; Moloney and Field (19xx) suggest $L^{-3/4} = W^{-1/4}$ laws for μ, g, and d_z xx?? based on xx.†

For the p matrix or function, we have assumed the ZP graze on the PP in a size range proportional to their own size with equal preference:

$$p(\omega, \omega') = \begin{cases} \dfrac{1}{\omega - \omega_z} & 0 \le \omega' \le \omega - \omega_Z \le w \\ \dfrac{1}{w} & \omega - \omega_Z - w \le \omega' \le \omega - \omega_Z \\ 0 & \text{else} \quad . \end{cases}$$

† However, as Smith (19xx) argues persuasively, empirical fits, especially when justified by visual comparison of points and a line on a log-log plot, obscure real physiological differences. In addition, correlation coefficents often give a misleading impression of how well the power law represents the data.

4.1.2 — Ranges and Steady States

Phytoplankton will only be able to grow in the range $0 \leq \omega \leq \omega_{Pmax}$ where the maximum possible size is given by

$$\mu(\omega_{Pmax}) = d_p(\omega_{Pmax}) \quad .$$

However, not all of this range may be occupied, depending on parameters such as

$$N_T = N + \int d\omega \; P(\omega) + \int d\omega \; Z(\omega) \quad .$$

Zooplankton require

$$a(\omega)g(\omega)C(\omega) > d_z(\omega)$$

but will generally be restricted by the amount of available food.

Let us now consider the sequence of steady states as N_T increases from zero:

1) Initially, N will equal N_T until the threshold

$$N > N_{c0} = \frac{d_{P0}N_{h,0}}{\mu_0 - d_{P0}}$$

is passed.

2) Next, N remains fixed at N_{c0} while P_0 increases ($= N_T - N_{c0}$). The food available for ZP in class j increases as $p_{j0}P_0$. By the assumptions about p_{ij}, the food for class Z_0 will be the largest, so that we expect to reach the critical level

$$F_0 = P_0 \rightarrow F_{c0} = \frac{d_{Z0}C_0}{a_0 g_0 C_0 - d_{z0}}$$

first.

3) P_0 now remains constant ($= F_{C0}$) and further increases in N_T result in Z_0 increasing. But N must also increase so that the $\frac{\partial}{\partial t}P_0$ equation can be balanced as the grazing pressure grows.

4) When N reaches the N_{c1} level, the second group of autotrophics, P_1, will be able to survive and the sequence described in stages 2-3 will repeat but at the $j = 1$ level, and then the $j = 2$ level, etc.

In practice, the problem is easier to solve in reverse: we choose a value for N and then find the classes which satisfy

$$\mu_j \frac{N}{N + N_h} > d_{Pj} \quad ;$$

these classes ($0 \leq j \leq j_N$) will be populated, with the same number of ZP classes. We then find the vector of F_i values from the steady state version of (4.2) and the Z_i values from (4.3) (involving inverting p_{ji}). Finally we invert (4.1) to obtain the P_i values and sum P_i, Z_i and N to get N_T. Repeating for a set of N's allows us to plot the steady states (figure 4.2). For these examples, we used the parameters in table 4.xx and show various Δ values; the figures suggest that the continuum case will also be well-behaved.

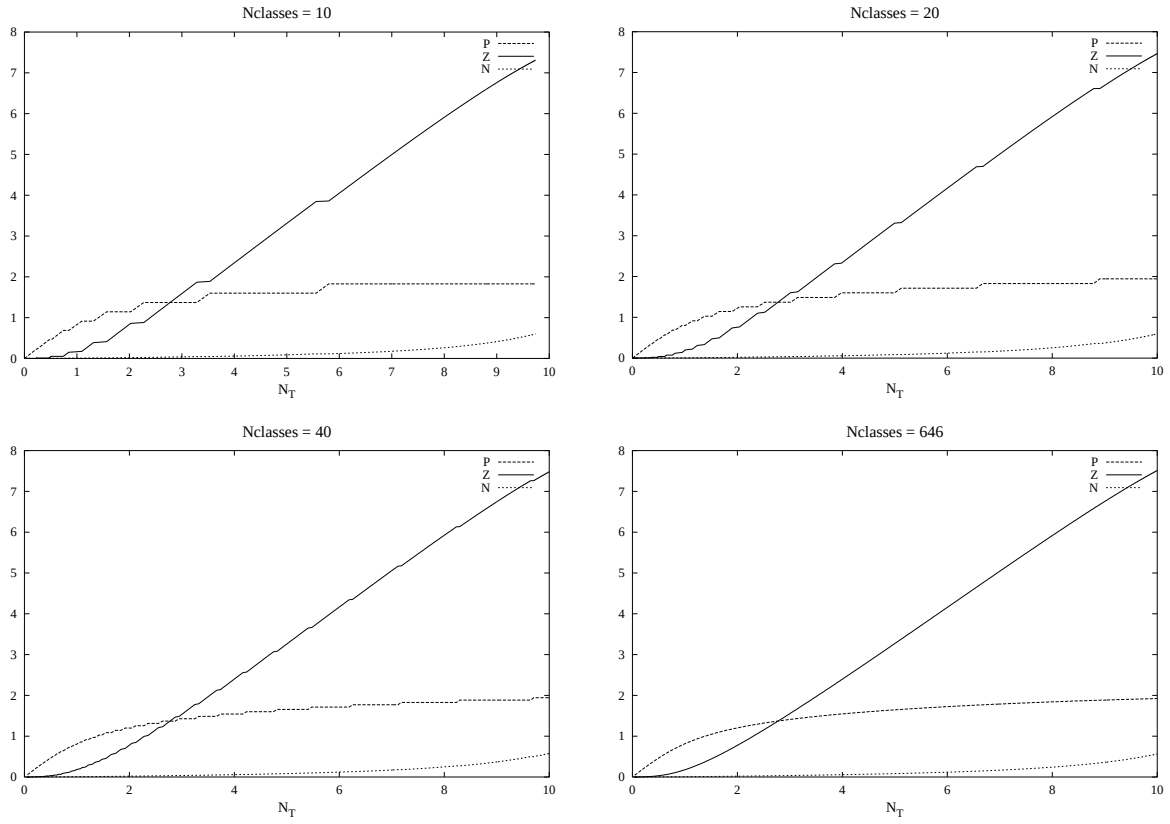

Figure 4.2: Net P, Z, and N for the size-spectrum model at different resolutions. The number of classes, in the title, is ω_{Pmax}/Δ. For the larger values of N_T, all phytoplankton size classes which can sustain growth ($\mu(\omega) > d_p$) are filled, and P levels off.

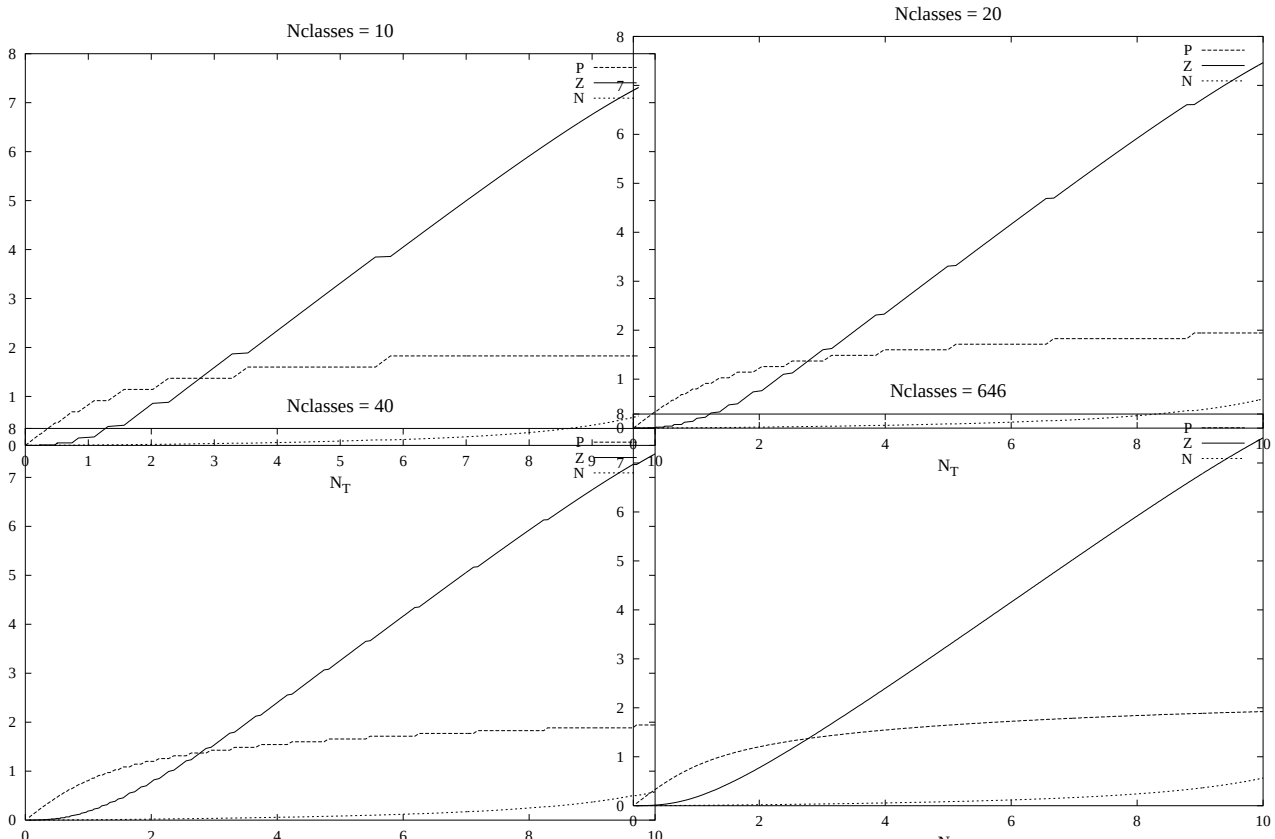

Figure 4.3: Net P, Z, and N for the size-spectrum model at different resolutions. The number of classes, in the title, is ω_{Pmax}/Δ. For the larger values of N_T, all phytoplankton size classes which can sustain growth ($\mu(\omega) > d_p$) are filled, and P levels off.

We can evaluate the stability of these steady states for the discrete case, since the system is a finite set of ODE's (although the stability matrix has the dimension of twice the number of occupied classes and thus can be very large). The steady states for 10, 20, 40 80, and 160 classes are unstable for N_T larger than 8.4, 5.9, 4.0, 2.7, and 2.1 respectively. The instability seems to lead to very irregular fluctuations (figure 4.3). Note that the instability of the full system is different from that of individual parts; for example, in the $N_T = 5$ case with 8 active size classes, any individual pair, P_i and Z_i, alone will grow and develop a limit cycle, but the system reaches a steady equilibrium when all the size classes are included in the initial conditions. For $N_T = 3$, only the smallest class has a limit cycle. These cycles are possible for the cases with high N_T levels but with only a few of the possible classes occupied because the N levels are also very high (2 to 3). When all of the different classes are active, the N levels are much lower (0.05); in effect, each class sees a much lower N_T level and is pushed into the steady state rather than the limit cycle regime.

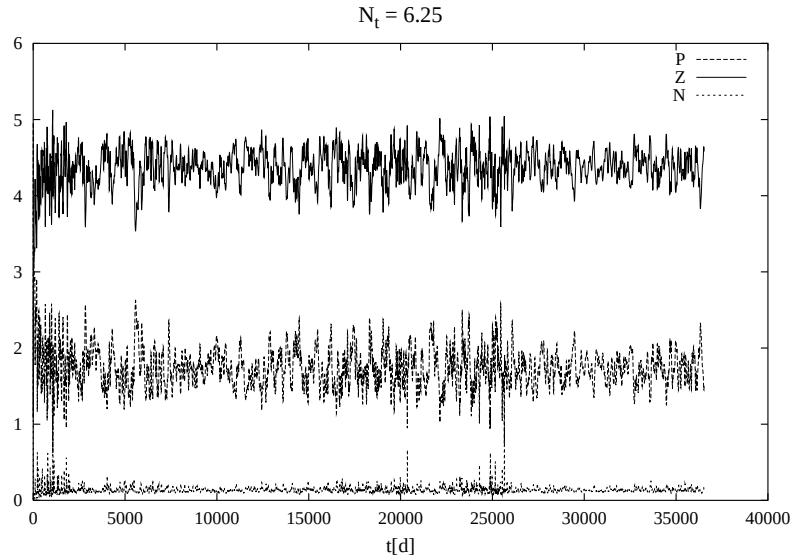

Figure 4.4: Time dependence of the unstable state $N_T = 6.25$.

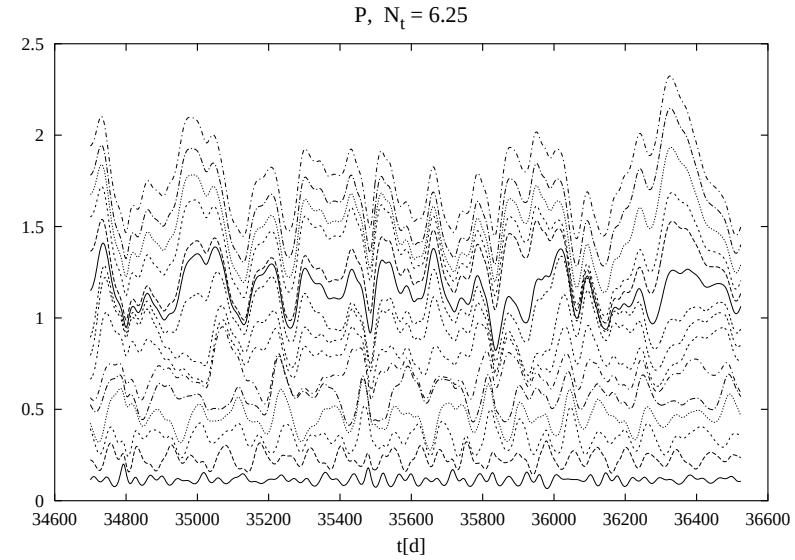

Figure 4.5: Cumulative PP biomass for the 15 active size classes.

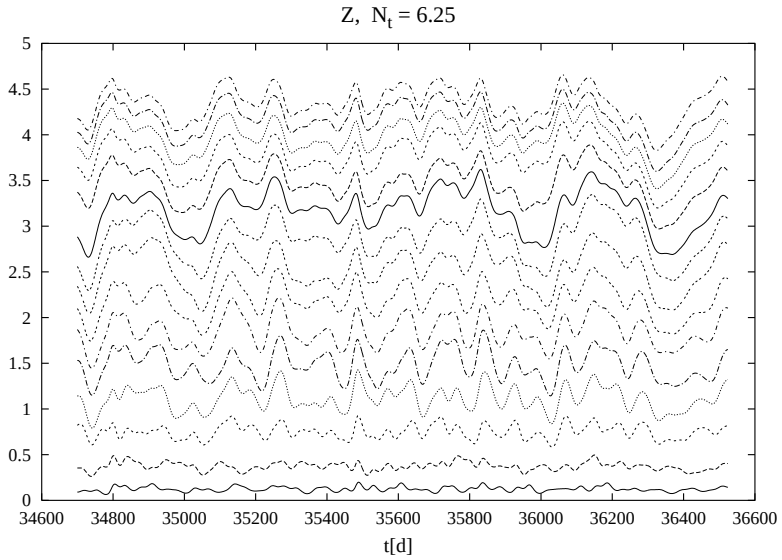

Figure 4.6: Same for the ZP.

The algorithm for finding steady states requires the lower-triangular assumption for p_{ij}, i.e., the lowest heterotroph class can feed only on the lowest autotroph class, $P_0 \rightarrow Z_0$). The higher classes, Z_j, prey on $P_0,\ P_1,\ \ldots P_j$. If this condition does not hold (e.g., if Z_0 feeds on P_0 and P_1, Z_1 on P_0, P_1, P_2, etc.), the p_{ij} matrix may be singular or we may end up with negative values for some of the Z_i. That does not mean we cannot use such a system, just that finding steady states becomes more difficult. Time-stepping shows that gaps open in the PP size-spectrum (and possibly in the ZP one as well), with some classes dying out (figure 4.6). Tilman's (19xx) theory ... xx.

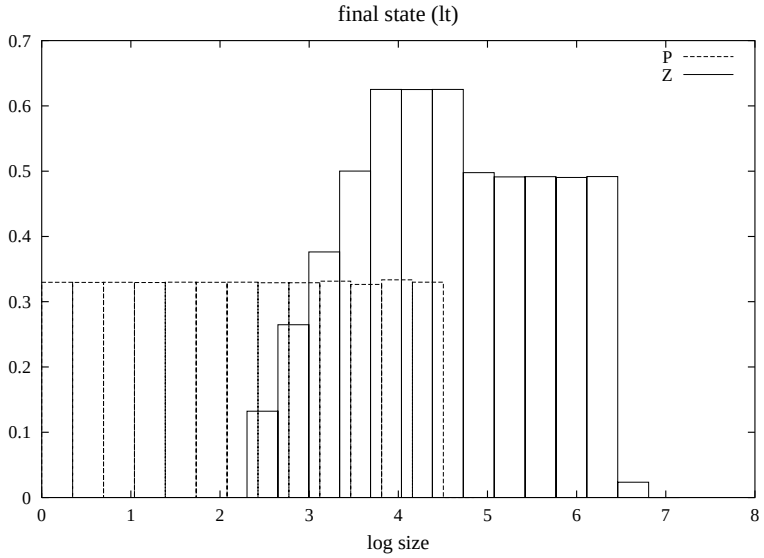

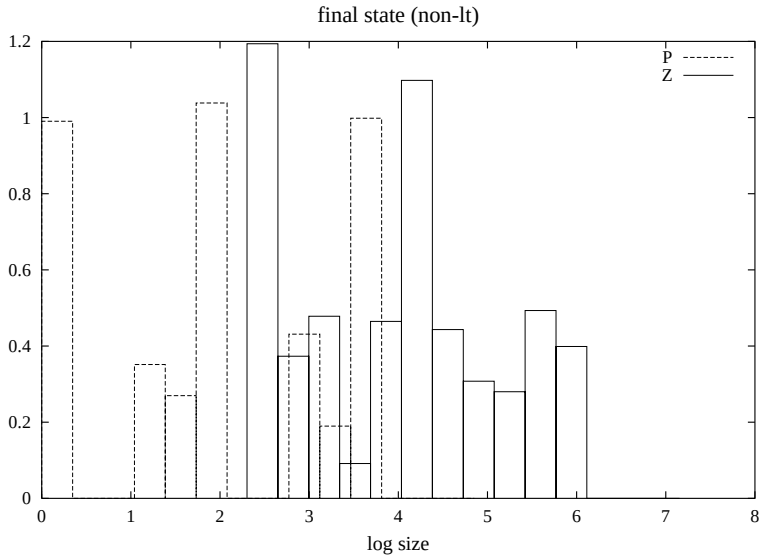

Figure 4.7: End states (after 80,000 days) in the case of a lower-triangular p_{ij} with food ranging from $L_Z/40$ to $L_Z/10$ and a case with the range being $L_Z/20$ to $L_Z/5$. Since the minimum L_P is one-tenth the minimum L_Z, the latter case is not lower-triangular. The second case also has persistent oscillations.

As formulated, the model implies that the ratio of sizes of the largest to the smallest ZP is the same as the ratio for the PP. Although this may appear to arise from the use of the same Δ values for both classes, that choice really stems from the way we specify the range of available food for ZP of size L_Z: we assume that they graze over weights

$$\alpha_0 \left(\frac{W_Z}{W_0}\right)^\gamma W_Z \leq W_P \leq \alpha_1 \left(\frac{W_Z}{W_0}\right)^\gamma W_Z$$

(applying allometric scaling). In log-size space, we have

$$\ln \alpha_0 + \gamma\omega_Z + \omega_Z \leq \omega_P \leq \ln \alpha_1 + \gamma\omega_Z + \omega_Z \quad .$$

To keep the classes synchronized, we should choose

$$(1+\gamma)\Delta_Z = \Delta_P \quad .$$

The size ranges will now satisfy

$$\frac{W_{Zmax}}{W_{Zmin}} \leq \frac{1}{1+\gamma}\frac{W_{Pmax}}{W_{Pmin}} \quad .$$

For the examples above, γ is zero, so that the ZP forage over a range of sizes which is a fixed fraction of their own, and the maximum/ minimum ratios are the same. If, however, the size of the food items foraged by ZP does not increase in proportion to the heterotroph's size but grows more slowly ($\gamma < 1$), the size range for ZP is larger than for PP. The factor is probably not large, so that we must increase the length of the food chain to include the larger zooplankton — these animals must must be omnivores or predators, rather than herbivores.

4.1.3 — Continuum case

We can find the steady state for the continuum model in much the same way. Given N, the largest sustainable size for PP is given by ω_{Pmax} such that

$$\frac{\mu(\omega_{Pmax})N}{N_h(\omega_{Pmax})+N} = d_p(\omega_{Pmax}) \quad .$$

We then find for the ZP food distribution

$$F(\omega) = \frac{d_z(\omega)C(\omega)}{a(\omega)g(\omega)C(\omega) - d_z(\omega)}$$

and solve the integral equation

$$\int_0^{\omega_{Pmax}} d\omega' p(\omega,\omega')P(\omega') = F(\omega)$$

for P. To determine Z, we are faced with a second integral equation

$$\int_{\omega_Z}^{\omega_Z+\omega_{Pmax}} d\omega' p(\omega',\omega)\frac{g(\omega')Z(\omega')}{1+F(\omega')/C(\omega')} = \frac{\mu(\omega)N}{N_h(\omega)+N} - d_p(\omega) \quad . \tag{4.7}$$

Finally, we compute N_T by

$$N_T = N + \int_0^{\omega_{Pmax}} P + \int_{\omega_Z}^{\omega_Z+\omega_{Pmax}} Z \quad .$$

For the example parameters we have been using, with C and a constant and with the allometric coefficients for $g(\omega)$ and $d_z(\omega)$ the same, $F(\omega)$ is constant. Since $\int d\omega' p(\omega,\omega') = 1$, $P(\omega)$ will be the same constant $P(\omega) = d_{Z0}C/(ag_0C - d_{Z0})$, $0 \le \omega \le \omega_m$. The only difficult part is solving the Z (or ζ) equation.

The results are not what one might expect. We would normally expect a continuous solution. Given that g and μ are proportional to $\exp(\beta\omega)$ and d_p is constant (for our choice of allometric scalings) and that $p(\omega',\omega) = 1/w$ for some range of ω', we would anticipate a solution like $Z_0 + Z_1\exp(-\beta\omega)$ might work. In the range where the largest prey would be larger than ω_{Pmax}, Z would be constant. But this solution does not integrate correctly when the range of integration overlaps the point joining the two solutions. Instead, we must write the integrals explicitly

$$\frac{\mu_0 N(1+F/C)}{(N_h+N)g_0}\exp(\beta\omega) - d_p = \begin{cases} \int_\omega^w d\omega' \frac{1}{\omega'}\exp(\beta\omega')Z(\omega_Z+\omega') + \\ \qquad \int_w^{\omega+w} d\omega' \frac{1}{w}\exp(\beta\omega')Z(\omega_Z+\omega') & \omega < w \\ \int_\omega^{\omega+w} d\omega' \frac{1}{w}\exp(\beta\omega')Z(\omega_Z+\omega') & w < \omega < \omega_{Pmax} - w \\ \int_\omega^{\omega_{Pmax}} d\omega' \frac{1}{w}\exp(\beta\omega')Z(\omega_Z+\omega') & \omega_{Pmax} - w < \omega < \omega_{Pmax} \end{cases} .$$

Differentiating these with respect to ω and dividing by $\exp(\beta\omega)$ gives a set of difference equations:

$$-w\beta\frac{\mu_0 N(1+F/C)}{(N_h+N)g_0} = \begin{cases} \frac{w}{\omega}Z(\omega_Z+\omega) - \exp(\beta w))Z(\omega_Z+\omega+w) & \omega < w \\ -\exp(\beta w)Z(\omega_Z+\omega+w) + Z(\omega_Z+\omega) & w < \omega < \omega_{Pmax} - w \\ Z(\omega_Z+\omega) & \omega_{Pmax} - w < \omega < \omega_{Pmax} \end{cases} .$$

Thus the $Z(\omega)$ values are step-wise constant on ranges $\omega_{Pmax}+\omega_Z-(n+1)w$ to $\omega_{Pmax}+\omega_Z-nw$, with a linear rise at the beginning. Figure 4.7 compares this solution with the (incorrect) continuous one and the discrete model.

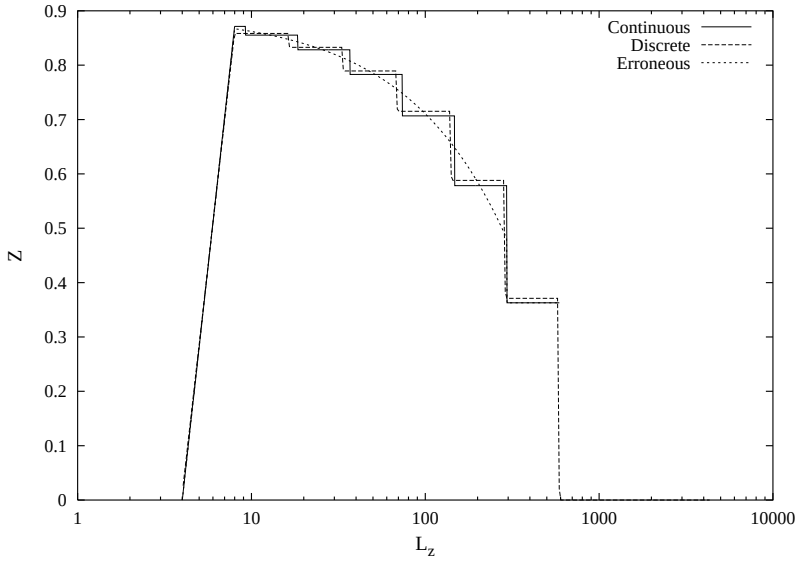

Figure 4.8: Steady state ZP structures for the continuous size class solution, the discrete case with 231 active classes $\Delta = \ln(2^{1/32})$, and the erroneous smooth case. The discrete model with $\Delta = \ln(2^{1/128})$ (922 active classes) is almost identical to the continuous solution.

4.1.4 — Prey switching

The previous system presumes that the ZP which prey on a range of PP weight classes will not alter their behavior depending on the range of food items available – the p_{ij}'s are constants. We've called this "indiscriminate" behavior above. Although we have used the same values for the constants, we could rationalize the factors being different in terms of varying ability to sense or to attack successfully prey types. However, a more significant alteration comes from introducing preferences as well, so that the ZP focuses foraging effort on the more abundant prey. Taking p_{ij} to be

$$p_{ij} = \frac{a_{ij}P_j}{\Sigma a_{ik}P_k}$$

(with the a_{ij}'s being constant) produces a modified Holling type III model. The resulting system is much more stable (figures 4.8-9).

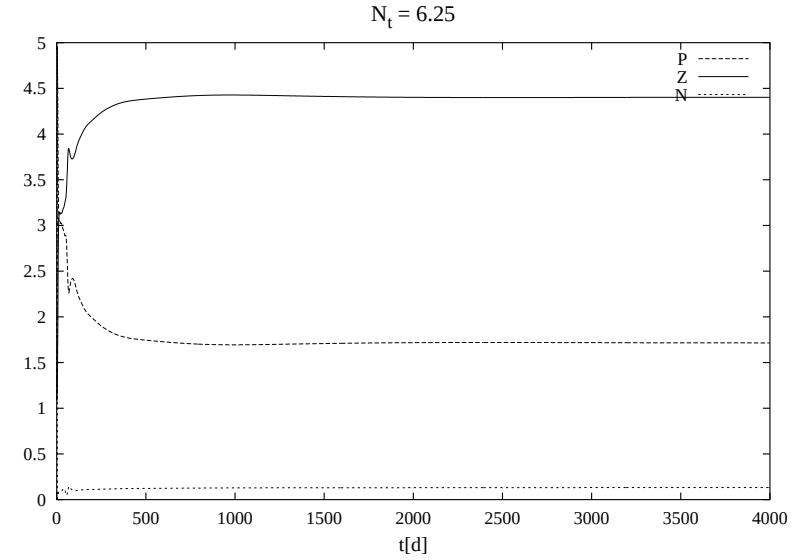

Figure 4.9: Time dependence of the case with switching; $N_T = 6.25$.

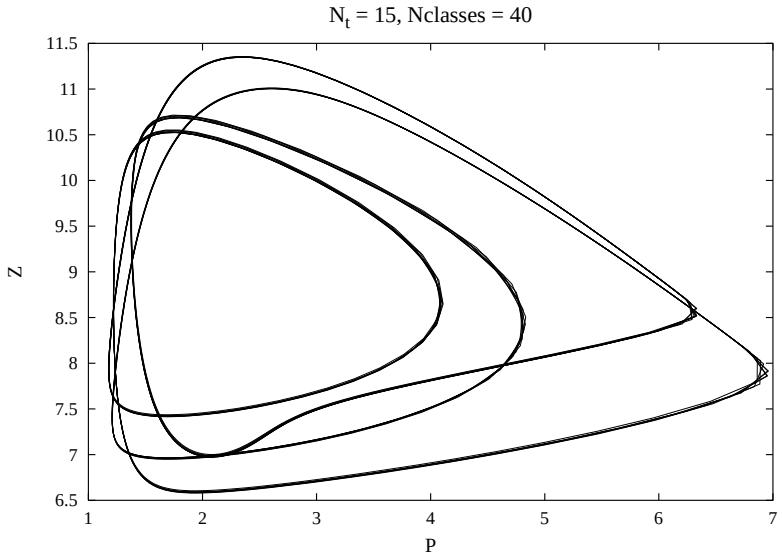

Figure 4.10: Regular cycles for very large N_T and smaller classes.

4.2 — Weight, length, or age models

In the size-spectrum models, all ingested resources are used to produce new biomass within the same size class. Different size classes implicitly contain different sets of species. However, the macrozooplankton (such as copepods or euphausiids) can increase in weight by several orders of magnitude from the larval to adult stages. The different stages or sizes vary significantly in terms of their foraging ability, ingestion rates, and the kind of prey they consume, as well as in their metabolic rates. Reproduction may occur seasonally, rather than continuously as assumed so far, and is limited to the adult part of the population. As we shall see, the time-delays between reproduction and the increase in adult biomass can significantly alter the dynamics.

"Structured population models," which incorporate effects of growth in size and age, can be formulated in discrete (matrix) or continuous forms, Since we are using continuum models when possible, we shall discuss the Von Foerster-McKendrik form. We describe the population by a number density $n(w, \mathbf{x}, t)$ such that the number (or probable number) of organisms per unit weight class and per unit volume of water. It satisfies an advection-like equation

$$\frac{D}{Dt}n(w,t) + \frac{\partial}{\partial w}\Big[g(w)n(w,t)\Big] = -d_z(w)n(w,t) + \int dw' E(w|w')n(w',t) \tag{4.8}$$

where g represents the rate of weight gain (dw/dt), d_z the mortality, and E the rate at which new organisms at size w are created by adults at size w' reproducing. We have suppressed many of the arguments for the various functions: they all can depend on space and time as well as environmental parameters, such as the density of food or the temperature. In addition, the rates can depend on functionals of n as well (e.g., when competition for food limits growth, decreases birth rates, or increases mortality).†

We shall factor E assuming that

- the newborn size does not depend on the adult size or conditions

$$E(w|w') = e_0(w)e_1(w',t)$$

- the birth rate is a function of the number of adults

$$N_A \equiv \int dw\alpha(w)n(w) \quad , \quad e_1(w) = R(N_A,t)\alpha(w) \quad \Rightarrow \quad \int dw' En = e_0(w)N_A R(N_A,t)$$

and we can normalize e_0 by

$$\int dw\ e_0(w) = 1 \quad , \qquad \int dw\ we_0(w) = w_0$$

† A functional maps a function into a number and can be represented as $F[n] = \int dw f(w)n(w)$ with a specified kernel f. E.g., we can represent competitive pressure at size w from other organisms as $C = \int dw' c(w|w')n(w')$, where c is peaked around $w - w'$; we then specify that the rate of growth $s(w)$ is some decreasing function of C.

- the weight range for newborn organisms is small – effectively a delta function

$$e_0(w) = \delta(w - w_0)$$

The last of these allows us to replace the source term in (4.8) with a boundary condition, giving

$$\frac{\partial}{\partial t}n + \frac{\partial}{\partial w}gn = -d_z n \quad , \quad g(w_0)n(w_0,t) = N_A R(N_A) \quad . \tag{4.9}$$

NUMERICS

Equation 4.9 can also be written as

$$\frac{\partial}{\partial t}n + g\frac{\partial}{\partial w}n = -(d_z + \frac{\partial}{\partial w}g)n \quad , \quad g(w_0)n(w_0,t) = N_A R(N_A)$$

which makes the connection to the scalar advection equation explicit. Since analytical solutions are rare, we again need to consider numerical methods. The previous equation can be solved in a Lagrangian form (method of characteristics) in which we start with a cohort at time t and weight w_0 and follow it

$$\frac{d}{dt}W = g(W,t) \quad , \quad W(t) = w_0$$
$$\frac{d}{dt}n = -[d(W,t) + \frac{\partial g(W,t)}{\partial W}]n \quad , \quad n(t) = n_0 \quad .$$

At each time, we have a set of cohorts of different numbers and weights. To calculate n_0 for the next cohort, we need to approximate the integral for this unequally spaced data, which can be done easily. This kind of model can be extended to cases where g, d_z are functionals of n by again approximating integrals (c.f., deRoos' "escalator-boxcar train" article, 19xx). After some cutoff time (or weight or number density), cohorts can be discarded; nonetheless, we could have a large number of cohorts active at any time.

For the Eulerian approach, we write discretized equations for $n_j = n(w_j)$, $w_j = w_0 + (j + \frac{1}{2})\delta w$ in terms of the fluxes F_j defined at $w_0 + j\delta w$

$$\frac{\partial}{\partial t}n_j = -(F_{j+1} - F_j)/\delta w - d_j n_j \quad , \quad F_0 = RN_A \quad , \quad N_A = \delta w\, \alpha_j n_j \quad .$$

The problem, as with the case of advection, lies in specifying the fluxes at the edge of each grid box. Various authors (xx) have discussed the accuracy, numerical diffusivity, and positivity of different schemes. We shall use an "upwind difference" in which the flux at weight w_j is given by $g(w_j)n(w_j - \frac{1}{2}\delta w)$ which maintains positivity ($n > 0$), but has a numerical diffusivity $\sim \frac{1}{2}g\delta w/\delta t$ causing a weight distribution to spread as the animals grow. Such spreading is realistic, since not all individuals grow at exactly the same rate; as the previous chapter demonstrates, we would expect a diffusivity

$$\mathcal{K} = \frac{\delta t}{2}\langle[g - \langle g\rangle]^2\rangle$$

which will match up with the numerical case if the variance in g is proportional to g (and an alteration to the mean growth rate). Unfortunately, the diffusion permits some individuals in sharp pulse of newborns to reach adult in a time $(w_A - w_0)\delta t/\delta w$ – much too rapidly. The same problem occurs even without discretization if we do represent the variability on g as a diffusivity; information can propagate infinitely rapidly. Usually, the errors are acceptably small since the newborns are distributed in time and the temporal changes in the coefficients are smooth, but one needs to verify that the model is not dominated by this kind of rapid propagation effect.

4.2.1 — Maps

The simplest form which makes the possibility of oscillatory/ chaotic behavior clear assumes that all reproduction occurs at a specific adult size: $\alpha(w) = \frac{g}{d_z}\delta(w - w_A)$, with the factor making α dimensionless and ensuring that $\int dw\, \alpha n$ results in a number of individuals. The reproducing population is $N_A = \frac{g}{d_z} n(w_A, t)$; all adults reproduce at a single weight. With this form, the flux of newborn animals is given by

$$gn(w_0, t) = N_A(t) R(N_A(t)) \quad .$$

Finally, we can solve the equation between w_0 and w_A easily if g and d_z are constant

$$n(w_A, t) = n\left(w_0, t - \frac{w_A - w_0}{g}\right) \exp\left(-d_z \frac{w_A - w_0}{g}\right) = n(w_0, t - T)\exp(-d_z T)$$

with $T = (w_A - w_0)/g$ being the generation time. Therefore

$$N_A(t) = \frac{1}{d_z}\exp(-d_z T) N_A(t - T) R(N_A(t - T))$$

Thus we can algebraically map the number of adults at one generation into the number at the next. If the growth rate and death rates vary with weight, the coefficient of $N_A R(N_A)$ changes, but the form remains the same.

As an example, let us assume the rate of producing offspring per adult depends on the food per adult $f = P/N_A$ in the form of a sigmoid curve

$$R = \frac{r}{T}\frac{(f/f_0)^\beta}{1 + (f/f_0)^\beta} = \frac{r}{T}\frac{1}{1 + (N/N_0)^\beta}$$

with $N_0 = P/f_0$ being the half-saturation value (figure 4.10). Then $X_n = N(nT)/N_0$ satisfies

$$X_{n+1} = \gamma \frac{X_n}{1 + X_n^\beta} \quad , \quad \gamma = \frac{r}{d_z T}\exp(-d_z T) \tag{4.10}$$

For this iterated map, we can show easily that

- The $X = 0$ steady state is unstable for $\gamma > 1$.
- The state $X = (\gamma - 1)^{1/\beta}$ to which the system bifurcates becomes unstable for $\gamma > \beta/(\beta - 2)$ to a period $2T$ oscillation.

- Further bifurcations to period $4T$, $8T$, $16T$, etc. occur at shorter and shorter increments in γ, leading to a non-repeating sequence for a finite value of γ. This is the "period-doubling" route to chaos. See figures 4.11-12.

This map demonstrates the potential for chaotic, unpredictable population fluctuations. In Appendix 4.xx, we reproduce a simple proof that a map can give non-repeating sequences.

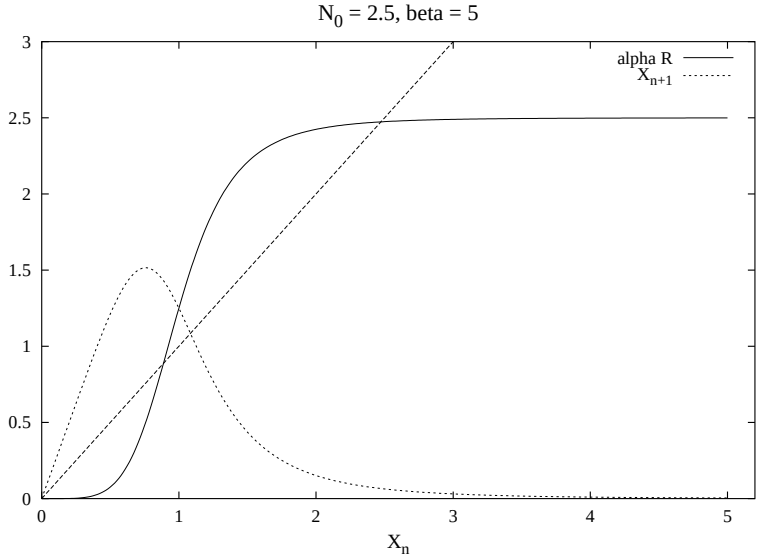

Figure 4.11: Iterated map structure for $\gamma = 2.5$, $\beta = 5$, showing the offspring production rate per adult as a function of the number of adults and the map $X_n \to X_{n+1}$.

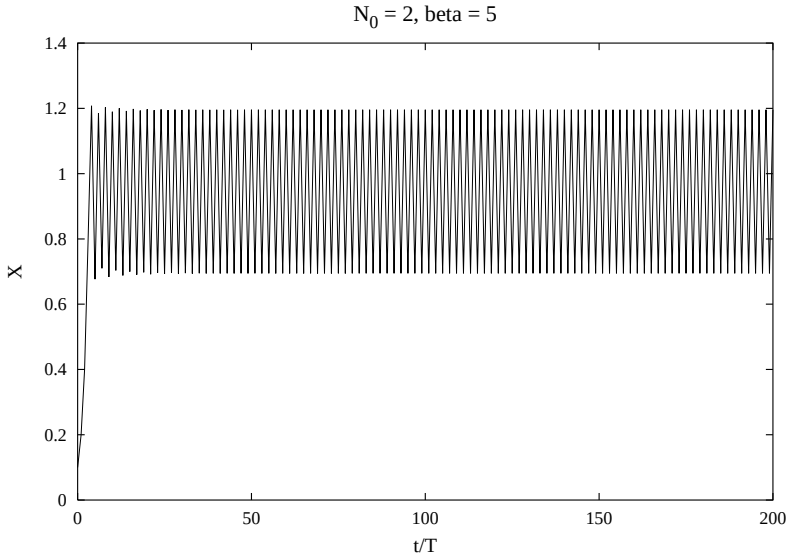

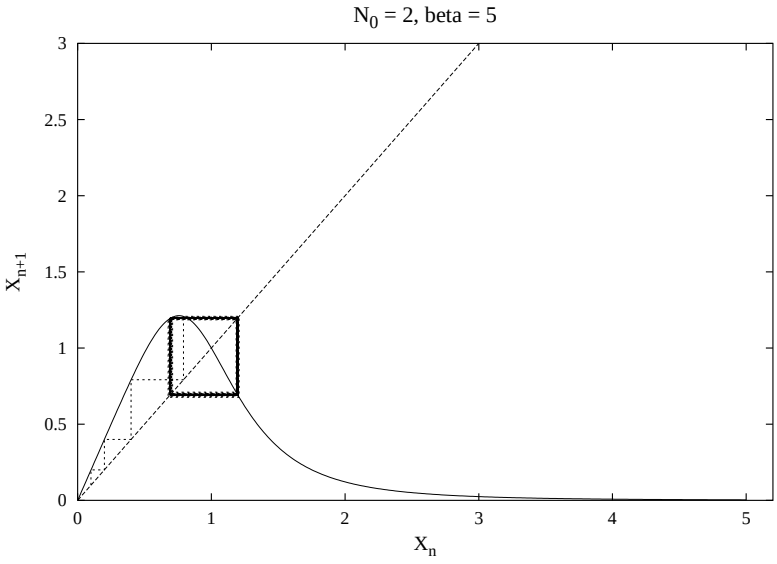
N0 = 2, beta = 5
Xn+1
Xn
0
0.5
1
1.5
2
2.5
3
0
1
2
3
4
5

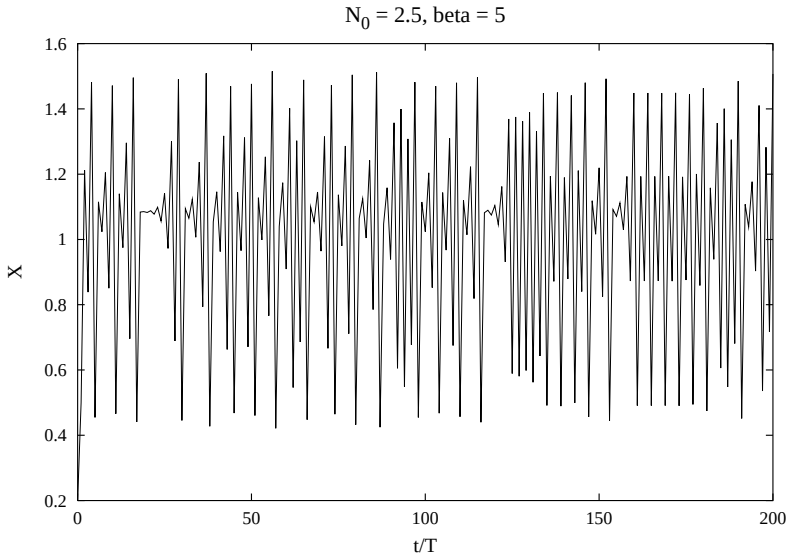
N0 = 2.5, beta = 5
X
t/T
0.2
0.4
0.6
0.8
1
1.2
1.4
1.6
0
50
100
150
200

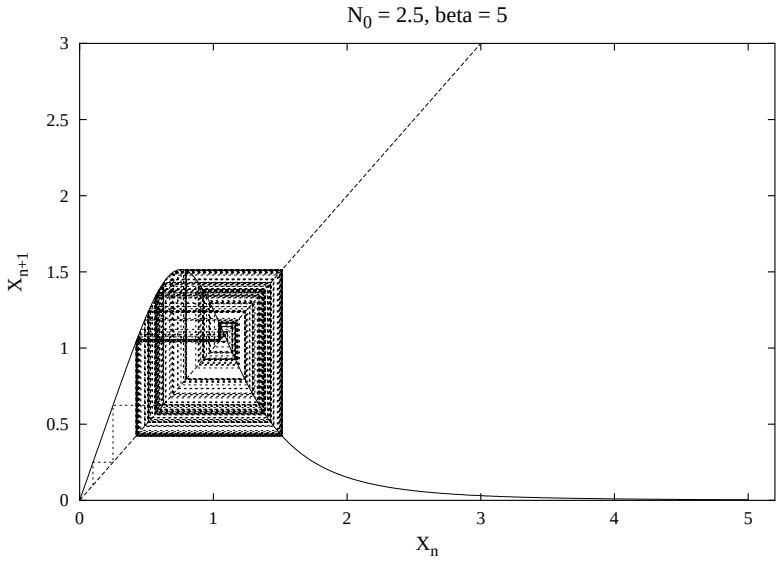

Figure 4.12: Two views of the number in successive generations. The upper plot shows a time-series, while the lower plot is a "cobweb diagram: starting at (X_0,X_0), we project vertically to the $N_0X/(1+X^\beta)$ curve, then move horizontally back to the diagonal arriving at (X_1, X_1). Repeating this procedure traces out the sequence and shows periodic solutions clearly in the $N_0 = 2$ case.

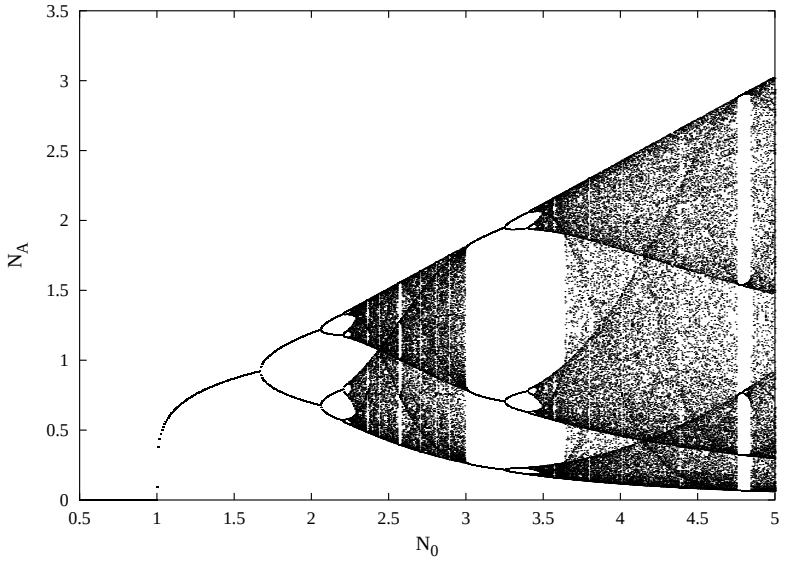

Figure 4.13: Bifurcation diagram showing 200 generations after spin-up of 5000 generations.

4.2.2 — Appendix 4.xx: Truly chaotic...

Here, we reproduce a simple proof (c.f. xx, 19xx) that the logistic map produces non-repeating patterns. Let

$$X_{n+1} = \gamma X_n (1 - X_n)$$

and look at the case $\gamma = 4$ (the maximum); we can then write

$$X_n = \sin^2 \theta_n \quad .$$

The recursion relation becomes

$$\sin^2 \theta_{n+1} = 4 \sin^2 \theta_n (1 - \sin^2 \theta_n) = \sin^2(2\theta_n)$$

$$\Rightarrow \quad \theta_n = 2^n \theta_0 \quad .$$

We note that $\sin^2(a\pi)$ depends only on the fractional part of a, not the part to the left of the decimal point. If we let $\theta_n = a_n \pi$, we have

$$a_n = 2^n a_0 \quad , \quad a_0 = \theta_0 / \pi \quad .$$

Now consider writing a_0 as a *binary* fraction. To find a_n, we shift a_0 to the left n places and discard the integer part. If θ_0/π is an irrational number, the fractional part of a_0 will not repeat; therefore, no matter how far we shift it, we will never find the exact same sequence of 0's and 1's as some previous value. In addition, two very close initial conditions will eventually reach the point where their fractions differ and the sequence of states will be entirely different thereafter. (On finite precision machines, the a_n series rapidly runs out of significant bits, while the standard iteration because of roundoff errors continues to generate changes in the least significant bits).

4.2.3 — Finite Range of Reproducing Adults

The iterated map version has a number of oddities: the cycles from each starting time in the range $[0, T)$ are independent of each other. Allowing reproduction over a range of sizes will couple neighboring times together, leading to smooth behavior; therefore, we might worry that the chaotic behavior disappears. To examine this issue, consider another case where all animals with weights greater than or equal to w_A are reproducing. Then $\alpha(w) = \mathcal{H}(w - w_A)$. We can find an equation for the number of adults

$$N_A = \int_{w_A}^{\infty} dw n(w)$$

by integrating (4.9) over the same limits

$$\frac{\partial}{\partial t} N_A = -d_z N_A + g(w_A) n(w_A) \quad .$$

Using the solution for n gives a delay-differential equation

$$\frac{\partial}{\partial t}N_A(t) = -d_z N_A(t) + e^{-d_z T} N_A(t-T) R(N_A(t-T))$$

with $T = (w_A - w_0)/g$ again being the generation time. Because of the delay term, this equation is not just a first order equation, and it can exhibit complex behavior.

We use the same form for R, define $X = N_A/N_0$, and nondimensionalize time by T to find

$$\frac{\partial}{\partial t}X(t) = -dX(t) + d\gamma \frac{X(t-1)}{1+X(t-1)^\beta} \quad , \quad d = d_z T \quad . \tag{4.11}$$

We can again show that the steady solution $\overline{X} = (\gamma - 1)^{1/\beta}$ exists for $\gamma > 1$.

The stability analysis of this solution illustrates some of the differences between a delay-differential equation and an ODE. We perturb around $\overline{X}$ to find

$$\begin{aligned}\frac{\partial}{\partial t}X'(t) &= -dX'(t) + dX'(t-1) - \beta d\frac{\gamma-1}{\gamma}X'(t-1) \\ &= -dX'(t) - d\left[\beta\frac{\gamma-1}{\gamma} - 1\right]X'(t-1) \quad .\end{aligned}$$

The term in square brackets is often positive, so it appears that the solutions should decay; however, if $X'(t-1)$ has the opposite sign as $X'(t)$, growth may be possible. Taking a solution form

$$X'(t) = X'_0 \exp(\sigma t - \imath\omega t)$$

gives

$$\sigma - \imath\omega = -d - d\left[\beta\frac{\gamma-1}{\gamma} - 1\right]e^{-\sigma}e^{\imath\omega}$$

with the last terms arising from the delay; separating into real and imaginary parts yields

$$\begin{aligned}\sigma &= -d - d\left[\beta\frac{\gamma-1}{\gamma} - 1\right]e^{-\sigma}\cos\omega \\ \omega &= d\left[\beta\frac{\gamma-1}{\gamma} - 1\right]e^{-\sigma}\sin\omega \quad .\end{aligned}$$

The critical point, $\sigma = 0$, can be found by eliminating the term in brackets between the two:

$$\omega = -d\tan\omega$$

which must be solved in the range $\frac{1}{2}\pi < \omega < \pi$ so that the cosine will be negative, and σ may be positive. Once we have found ω, the second equation gives

$$\gamma = \left[1 - \frac{1}{\beta}\left(\frac{\omega}{d\sin\omega} + 1\right)\right]^{-1} \quad .$$

For the parameters in the example, $\beta = 5$ and $d = 4$, the instability occurs at $\gamma = 1.78$. Since $\omega/\sin\omega \geq \pi/2$, the expressions above show that instability in general requires

$$d > \frac{\pi}{2(\beta - 1)} \quad .$$

A population for which a small fraction dies over one generation will have stable steady solutions; otherwise, the populations will begin to oscillate when γ is high enough – when each individual has many offspring [we can consider the net production of offspring as approximately the rate times the expected lifetime $1/d_z$ giving $g/d_z T = \gamma \exp(d)$ – order 200 for the chaotic state below].

Numerical solutions can be obtained easily. Given a time step, dt, we define a vector of previous N_A values at times t, $t - dt$, $t - 2dt$, $t - 3dt$,..., $t - 1$ (initially filled with the steady state value plus random perturbations). The last element gives the delayed value $N_A(t - 1)$ required in stepping $N_A(t)$ forward. The array is then shifted one position so that the last element becomes $N_A(t + dt - 1)$ and the new value $N_A(t + dt)$ is put into the first slot. We can display the time-series of N_A; however, it is easire to spot periodic or chaotic behavior by looking at delay plots of $N_A(t + 1)$ vs. $N_A(t)$. Figure 4.13 gives a number of examples and shows that instability to a periodic oscillation indeed begins at $\gamma = 1.78$; period doubling occurs, and we reaching chaotic states by $\gamma = 3.5$. For larger γ values, we return to periodic states.

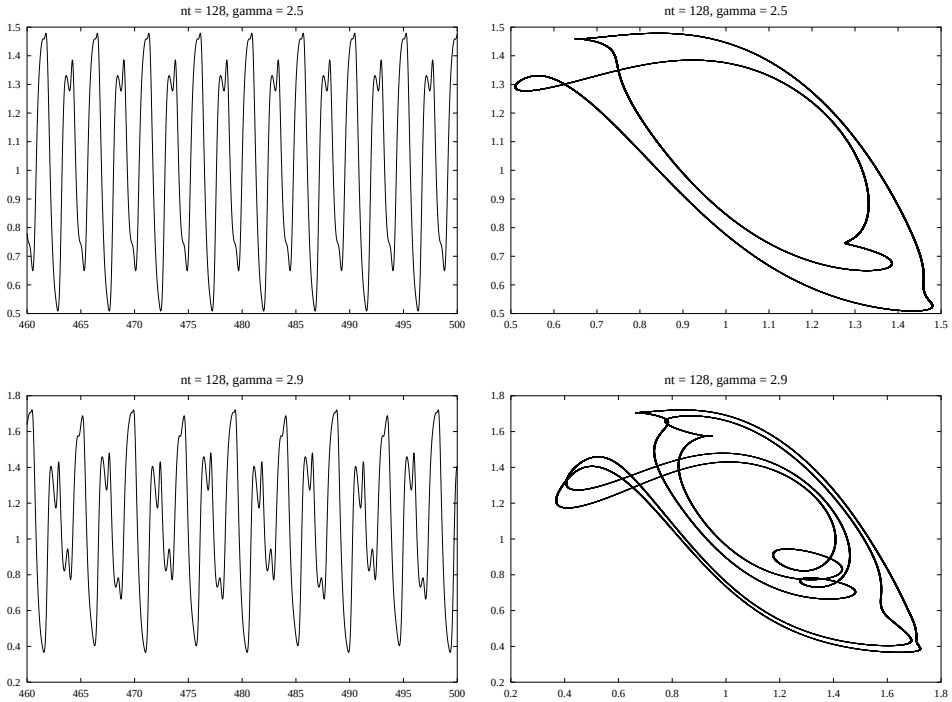

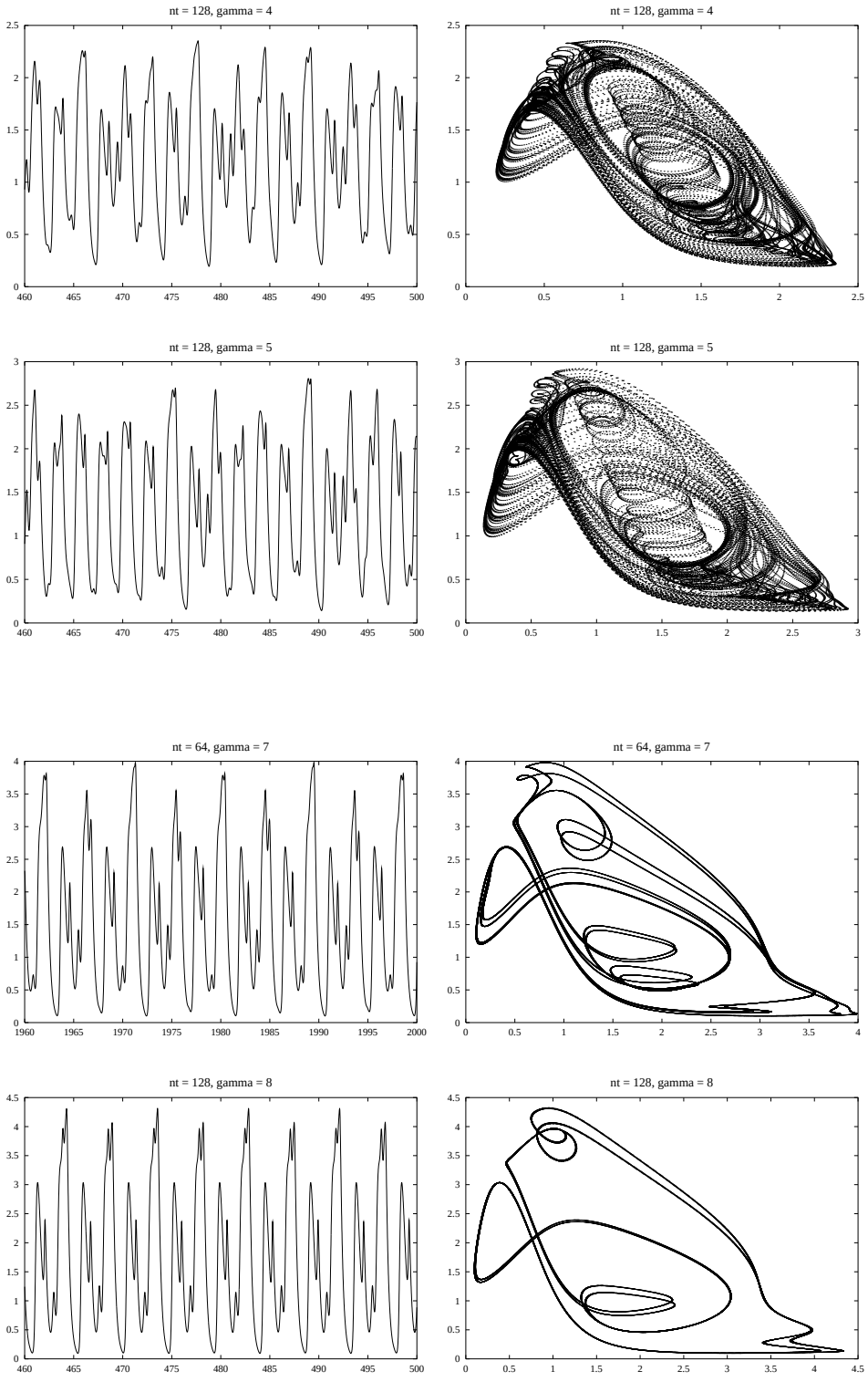

Figure 4.14: Figures showing (left) time-series of the number of adults N_A and (right) $N_A(t+1)$ vs. $N_A(t)$ for $\gamma = 2.5$, 2.9, 4, 5, 7, 8.

4.2.4 — Coupling to food source

To link this kind of model to lower trophic levels, we need to consider the biomass changes implied in (4.9). Although the numbers in any weight class other than w_0 can only decrease, the movement of numbers from one class to a larger class imply an increase in biomass which must have derived from the animals' food source. For a single organism, the rate of change of mass is just

$$\frac{d}{dt}w = g$$

(in the Lagrangian sense), and the net biomass changes by

$$\frac{d}{dt}b = n\frac{d}{dt}g = ns = \frac{g}{w}b$$

(not counting biomass loss by death, which does not affect the food source). This, then, represents the rate of biomass assimilation by ZP at size w. To derive this from the number equation, we examine changes in the net biomass

$$\begin{aligned}\frac{\partial}{\partial t}\int wn &= w_0 N_A R - \int w\frac{\partial}{\partial w}gn - \int d_z wn \\ &= w_0 N_A R + \int gn - \int d_z wn \quad .\end{aligned}$$

The first two terms represent biomass increases; we must relate these to depletion of the resources. Of course, ZP of different weights may draw from diffrent PP groups, in which case the terms can be suitably partitioned.

As written, the reproduction draws directly on the prey for its biomass. We would then think of both R and g as being functions of P, functions which vanish as $P \to 0$. Therefore, we have a PP equation of the form

$$\frac{\partial}{\partial t}P = uptake - \frac{1}{a}\int g(P,w)n - \frac{1}{a}w_0 R(P,N_A)N_A - death \quad .$$

As an alternative, suppose that the biomass of offspring is drawn from the adult biomass directly at a rate which could be independent of the food supply. Then the $w_0 N_A R$ term must be offset by one of the other two integrals – either the death rate must increase or the growth rate decrease to compensate. We can represnt these possibilities as

$$d_z \to d_z + \frac{w_0}{w}R\alpha$$

(so that the integral of the last term times wn cancels $w_0 N_A R$) or

$$g \to g(P,w) - w_0 R\alpha$$

(with the integral times n providing the reproductive biomass). In those cases, the PP equation will be

$$\frac{\partial}{\partial t}P = uptake - \frac{1}{a}\int g(P,w)n - death \quad .$$

To maintain some generality, we shall use a system including both externally provided biomass (R_e) and one which redistributes it within the ZP (R_i), expecting one or the other to be zero:

$$\begin{aligned} \frac{\partial}{\partial t}n &= -\frac{\partial}{\partial w}gn - (d_z + \frac{w}{w_0}R_i\alpha)n \\ g(w_0)n(w_0) &= (R_i + R_e)\int \alpha w \\ \frac{\partial}{\partial t}P &= uptake - \frac{1}{a}\int gn - \frac{1}{a}w_0 R_e N_A - death \quad . \end{aligned} \tag{4.12}$$

Example:

Let us consider the equivalent of the NPZ model using a structured zooplankton population. We assume that the growth rate is $g = G(P)g_w(w)$, the assimilation efficiency is constant, and the birth rate is $R = R_e(P)$ ($R_i = 0$), so that reproduction biomass derives from food intake. The equations become

$$\begin{aligned} \frac{\partial}{\partial t}P &= \mu P\left(N_T - P - \int dw\, wn\right) \\ &\quad - \frac{1}{a}G(P)\int dw\, g_w n - \frac{1}{a}w_0 R(P)\int \alpha n - d_p P \qquad (4.13a) \\ \frac{\partial}{\partial t}n &= -G(P)\frac{\partial}{\partial w}g_w n - d_z n \quad , \quad G(P)g_w(w_0)n(w_0) = R(P)\int \alpha n \qquad (4.13b) \quad . \end{aligned}$$

For future use, we note that the ZP biomass $Z = \int wn$ satisfies

$$\frac{\partial}{\partial t}Z = G(P)\int g_w n + w_0 R(P)\int \alpha n - \int d_z wn \quad .$$

STEADY STATES:

The steady state equation

$$G(\overline{P})\frac{\partial}{\partial w}g_w\overline{n} = -d_z\overline{n} \quad , \qquad G(\overline{P})g_w(w_0)\overline{n}(w_0) = R(\overline{P})\int \alpha\overline{n}$$

can be solved by discretizing it to derive a matrix multiplying the vector of $\overline{n}$ values. An upwind scheme is suitable, since the diffusion in weight space will give a representation of the effects of variability in the growth rate. The $\overline{P}$ which makes one eigenvalue zero can be found by searching, and the corresponding eigenvector gives the shape of $\overline{n}$. We can also find the steady state analytically: the number equation

$$\frac{\partial}{\partial w}g_w\overline{n} = -\frac{d_z}{G(\overline{P})}\overline{n}$$

yields

$$\frac{\overline{n}(w)}{\overline{n}(w_0)} = \frac{g_w(w_0)}{g_w(w)}\exp\left(-\int_{w_0}^{w} dw' \frac{d_z(w')}{G(\overline{P})g_w(w')}\right) \quad .$$

For this form, we find $\overline{P}$ from the birth equation

$$g_w(w_0)G(\overline{P}) = R(\overline{P})\int_0^\infty dw\,\alpha(w)\frac{\overline{n}(w)}{\overline{n}(w_0)} \quad .$$

Because the decay of $\overline{n}$ with weight depends on $\overline{P}$, the case with R proportional to G (all resource dependence arising from the grazing function) still provides the necessary information.

The PP equation gives $\overline{n}(w_0)$:

$$\mu\overline{P}\left(N_T - \overline{P} - \overline{n}(w_0)\int w\frac{\overline{n}(w)}{\overline{n}(w_0)}\right) = \overline{n}(w_0)\frac{1}{a}\int w d_z(w)\frac{\overline{n}}{\overline{n}(w_0)} + d_p\overline{P}$$

(using the steady version of the ZP biomass equation).

STABILITY:

Perturbations to the steady state n have an $\exp(\sigma t)$ dependence and a weight structure satisfying

$$\sigma n' + G\frac{\partial}{\partial w} g_w n' + d_z n' = -P'\frac{G'}{G} G \frac{\partial}{\partial w} g - w\overline{n} = P' d_z \frac{G'}{G}\overline{n}$$

$$G g_w(w_0) n'(w_0) - R\int \alpha n' = P'\left[\frac{R'}{R} R\int \alpha\overline{n} - \frac{G'}{G} G g_w(w_0)\overline{n}(w_0)\right] = P'\left[\frac{R'}{R} - \frac{G'}{G}\right] R\int \alpha\overline{n}\ .$$

Here functions such as G or $G' \equiv \frac{\partial G}{\partial P}$ are evaluated at $\overline{P}$.

In general, the solution for n' will be proportional to P'

$$n'(w) = P'\hat{n}(w,\sigma)$$

and the PP equation will reduce to

$$\begin{aligned}
\frac{1}{P'}\frac{\partial P'}{\partial t} &= -\mu\overline{P} + \frac{1}{a}\left[\frac{G}{\overline{P}} - G'\right]\int g_w\overline{n} + \frac{w_0}{a}\left[\frac{R}{\overline{P}} - R'\right]\int \alpha\overline{n} \\
&\quad - \mu\overline{P}\int w\hat{n} - \frac{1}{a}G\int g_w\hat{n} - \frac{w_0}{a}R\int \alpha\hat{n} \\
&= -\mu\overline{P} + \frac{w_0}{a}\left[\frac{G'}{G} - \frac{R'}{R}\right] R\int \alpha\overline{n} + \frac{1}{a}\left[\frac{G}{\overline{P}} - G'\right]\int \frac{d_z}{G} w\overline{n} \\
&\quad - \mu\overline{P}\int w\hat{n} - \frac{1}{a}G\int g_w\hat{n} - \frac{w_0}{a}R\int \alpha\hat{n}
\end{aligned}$$

however, finding σ is still non-trivial, since $\hat{n}$ depends on the growth rate.

SIMPLIFICATION:

If we examine the special case d_z constant and $R(P)$ proportional to $G(P)$, we can obtain a somewhat surprising result. Since $R'/R = G'/G$, the perturbation equation has the solution

$$n' = P'\frac{d_z}{\sigma}\frac{G'}{G}\overline{n} \quad or \quad \hat{n} = \frac{d_z}{\sigma}\frac{G'}{G}\overline{n} \equiv \frac{G'}{\sigma}\gamma\overline{n}$$

with $\gamma = d_z/G(\overline{P})$, leading to a PP equation

$$\begin{aligned}
\sigma &= -\mu\overline{P} + \frac{1}{a}\left[\frac{G}{\overline{P}} - G'\right]\gamma\int w\overline{n} - \frac{\mu\overline{P}G'}{\sigma}\gamma\int w\overline{n} - \frac{1}{a}\frac{\gamma G'}{\sigma}\left[G\int g_w\overline{n} + w_0 R\int \alpha\overline{n}\right] \\
&= -\mu\overline{P} + \frac{1}{a}\left[\frac{G}{\overline{P}} - G'\right]\gamma\int w\overline{n} - \frac{\mu\overline{P}G'}{\sigma}\gamma\int w\overline{n} - \frac{1}{a}\frac{\gamma G'}{\sigma} d_z\int w\overline{n} \\
&= -\mu\overline{P} + \frac{1}{a}\left[\frac{G}{\overline{P}} - G' - \frac{d_z G'}{\sigma}\right]\gamma\int w\overline{n} - \frac{\mu\overline{P}G'}{\sigma}\gamma\int w\overline{n}\ .
\end{aligned} \tag{4.14}$$

But a simple ODE model

$$\frac{\partial}{\partial t}P = \mu P(N_T - P - Z) - \frac{1}{a}\gamma G(P)Z - d_p P$$
$$\frac{\partial}{\partial t}Z = \gamma G(P)Z - d_z Z$$

gives the same growth rate equation

$$\sigma = -\mu\overline{P} + \frac{1}{a}\left[\frac{G}{\overline{P}} - G' - \frac{G'd_z}{\sigma}\right]\gamma\overline{Z} - \frac{\mu\overline{P}d_z G'}{\sigma G}\overline{Z} \quad .$$

Thus the stability properties of the size-resolved model match exactly the ODE stability conditions if the measure of the efficiency of converting grazed food into ZP biomass, γ, is chosen suitably. The steady state will be unstable if

$$\frac{G}{\overline{P}} - G' > \frac{\mu a}{\gamma}\frac{\overline{P}}{\overline{Z}} \quad .$$

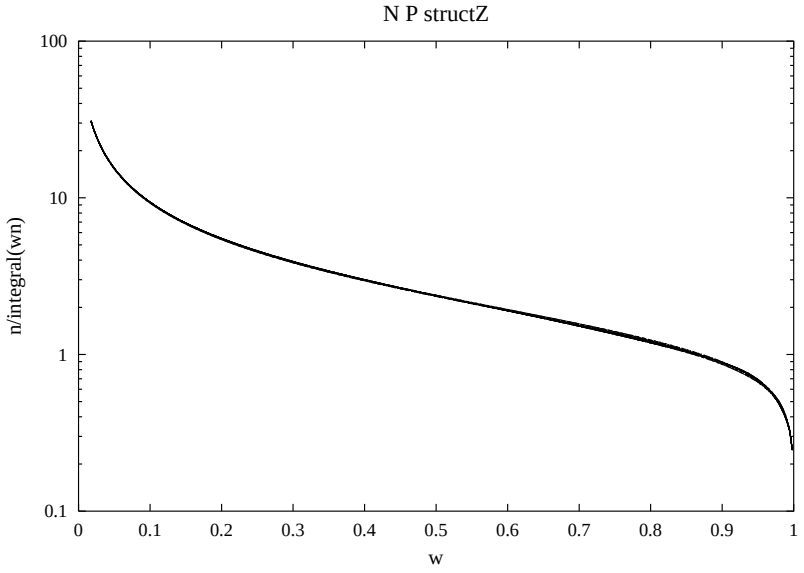

Figure 4.15: Size spectrum at various times in fluctuating regime.

But the resemblence between the two models is much deeper: numerical solutions show that the shape of n remains constant even when the amplitude is fluctuating (figure 4.14). This result suggests the continuous model can have a solution

$$n(w,t) = Z(t)\frac{\overline{n}(w)}{\int w\overline{n}}$$

where the normalization ensures that Z is the biomass. If we substitute this into the equation 4.9, we find

$$\begin{aligned}\overline{n}\frac{\partial}{\partial t}Z &= Z\left[-G(P)\frac{\partial}{\partial w}g_w\overline{n} - d_z\overline{n}\right] \\ &= Z\left[\frac{G(P)}{G(\overline{P})}d_z\overline{n} - d_z\overline{n}\right]\end{aligned}$$

and

$$ZG(P)g_w(w_0)\overline{n}(w_0) = ZR(P)\int \alpha\overline{n} = Z\frac{R(P)G(\overline{P})}{R(\overline{P})}g_w(w_0)\overline{n}(w_0)$$

which holds since $R(P)/R(\overline{P}) = G(P)/G(\overline{P})$. Therefore, the ZP dynamics becomes

$$\frac{\partial}{\partial t}Z = Z\left[\gamma G(P) - d_z\right] \quad .$$

The PP equation

$$\frac{\partial}{\partial t}P = P(N_T - P - Z) - \frac{1}{a}G(P)Z\frac{\int g_w\overline{n}}{\int w\overline{n}} - \frac{w_0}{a}R(P)Z\frac{\int \alpha\overline{n}}{\int w\overline{n}} - d_pP$$

can be transformed using the integral of w times the equation for $\overline{n}$ to

$$\begin{aligned}\frac{\partial}{\partial t}P &= P(N_T - P - Z) - \frac{1}{a}d_z\frac{G(P)}{G(\overline{P})}Z - d_pP \\ &= P(N_T - P - Z) - \frac{1}{a}\gamma G(P)Z - d_pP\end{aligned}$$

so that the two equations for Z and P are precisely the ODE forms with $\gamma = d_z/G(\overline{P})$.

For this system, then, we can dispense with the structured model and simply solve for the biomass. Of course, we are not assured that the solution above is the one actually obtained; it could be unstable to perturbations in the weight distribution (e.g. pulses of high population). While that cannot happen for the steady state (by eqn. 4.14), we have neither shown the limit cycle is stable nor ruled out other equilibria or cycles which are far enough from $Z\overline{n}/\int w\overline{n}$. Numerically, however, we find no evidence of such solutions: after a period of adjustment, the weight distribution settles to $\overline{n}$ and stays there.

We can easily think of ways that this simplification process will fail: for example, d_z may include predation, which would depend on the size/ weight of the ZP. Reproduction could have a seasonal modulation (via temperature or other cues) which differs from the changes in the growth rate. We shall discuss approximate approaches to these kinds of problems below and in chapter xx.

Second example:

Most problems cannot be reduced to a low order system in the manner above, and the dynamics including a structured ZP population will generally be richer than the standard ODE models. To illustrate this, we consider the case where the reproduction biomass is drawn from the adult population. We assume that $R_i = R$ is simply a constant, that $G(P) = P$ to match the QNPZ model, and that the biomass of the offspring can be neglected ($w_0\alpha/w \to 0$). The last assumption is not necessary but simplifies the analysis significantly; numerically, we can show that the finite w_0 case is quite similar to the results from the approximated set:

$$\frac{\partial}{\partial t}P = \mu P\left(N_T - P - \int dw\, wn\right) - \frac{1}{a}P\int dw\, g_w n - d_p P \tag{4.15a}$$

$$\frac{\partial}{\partial t}n = -P\frac{\partial}{\partial w}g_w n - d_z n \tag{4.15b}$$

$$P g_w(0) n(0) = R\int dw\, \alpha n \quad . \tag{4.15c}$$

We change the weight variable to one representing the time required to grow to a particular weight

$$\xi = \int_{w_0}^{w} dw' \frac{1}{g_w(w')} \quad \Rightarrow \quad d\xi = dw/g_w(w) \quad .$$

Multiplying (4.15b) by g_w and defining $N \equiv g_w n$ gives

$$\frac{\partial}{\partial t}P = \mu P\left(N_T - P - \int d\xi\, wN\right) - \frac{1}{a}P\int d\xi\, g_w N - d_p P \tag{4.16a}$$

$$\frac{\partial}{\partial t}N = -P\frac{\partial}{\partial \xi}N - d_z N \tag{4.16b}$$

$$PN(0) = R\int d\xi\, \alpha N \quad . \tag{4.16c}$$

In the case where α is a step-function, the steady state is

$$\begin{aligned}
\overline{N} &= N_0 \exp(-d_z\xi/\overline{P}) \\
\overline{P} &= -\frac{d_z \xi_A}{\ln(d_z/R)} \\
N_0 &= \frac{\mu N_T - \mu\overline{P} - d_p}{\int \left(\mu w + \frac{1}{a}g_w\right)\exp(-d_z\xi/\overline{P})} \quad .
\end{aligned}$$

The stability problem for the population structure is also simple:

$$\sigma N' + \overline{P}\frac{\partial \xi}{\partial N}' + d_z N' = \frac{P'}{\overline{P}} d_z \overline{N} \quad , \quad \overline{P}N'(0) + P'N_0 = R\int d\xi\, \alpha N'$$

giving

$$N' = N_0 \frac{P'}{\overline{P}} [\frac{d_z}{\sigma} \exp(-d_z \xi/\overline{P}) + \beta \exp(-(d_z+\sigma)\xi/\overline{P})]$$

with

$$\beta = \left[\frac{d_z}{d_z+\sigma} \exp(-\sigma \xi_A/\overline{P}) - 1 \right]^{-1} \quad .$$

The equation for σ from the perturbation form of (4.16) becomes

$$\sigma = -\mu\overline{P} - \frac{d_z}{\sigma} N_0 \int (\mu w + \frac{g_w}{a}) \exp(-d_z \xi/\overline{P}) - \beta N_0 \int (\mu w + \frac{g_w}{a}) \exp(-[d_z+\sigma]\xi/\overline{P}) \quad .$$

If β were zero, we would recover the quadratic form for σ found before; in the case here with $G = P$, these terms lead to stability. The new terms add not only additional factors of σ from the integrals but also the transcendental term in β. Instead of solving this equation, we examine the discretized version of the equations

$$\frac{\partial}{\partial t} n_i = \delta_{i,0} R \alpha_j n_j + P(g_{i-\frac{1}{2}} n_{i-1} - g_{i+\frac{1}{2}} n_i)/\delta w - d_z n_i$$
$$\frac{\partial}{\partial t} P = P \left[\mu(N_T - P - w_i n_i \delta w) - \frac{1}{a} g_{i-\frac{1}{2}} n_i \delta w - d_p \right]$$

(for $g_{jmax+\frac{1}{2}} = 0$; modifications for $w_0 \neq 0$ are obvious) or

$$\frac{\partial}{\partial t} \mathbf{b} = b_1 \mathbf{L}_1 \mathbf{b} + \mathbf{L}_2 \mathbf{b}$$

with $\mathbf{b} = (P, n_0, n_1, \ldots, n_{max})$ being the vector of variables. We need to solve for the mean

$$\overline{b}_1 \mathbf{L}_1 \overline{b} + \mathbf{L}_2 \overline{b} = 0$$

and then can pose the perturbation problem as an ordinary matrix eigenvalue problem:

$$\frac{\partial}{\partial t} \mathbf{b}' = \Big[(\mathbf{L}_1 \overline{\mathbf{b}}) \times [1, 0, 0, \ldots, 0] + \overline{b}_1 \mathbf{L}_1 + \mathbf{L}_2 \Big] \mathbf{b}' \equiv \mathbf{L}' \mathbf{b}' \quad . \tag{4.17}$$

We can search for the $\overline{P} = \overline{b}_1$ which makes $\overline{P}\mathbf{L}_1 + \mathbf{L}_2$ have a zero eigenvalue; the eigenvector renormalized by the value of $\overline{P}$ gives the basic state. Alternatively, we can solve the problem in reverse: given a guess of $\overline{P}$, we can start with $\overline{n}_0 = 1$ and iterate the $n_1,\ n_2,\ n_3, \ldots$ equations to find the population structure. The n_0 equation then tells us the value of R corresponding to that $\overline{P}$. We search for the $\overline{P}$ which gives the desired R value. Once we have this, the P equation gives us the value of n_0 and the population vector scales by this number to yield the full steady solution.

The results for the stability calculation in figure 4.15 indicate perturbations will grow for $R \geq 0.5$. Numerical simulations (figure 4.16) show limit cycles developing. These fluctuations are associated with changes in the weight distribution: a PP bloom triggers

rapid growth so that a larger percentage of the ZP reach adult size. These reproduce, and the larger generation depletes the food supply further. As the ZP die out, the nutrients build back up, setting the stage for a new PP bloom (figure 4.16b).

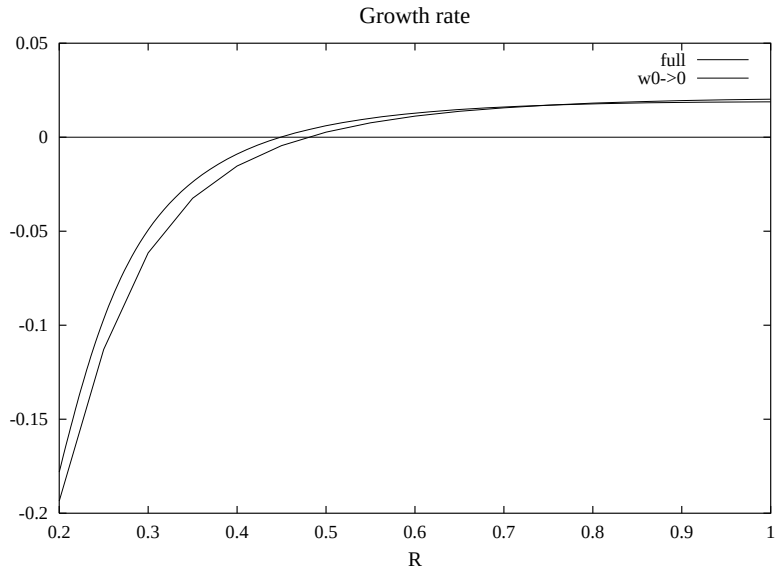

Figure 4.16: Growth rate for perturbations as a function of R. The case neglecting the biomass of the offspring is not dramatically different when $w_0 = \frac{1}{64} w_{max}$.

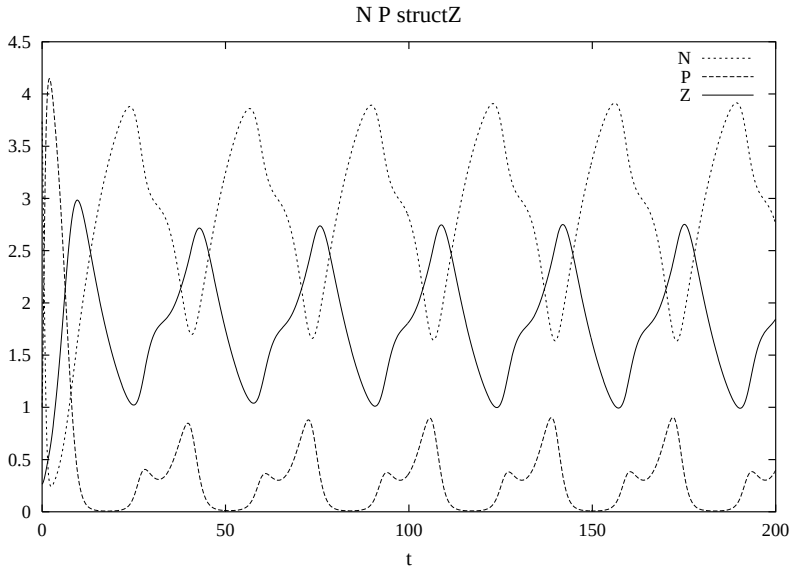

Figure 4.17a: Limit cycles when $R = 1$.

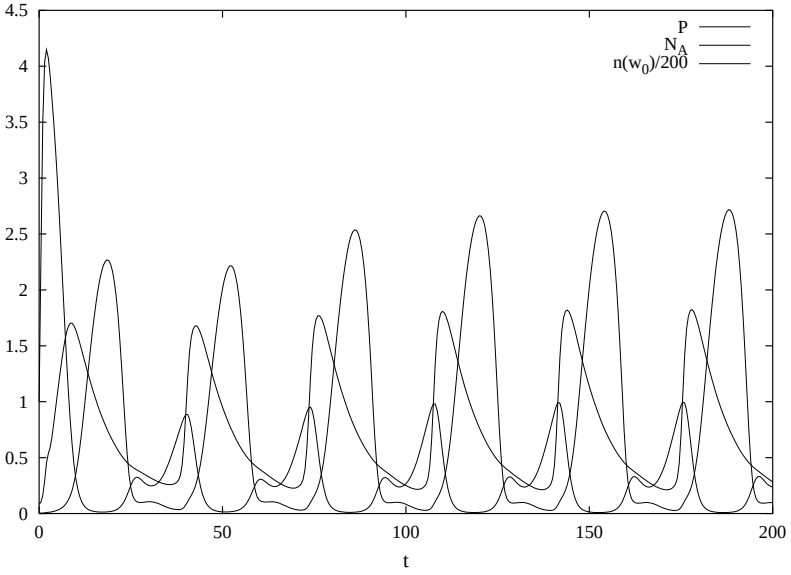

Figure 4.17b: Time series of P, N_A, and $n(0,t)$.

N P structZ

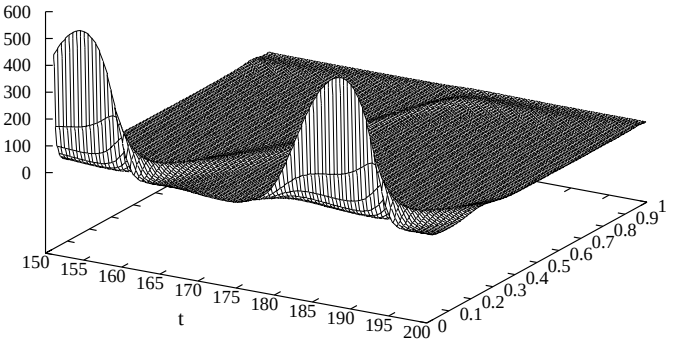

Figure 4.17c: $n(w,t)$.

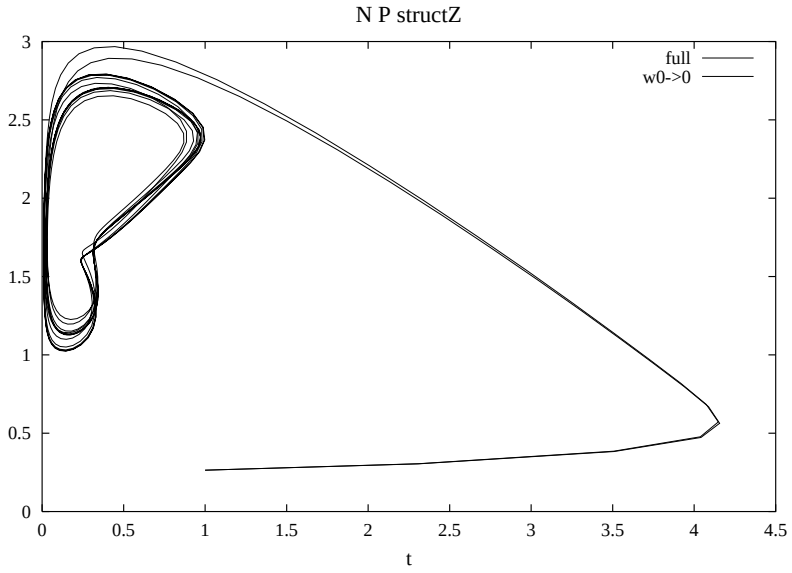

Figure 4.17d: Comparison of the approximation $w_0 << w_{max}$ to the full case.

MOMENTS

For some problems, we can reduce the full structured model to a few ODE's by a moment method (xx, 19xx). We project the number density equation on a set of functions $\phi_m(w)$. If

$$N_m = \int dw\, \phi_m(w) n$$

then

$$\frac{\partial}{\partial t} N_m = -P \int dw\, \phi_m \frac{\partial}{\partial w} g_w n - d_z N_m = \phi_m(0) R \int dw\, \alpha n + P \int dw\, n g_w \frac{\partial}{\partial w} \phi_m - d_z N_m \quad .$$

We can close the system exactly if α can be represented by a finite sum of ϕ's and $g \frac{\partial}{\partial w} \phi_m$ is a sum of the ϕ_n's with $n \leq m$. To couple to the P equation, $\int wn$ and $\int g_w n$ must also be expressible in terms of the projection.

For example, we can take g_w to be constant and $\phi_m = w^m/m!$. If $\alpha = w^s/s!$, then

$$\begin{aligned}
\frac{\partial}{\partial t} P &= \mu P(N_T - P - N_1) - \frac{g_w}{a} P N_0 - d_p P \\
\frac{\partial}{\partial t} N_0 &= R N_s - d_z N_0 \\
\frac{\partial}{\partial t} N_m &= g_w P N_{m-1} - d_z N_m \quad (1 \leq m \leq s) \quad .
\end{aligned}$$

From these, we find the steady state values

$$\begin{aligned}\overline{P} &= d_z^{(1+s)/s} g_w^{-1} R^{-1/s} \\ \overline{N}_0 &= \frac{\mu N_T - \mu\overline{P} - d_p}{\mu g_w \overline{P}/d_z + g_w/a} \\ \overline{N}_m &= (g_w\overline{P}/d_z)^m \overline{N}_0 \quad .\end{aligned}$$

The perturbation problem will generally be an order $s+2$ polynomial in the growth rate, and we can write an equation for it. Computationally, however, it is simpler to phrase the problem in the same matrix form as we did above

$$\frac{d}{dt}\mathbf{b} = b_1\mathbf{L}_1\mathbf{b} + \mathbf{L}_2\mathbf{b}$$

with different matrices, of course. The results in figure 4.17 indeed show an instability as R increases; this occurs as a pair of complex roots moves from the negative real half plane to the positive side (a Hopf bifurcation). Thus the population develops a limit cycle.

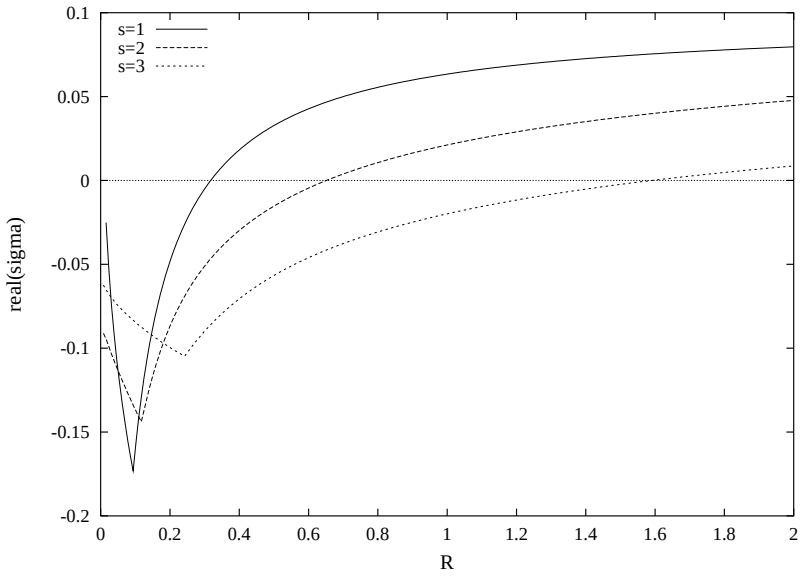

Figure 4.18: Growth rates for various s values.

For the von Bertalanffy growth equation, we can also solve using moments with the functions $\phi_m = (w/w_m)^{m/3}$ for which

$$g_0\left[\left(\frac{w}{w_m}\right)^{2/3} - \left(\frac{w}{w_m}\right)\right]\frac{\partial}{\partial w}\phi_m = \frac{g_0}{w_m}\frac{m}{3}[\phi_{m-1} - \phi_m] \quad .$$

From this, we find

$$\frac{\partial}{\partial t}N_m = \delta_{m,0}R\int dw\,\alpha n + P\frac{g_0}{w_m}\frac{m}{3}[N_{m-1} - N_m] - d_z N_m$$

and

$$\frac{\partial}{\partial t}P = \mu P(N_T - P - w_m N_3) - \frac{g_0}{a}P(N_2 - N_3) - d_p P \quad .$$

To obtain a sigmoid form for α, we use $\alpha = s(w/w_m)^{(s-1)/3} - (s-1)(w/w_m)^{s/3}$ so that

$$\frac{\partial}{\partial t}N_m = \delta_{m,0}R[sN_{s-1} - (s-1)N_s] + P\frac{g_0}{w_m}\frac{m}{3}[N_{m-1} - N_m] - d_z N_m \quad .$$

For this problem, instability requires very large values of s (order 40) with the parameters we are using; increasing g_0 by a factor of 3 permits instability even for the smallest value $s = 3$. In any case, the moment calculations give persuasive evidence that the limit cycles are not numerical artifacts and that the NP-structured Z model can have different dynamics from the QNPZ model of chapter one.

Simplification

The previous discussion concentrated on cases where the structured model differs from the stable, steady QNPZ model. However, for some parameter values (or $g_w(w)$, $alpha(w)$ functional forms), the structured model still has steady solutions, and we might wish to explore simplifying the model to obtain a much lower dimension system which can be used in simulations with space or time-dependent variability. If we write $n(w,t)$ as a product of the biomass, Z, and the weight structure $\hat{n}(w,t)$

$$n(w,t) = Z(t)\hat{n}(w,t) \quad , \qquad \int dw\, w\hat{n}(w,t) = 1$$

and substitute into the dynamics, we find

$$\hat{n}\frac{\partial}{\partial t}Z + Z\frac{\partial}{\partial t}\hat{n} = -ZP\frac{\partial}{\partial w}g_w\hat{n} - d_z Z\hat{n} \quad .$$

Multiplying by w and integrating gives

$$\frac{\partial}{\partial t}Z = PZ\gamma(t) - d_z Z$$

with $\gamma = \int g_w\hat{n}$ and a structure equation

$$\frac{\partial}{\partial t}\hat{n} = -P\frac{\partial}{\partial w}g_w\hat{n} - P\gamma\hat{n} \quad , \qquad Pg_w(0)\hat{n}(0,t) = R\int dw\,\alpha\hat{n} \quad .$$

The PP equation

$$\frac{\partial}{\partial t}P = \mu(N_T - P - Z) - \gamma PZ - d_p P$$

likewise has the appropriate form. As a comparison, consider the case when the light level varies seasonally, so that the PP uptake rate varies. We presume a sinusoidal dependence with μ changing from 0.6 to 1.4 times the mean value. Figure 4.18 shows that the simplification works quite well in the stable case; when limit cycles occur, the approximation

represents the average trajectory reasonably well, but does not produce the large cyclic variations (figure 4.19). However, the detailed cycling depends on initial conditions and thus is not likely to be realistic. Figure 4.20 compares the simplified model to the average of runs of the full model with different starting phases; we can predict the expected trajectory fairly well, although there is a noticeable offset in the ZP field.

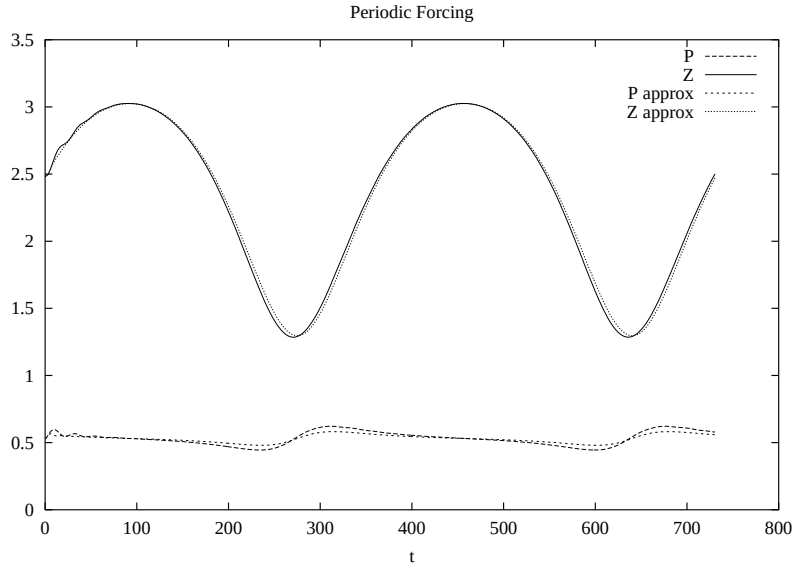

Figure 4.19: Comparison of a two-year cycle of the full model and the simplified two-variable representation for $R = 0.4$.

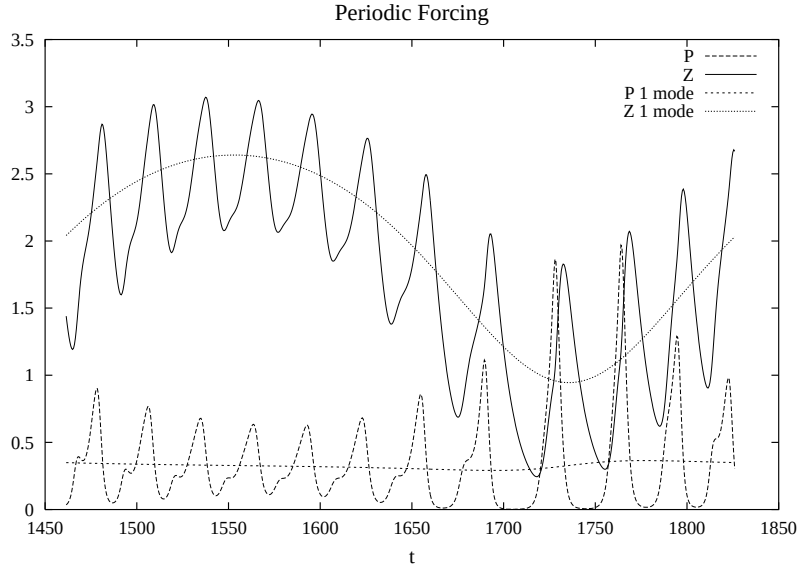

Figure 4.20: Comparison for $R = 1.0$.

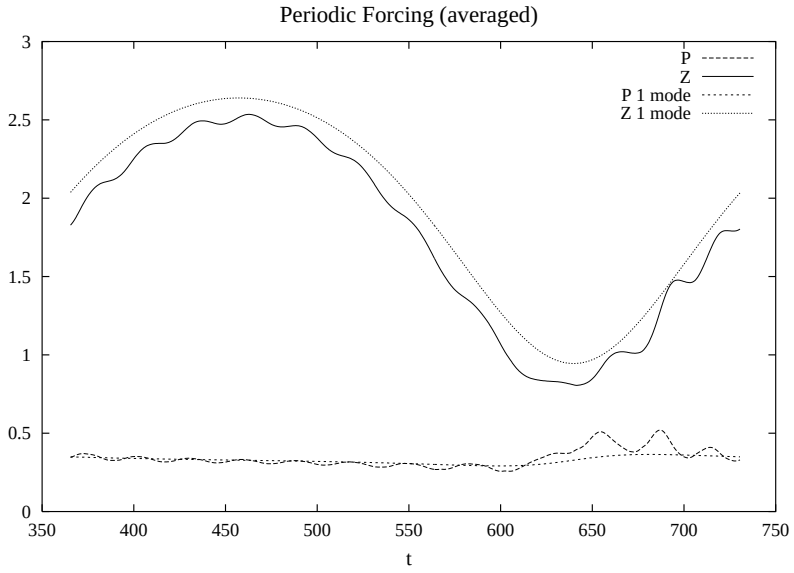

Figure 4.21: Comparison to phase-averaged cycles for $R = 1.0$.

Other simplifications

The oscillations in $\mathbf{b}(t)$ certainly have a biological basis in the delay in maturation and the intra-species competition for food. The amplitudes and periods will not be so regular in nature, and the phases and other details will be very sensitive to model error as well as initial conditions. Yet we can certainly imagine circumstances in which the delays implied by the structured model will be be an essential part of the dynamics (for example, seasonally modulated reproduction or the response to impulsive events such as the onset of upwelling winds). In these situations, the change in structure of the population will be essential; however, carrying a large number of weight classes (126 in the examples above), perhaps multiplied by the number of ZP species, becomes prohibitive in a spatially resolved system. We need to consider methods for reducing the number of variables while retaining the important aspects of the dynamics.

The problem of simplified representations is, of course, much broader than just the issue of dealing with structured populations, and we shall return to it later. For now, consider the projection or Galerkin method: we approximate n using a small set of functions

$$n(w,t) = a_n(t)\phi_n(w)$$

and also pick a set of orthogonal functions $\tilde{\phi}_m$

$$\int dw\, \tilde{\phi}_m(w)\phi_n(w) = \delta_{mn} \quad .$$

If we substitute the approximation into the dynamical equation, multiply by one member of the set of $\tilde{\phi}$'s and integrate, we end up with a dynamical system

$$\begin{aligned}\frac{\partial}{\partial t}a_m &= -P\left[\int dw\,\tilde{\phi}_m \frac{\partial}{\partial w} g_w \phi_n\right] a_n - d_z a_m \\ &= \left[R\,\phi_m(0)\int dw \alpha(w)\phi_n(w)\right] a_n + P\left[\int dw\,\frac{\partial \tilde{\phi}_m}{\partial w} g_w \phi_n\right] a_n - d_z a_m \quad .\end{aligned}$$

The procedure is straightforward, but the choice of basis functions ϕ_m and the adjoint functions $\tilde{\phi}_m$ seems much less so. If the basic dynamics is expressed in matrix form, the $\phi_m(w)$ functions become a matrix of size length($\mathbf{b}$) $\times$ # modes (including P within the projection; we choose Φ and $\tilde{\Phi}$ so that one mode picks out just P with no amplitude in the n variables). The dynamics has the same form but with smaller matrices

$$\frac{\partial}{\partial t}\tilde{\mathbf{b}} = \tilde{b}_1[\tilde{\Phi}\mathbf{L}_1\Phi]\tilde{\mathbf{b}} + [\tilde{\Phi}\mathbf{L}_2\Phi]\tilde{\mathbf{b}} = \tilde{b}_1\tilde{\mathbf{L}}_1\tilde{\mathbf{b}} + \tilde{\mathbf{L}}_2\tilde{\mathbf{b}}$$

As a first example, we divide the weight space up into discrete bins and let ϕ_m select and average over the m^{th} bin

$$\phi_m(w) = [(w > w_{m-1}) - (w > w_m)]/(w_m - w_{m-1})$$

using the programming notation $a > b$ being 1 when true and zero when false. The reduced model is essentially the same as produced by a coarser w-grid. As figure 4.21 shows, the oscillations are not well-reproduced even with twenty weight classes; with ten, the fluctuations only occur in the phase when the ZP biomass is increasing, and they are scarcely present with five classes.

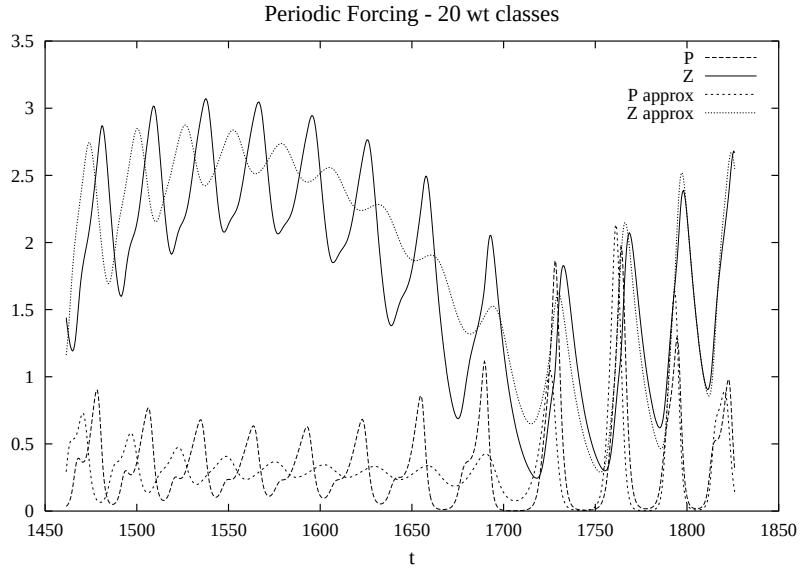

Figure 4.22: Representation using twenty weight classes.

For the second example, we employ the unstable eigenmode for the steady state with $R = 1$ – the solution $\mathbf{b}'$ to (4.17). We also find the left eigenvector corresponding to the same mode $\mathbf{y}$ such that $y_i L'_{ij} = \sigma y_j$ and normalize it so that $y_i b'_i = 1$. We begin with

$$\Phi_{\text{init}} = \begin{pmatrix} 1 & & & & \\ 0 & & & & \\ \dots & \overline{\mathbf{b}} & \Re(\mathbf{b}') & \Im(\mathbf{b}') & \\ 0 & & & & \\ 0 & & & & \end{pmatrix} \quad and \quad \tilde{\Phi}_{\text{init}} = \begin{pmatrix} 1 & 0 & 0 & \dots & 0 & 0 \\ 0 & w_1 & w_2 & \dots & w_{max-1} & w_{max} \\ & & & \Re(\mathbf{y}) & & \\ & & & \Im(\mathbf{y}) & & \end{pmatrix}$$

and perform the equivalent of Gram-Schmidt orthonormaliztion so that $\tilde{\Phi}\Phi = \mathbf{I}$. The resulting four-mode model captures the overall cycle but overestimates the variability.

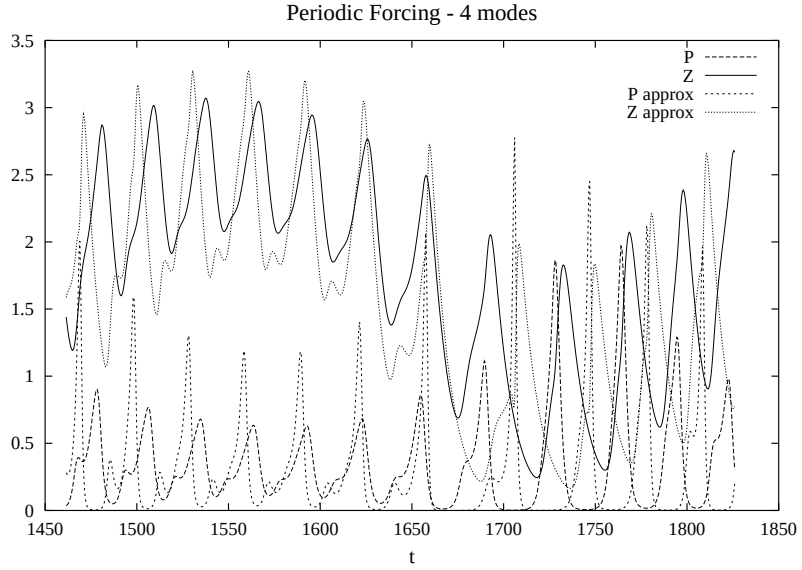

Figure 4.23: Representation using four modes.

Because the third and fourth modes have both positive and negative lobes, we are not assured that our estimated n or even Z values will always be positive. The weight-grouping approximation does not have this problem, but requires a large number of modes. We shall expand on these issues in Chapter xx.

4.3 — Species-Weight

We have the pieces required to construct a model such as figure 3.1: transfer of biomass between trophic levels, multiple limitations, size-dependent processes, and growth in size within a population. We can also reformulate the structured-population model in terms of biomass in log-weight classes as follows:

First, we note that the flux form still holds

$$\frac{\partial}{\partial t}n = -\frac{\partial}{\partial \omega}\tilde{g}n - dn \tag{4.18}$$

where $n\,d\omega$ is the number density in the class ω to $\omega + d\omega$ and $\tilde{g}$ is the rate of growth in terms of log weight

$$\tilde{g} = \frac{d}{dt}\omega = \frac{1}{w}\frac{d}{dt}w = \frac{g}{w} \quad .$$

The biomass in a particular log-weight class is just $b = wn = w_0 \exp(\omega)n$, so we can find the evolution equation for b by multiplying (4.19) by $w_0 \exp(\omega)$

$$\begin{aligned} \frac{\partial}{\partial t}b &= -\frac{\partial}{\partial \omega}\tilde{g}b + (\tilde{g} - d)b \\ \tilde{g}(\omega_0)b(\omega_0) &= \int d\omega\, r(\omega)b(\omega) \quad . \end{aligned} \tag{4.19}$$

In the second form, the $\frac{\partial}{\partial \omega}$ term moves biomass ($b\,d\omega$) conservatively from weight to weight while the $\tilde{g}b$ terms represents the biomass which must be added for the organisms to gain weight. Transfer of biomass from other parts of the size-species domain must be adequate to account for this term as well as any residual biomass gain needed for reproduction (recognizing, of course, the inefficiency of grazing).

The somewhat different form of the reproduction term just makes relating the newborn biomass produced by adults of weight w to intake easier. Competitive nonlinearities can still be included, both here and in the growth term, by making $r(\omega, s)$ and/or $\tilde{g}(\omega, s)$ functionals of $b(\omega, s)$.

To connect species s to the others on which it feeds or for which it is prey, we define the transfer function $p(\omega, s|\omega', s')$ – the amount of food from weight class ω' in species s' available to weight class ω in s. From this definition and the Holling type III form, we have the total amount of biomass grazed by the predators

$$G(\omega, s) = g_\omega(\omega, s)\frac{\int d\omega' ds' p(\omega, s|\omega', s')b^2(\omega', s')}{A(\omega, s)}$$

with

$$A(\omega, s) = \int d\omega' ds' p(\omega, s|\omega', s')b(\omega', s') + \frac{1}{C(\omega, s)}\int d\omega' ds' p(\omega, s|\omega', s')b^2(\omega', s')$$

and the rate at which grazing removes biomass from prey in class ω, s per unit biomass

$$D(\omega, s) = \int d\omega' ds' \frac{g_\omega(\omega', s'|\omega, s)\, b(\omega', s')}{A(\omega', s')}\, b(\omega, s) \quad .$$

The intake of food by the predators will either go to growth or reproduction

$$\tilde{g} = (a - a_r)G \quad , \quad r = a_r G$$

with the a_r factor acting like α to isolate the adult portion of the weight spectrum.

With these definitions and choices, the equation for species s becomes

$$\begin{aligned} \frac{\partial}{\partial t} b &= -\frac{\partial}{\partial \omega}\big[(a - a_r)Gb\big] + \big[(a - a_r)G - D - d\big]b \\ a(\omega_0)G(\omega_0)b(\omega_0) &= \int d\omega a_r G b \quad . \end{aligned} \tag{4.20}$$

(assuming $a_r(\omega_0) = 0$) with the various quantities being functions of ω and s. If we integrate with respect to log-weight, we find the biomass equation [$\tilde{b}(s) = \int d\omega\, b(\omega, s)$]:

$$\frac{\partial}{\partial t}\tilde{b} = aGb\Big|_{\omega_0} + \int (a - a_r)Gb - \int (D + d)b = \int (aG - D - d)b$$

If we integrate over species and set the assimilation factor a to one, the G and D terms would cancel – they simply move biomass around, with the only losses arising from incomplete assimilation.

4.3.1 — Fixed Size Structure Species

Under some rather strong restrictions, we can again find solutions with a stable population structure for species s, so that $b(\omega, s, t) = Z(s, t)\overline{b}(\omega)$. If we substitute this ansatz into (4.20), we can see that the $\overline{b}$ factors will cancel out G can be factored into a part dependent on weight, but not environment (food, temperature, etc.) and a weight-independent environmental term, $G = \hat{G} g_\omega$. D and d must be independent of weight. The reproductive term was already assumed to be proportional to G. The resulting structure equation is

$$\begin{aligned} \hat{G}_0 \left[\frac{\partial}{\partial \omega}(a - a_r)g_\omega \overline{b} - (a - a_r)g_\omega \overline{b}\right] &= -(D_0 + d)\overline{b} \\ a(\omega_0)g_\omega(\omega_0)\overline{b}(\omega_0) &= \int a_r g_\omega \overline{b} \\ &\Rightarrow \\ \int a g_\omega \overline{b} &= \frac{D_0 + d}{\hat{G}_0} \end{aligned} \tag{4.21}$$

where $\hat{G}_0$ and D_0 are constants, chosen to give a value of $(D_0+d)/\hat{G}_0$ making the solution to the structure equation consistent with the boundary condition. With this form, the temporal changes of the biomass satisfy

$$\frac{\partial}{\partial t}Z = Z\frac{\hat{G}}{\hat{G}_0}\int a\hat{G}_0 g_\omega \overline{b} - DZ - dZ = Z\left[\frac{\hat{G}}{\hat{G}_0}(D_0+d) - D - d\right] \quad . \tag{4.22}$$

For the conditions to apply for species s, F and D must be independent of ω, so that $p = p(s|\omega', s')$ for all s' which are prey and $p = p(s', \omega'|s)$ for all s' which are predators. As an example, consider single-celled organisms which reproduce by cell division: we can think of $\alpha_g = 1$ so that all intake of nutrient goes to growth. Reproduction takes the flux into weight $2\omega_0$ and redirects it to new cells at weight w_0 so that $g(\omega_0)b(\omega_0) = g(2\omega_0)b(2\omega_0)$ or $r = \delta(\omega - 2\omega_0)g(\omega)$. In (4.20), we replace the integral condition by $G(\omega_0)b(\omega_0) = G(2\omega_0)b(2\omega_0)$. The factorization of G and the idea that grazers do not distinguish between cell sizes seem quite reasonable, and the reproduction indeed scales the same way with environmental variability as growth. Of course, we do need to account for the variations in parameters with different species. Even for single-celled organisms, however, this picture may be oversimplified: Pascual and Caswell (19xx) discuss the case where only part of the cell cycle proceeds at a nutrient-dependent rate and demonstrate that cell numbers can have oscillatory or chaotic fluctuations with, respectively, steady or periodic nutrient supply. Thus even the simplest organisms may show significant effects from varying weight distribution.

If we carry the fixed-weight distribution idea to an (unwarranted) extreme, by assuming $p = p(s|s')$, $C = C(s)$, $d = d(s)$, all species will have fixed distributions

$$b = Z(s,t)\overline{b}(\omega, s) \quad , \qquad \int d\omega\, \overline{b} = 1$$

with the equations for the structure and the dynamics given by (4.21-22); the food, grazing, and predation mortality are set by

$$\begin{aligned} F(s) &= \int ds' p(s|s') Z(s') \\ \hat{G}(s) &= \frac{F(s)}{1 + F(s)/C(s)} \\ D(s) &= \int ds' p(s'|s) \frac{Z(s')}{1 + F(s')/C(s')} \left[\int d\omega'\, g_\omega(\omega, s')\overline{b}(\omega, s')\right] \quad . \end{aligned} \tag{4.23}$$

(If a is independent of weight, the last integral becomes $[D_0(s') + d(s')]/[a(s')\hat{G}_0(s')]$ but this is not a fundamental change.) In essence, the model reduces to a multispecies "compartment" model like those in Chapter 3, conceivably with a much larger set of variables (limiting to the case where s is treated as continuous).

While some of the effects of weight have been removed, the models in (4.23) can still be developed within this context; indeed, the grouping chosen in that section could be

just as well be phrased in terms of s rather than ω. If species are sorted by their mean weight, then the allometric relationships still make sense. (However, such scaling for the grazing rates does not account for differences in preference among prey species which have similar mean weights; this kind of information can be incorporated into (4.23), but makes specification of $p(s|s')$ more complex.)

EXAMPLE:

As an example, we generalize the model in (4.4-6) to include carnivory. We take a species/ weight diagram like 4.1 with the heterotrophs (PP) separated from the autotrophs (ZP) and sorted by mean weight. Now $p(s|s')$ for s' in the ZP will have contributions from both smaller PP and smaller ZP classes. But this change enables the larger size classes to grow and persist. In the case with Monod forms, the model is generally quite noisy (figure 4.23a); many species fluctuate to small values, with some becoming extinct (i.e., below the precision of the calculation). Roughly 40% of the species die out over the long term (10^7 days or 27,000 years). The results will also be sensitive to the numerical method; the implication is that it can be very difficult to find the long-term statistics for this model.

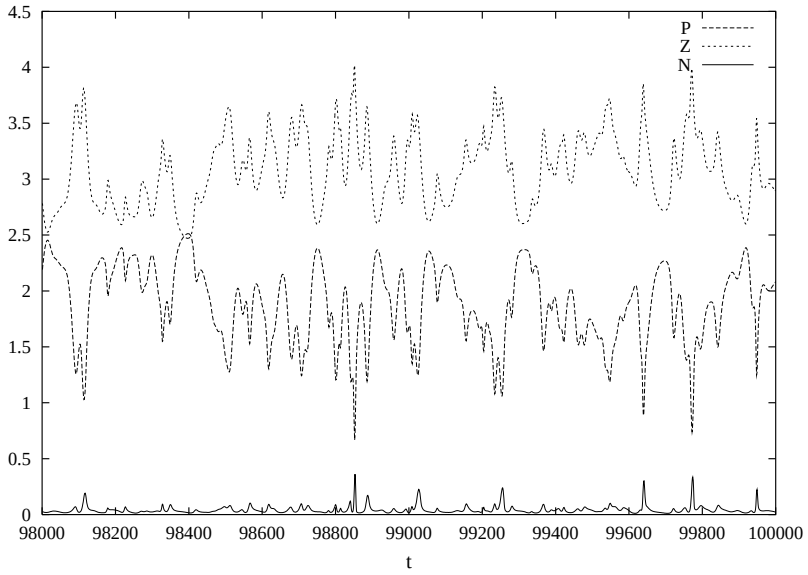

Figure 4.24a: Time series of total autotroph and heterotroph biomasses.

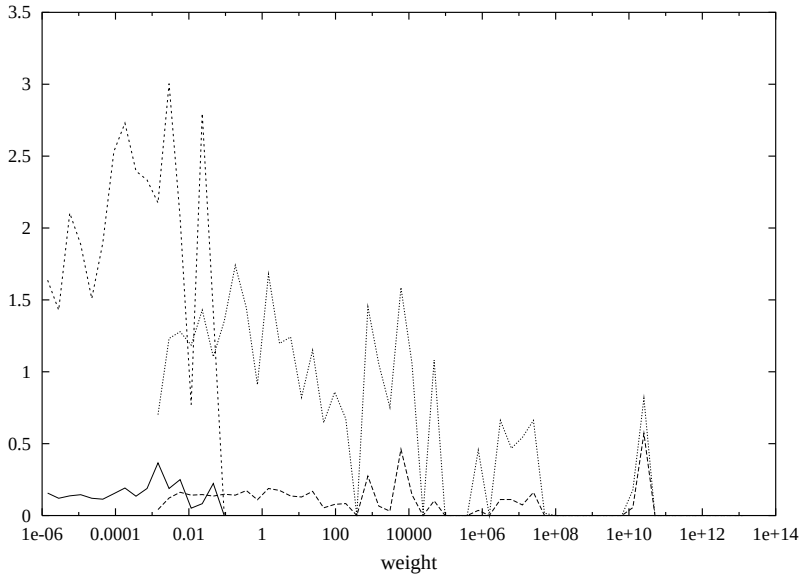

Figure 4.24b: Weight distributions (mean and maximum over time 80,000-100,000 *d*.

If prey-switching is included, the system settles rapidly (4.24a), although the large classes are still changing slowly (since their intrinsic rates are very small). We find the system organizes into distinct weight groups (4.24b). Extinctions of the kind described above do not occur, although gaps do form in the size spectrum and the number of species does decline (again slowly as the largest organisms die out).

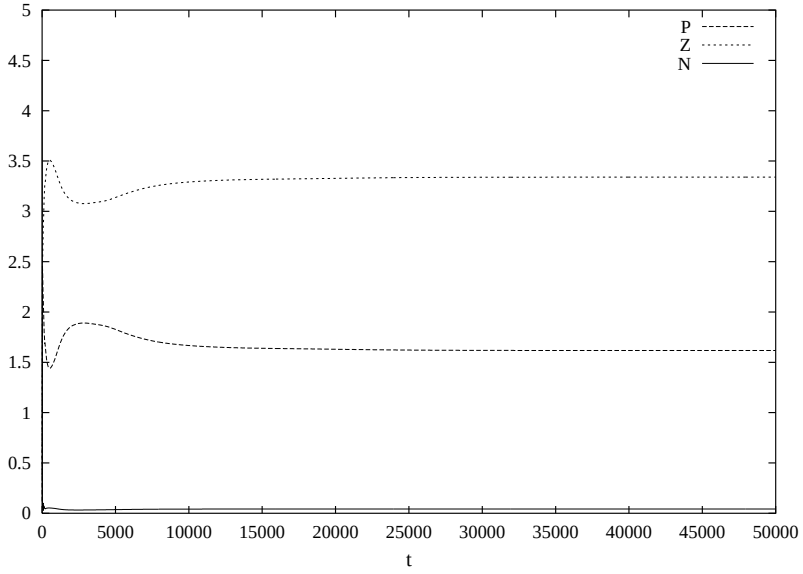

Figure 4.25a: Time series of total autotroph and heterotroph biomasses with prey-switching.

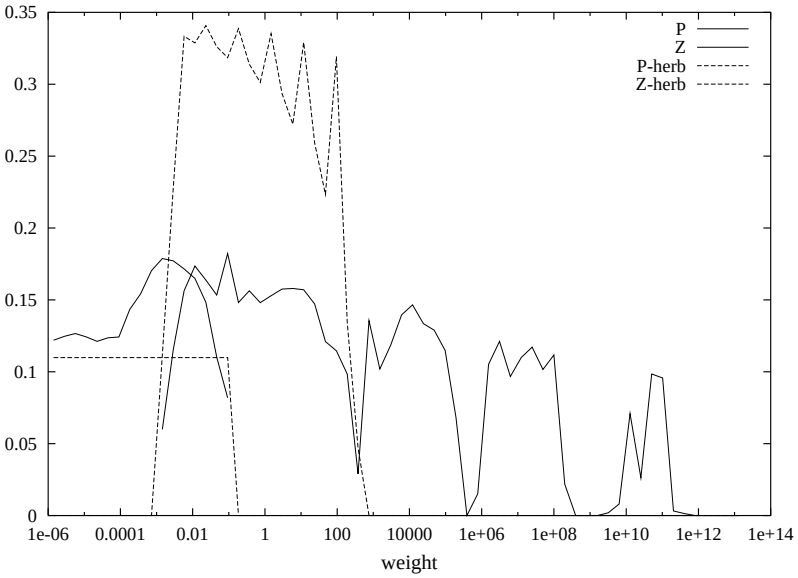

Figure 4.25b: Weight distributions with prey-switching. The dashed lines show the case with only herbivory.

4.3.2 — More general case

Finally, we discuss some cases including both multiple species and weight structure within a species. Assume that the larger ZP have a life-history so that $b(\omega, s)$ has a finite range in ω; the grazing then produces movement to higher weight classes (the $\frac{\partial}{\partial \omega}$ term). We've used two different ways of specifying the minimum weight vs. the adult weight: (1) $min(w/128, max(w_{PP}))$ or $(w/w_{z0})^{0.85}$ (figure 4.25). Grazing is size-based: ZP of weight w feed on all organisms in the range $1.25 \times 10^{-4}w$ to $10^{-3}w$.

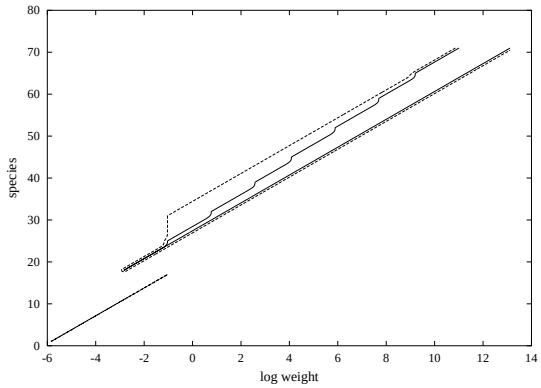

Figure 4.26: Species-weight for the $w/128$ (dashed) and $(w/w_0)^{0.85}$ (solid) choices.

These runs (with prey-switching) lead to a full suite of PP and small ZP, but only a few species of the larger ZP (figure 4.27). Apparently, species in the gaps have at least some period within their life-cycle when the food is inadequate, so that their net growth rate is not large enough to overcome the net mortality. Changing the allometric coefficient for ZP growth to 0.225 rather than 0.25 allows the higher weight organisms to persist (figure 4.27c).

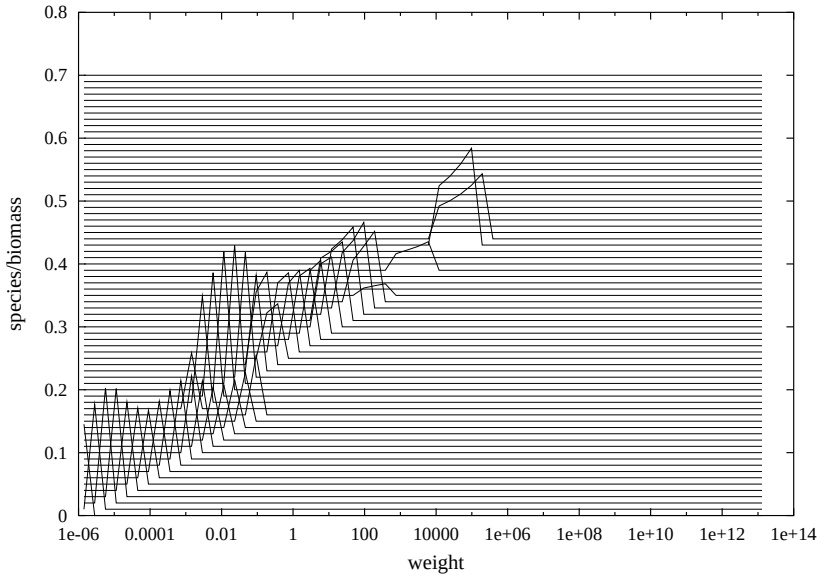

Figure 4.27a: Species-weight distribution with $w_{min} = (w/w_0)^{0.85}$.

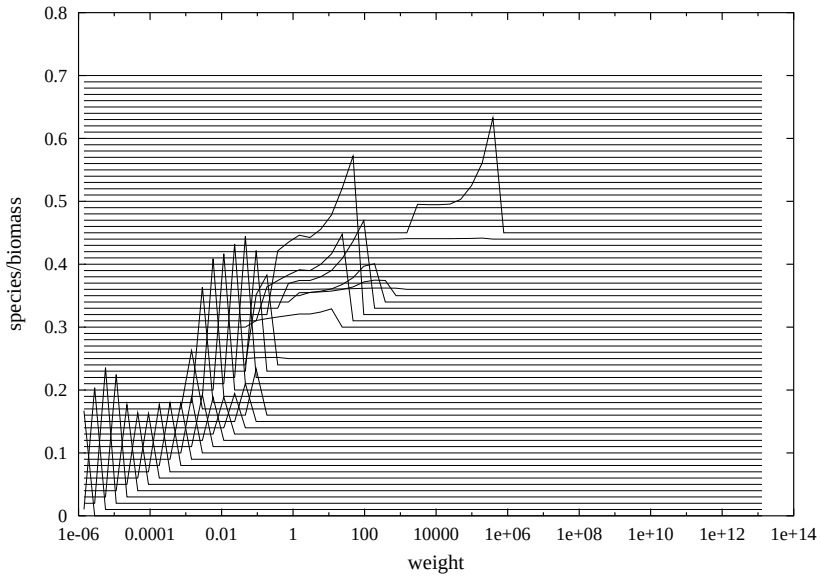

Figure 4.27b: Species-weight distribution with $w_{min} = w/128$.

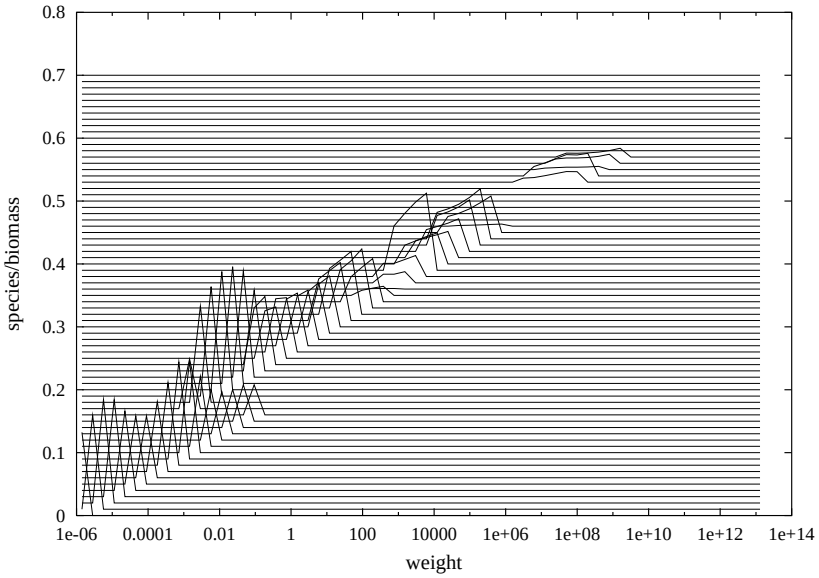

Figure 4.27c: Species-weight distribution with $w_{min} = (w/w_0)^{0.85}$ and an allometric coefficient of 0.225 for g.

4.3.3 — Size-spectrum

Particle counters provide a way to survey the ocean rapidly, assessing the number or volume of particles in size bins. After Sheldon et al. (1977) proposed that the biomass in logaritmic volume bins was roughly constant (with their data showing variations of the order of factors of 5), Platt and Denman (1977) suggested that the size-spectrum of oceanic organisms could be modelled by taking transfers of biomass to be local so that grazing gives a flux of biomass to slightly larger organsims. Zhou and Huntley (1997) examined another possibility, that the wieght gain term could also lead to a specific spectral shape (as we have seen in section 4.xx). The species-weight kind of structure has both mechanisms, so we can investigate the size spectrum. The results may not be simple: summing the data in fig. 4.27c gives a size spectrum which is not particularly smooth (fig. 4.xx).

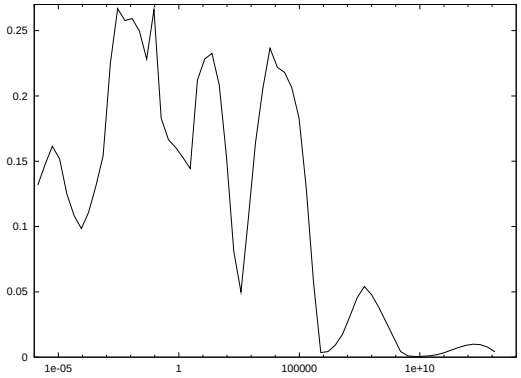

Figure 4.28: Size spectrum $\int dsb(s,\omega)$ (biomass in a unit log weight class) vs. log weight.

We start with the quadratic form of the model with weight as one of the traits

$$\frac{\partial}{\partial t}b(\omega,\mathbf{s})+\frac{\partial}{\partial\omega}\tilde{g}b=\tilde{g}b-db+\int d\omega' r(\omega,\omega',\mathbf{s})b(\omega',\mathbf{s}) \quad ;$$

we can always define averaged quantities by

$$\int d\mathbf{s} f(\omega,\mathbf{s},t)b(\omega,\mathbf{s},t)=\overline{f}(\omega,t)\int d\mathbf{s} b(\omega,\mathbf{s})=\overline{f}(\omega,t)\overline{b}(\omega,t)$$

so that the biomass density equation, integrated over $\mathbf{s}$ becomes

$$\frac{\partial}{\partial t}\overline{b}(\omega,t)+\frac{\partial}{\partial\omega}\overline{g}\overline{b}=\overline{g}\overline{b}-\overline{d}\,\overline{b}+\int d\omega'\overline{r}(\omega,\omega',t)\overline{b}(\omega',t)$$

The apparent simplicity arising form the dependence only on weight is, of course, misleading: terms like $\overline{d}$ which depend on predation cannot generally be predicting knowing only $\overline{b}(\omega,t)$. For example, the form we've been using

$$d(\omega,\mathbf{s})=d_0(\omega,\mathbf{s})+\int d\omega' d\mathbf{s}' G(\omega',\mathbf{s}'|\omega,s)b(\omega',\mathbf{s}')$$

(with time-dependence of terms implicit) gives

$$\overline{d}(\omega)\overline{b}(\omega)=\int d\mathbf{s}\, d_0(\omega,\mathbf{s})b(\omega,\mathbf{s})+\int d\omega' d\mathbf{s}\, d\mathbf{s}' b(\omega,\mathbf{s})G(\omega',\mathbf{s}'|\omega,\mathbf{s})b(\omega',\mathbf{s}')$$

If all the vital rates are the same across traits other than weight (i.e, $d_0=d_0(\omega)$, this would become

$$\overline{d}(\omega)\overline{b}(\omega)=d_0(\omega)\overline{b}(\omega)+\overline{b}(\omega)\int d\omega')G(\omega'|\omega)\overline{b}(\omega') \tag{4.24}$$

however, the condition on vital rates is very stringent and not very likely. Organisms with the same weight will still have different predation strategies, prey, vullnerability to other causes of mortality, etc. Evolutionary processes (Chapter xx) will work on these differences to separate opulations geographically or temporally. An alternative reduction, assuming fixed proportions of species in a weight class $b(\omega,\mathbf{s},t)=\overline{b}(\omega,t)\beta(\omega,\mathbf{s})$ with $\int d\mathbf{s}\,\beta(\omega,\mathbf{s})=1$ gives

$$\overline{d}=\int d\mathbf{s}\, d_0(\omega,\mathbf{s})\beta(\omega,\mathbf{s})+\int d\omega'\overline{b}(\omega')\int d\mathbf{s}\, d\mathbf{s}'\beta(\omega,\mathbf{s})G(\omega',\mathbf{s}'|\omega,\mathbf{s})\beta(\omega',s')$$

which has the same form, but with coefficients that depend on the species distribution and the variation of vital rates. So we'll continue to use 4.xx, with the understanding that the coefficients could be weighted averages.

If we assume allometric forms $\overline{g}=g_a o\exp(-\gamma\omega)$, $\overline{d}=d_a\exp(-\delta\omega)$, and take $\overline{r}(\omega,\omega')=r_a\delta(\omega-\omega'+\ln W)\exp(-\rho\omega)$ so that reproducing adultls are a factor W heavier than their

offspring, we can find a size spectrum $\overline{b} \propto \exp(-\beta\omega)$ when the coefficents satisfy $\gamma = \delta = \rho$ and

$$d_a = g_a(1+\beta+\gamma) + r_a \exp(-[\rho+\beta]W)$$

$$\frac{\partial}{\partial t}b(\omega,\mathbf{s}) + \frac{\partial}{\partial \omega}\tilde{g}b = \tilde{g}b - db + \delta\big(\omega - \omega_0(\mathbf{s})\big)\int r(\omega',\mathbf{s})b(\omega',\mathbf{s})$$

$$d = d_0 + \int d\omega' d\mathbf{s}'\, G(\omega',\mathbf{s}'|\omega,\mathbf{s})b(\omega',\mathbf{s}')$$

$$\tilde{g} = [1-\alpha]\, a\left[\mu N + \int d\omega' d\mathbf{s}' G(\omega,\mathbf{s}|\omega',\mathbf{s}')b(\omega',\mathbf{s}')\right]$$

$$r = \alpha\, a\left[\mu N + \int d\omega' d\mathbf{s}' G(\omega,\mathbf{s}|\omega',\mathbf{s}')b(\omega',\mathbf{s}')\right]$$

with the coefficients d_0, α, a, μ all functions of ω and $\mathbf{s}$, we can try to see when the biomass in a log weight class $B(\omega) = \int d\mathbf{s}\, b(\omega,\mathbf{s})$ might have a simple shape. If we assume grazing depends only on the difference in weights of predator and prey, then d, $\tilde{g}$, and r are functionals of B, although they may still depend on $\mathbf{s}$.

4.4 — Remarks

We have discussed a variety of models with a range of complexity, but have not tried to produce a "best model." Indeed, the arguments of Oreskes, *et al.*(1994) that models of natural systems can never be "verified," because of our imperfect knowledge of processes, parameters, initial and boundary distributions, apply even more strongly to ecological models. Instead, modellers face three tasks: (1) choose basic variables and functional forms (2) determine that the numerics solves the underlaying mathematical equations accurately, and (3) select parameters such that the model gives a reasonable estimate of the available data or its statistics. At that point, one can accept that the model may be a useful tool for interpreting the observations and for estimating the effects of changes in, for example, ocean temperatures.

But we should always remain aware that models are imperfect tools and cannot capture nature's complexity. In the case of predictive models, we should expect that new data will lead to modifications to keep the model on track. In meteorology and physical oceanography, for example, "data assimilation" procedures alter the values of imperfectly known variables or parameters so that the model-data fit remains acceptable. Similar issues apply to our problems. A model of copepod distribution of Georges Bank could incorporate information about the life-history with some parameters estimated from laboratory work (c.f. Davis, 19xx). Other values, such as mortality rates, are much less well-knowm as are the boundary conditions giving the input from the Gulf of Maine. Using filtering techniques such as adjoint methods (McGillicuddy, 19xx) for runs over several years would allow us to develop a picture of how such parameters/ boundary conditions vary seasonally; information which could be used to project into the future. Thus, predicting from such a model would be possible, but with limited accuracy. More likely, we would continue to incorporate new data, in the expectation that estimates of values in the future or of unobservable quantities such as the net predation (related in some way to the uptake of

food by larval fish) will be better. The success of the model would be judged by the degree to which it contribute to making the forecast better than an empirical/ statistical rule.

Similar caveats apply for more abstract models intended to help understand the underlying dynamics. One model may suggest that some process (e.g. upwelling of nutrient) is less significant than others (such as iron supply), while a different model could suggest quite different balances or argue that some other effect plays a major role. Disagreements among models can be difficult to resolve, although sometimes a more comprehensive system which includes both models can be used to get at the relative importance of processes.

To illustrate some of these issues, consider applying some of the models in these chapters to the Bermuda Atlantic Time Series (BATS) data (Michaels, et al., 19xx). Characteristics such as the net biomasses in the autotrophs and heterotrophs obviously depend both on the model and on the parameters. While we may be able to choose the parameters for a given model to match desired b values, such a procedure is not really satisfactory. As an example, we take four of the models above and adjust the constants such that the steady-state values are the same (and close to the mean values from BATS). We assume that the models represent the upper 50 m of the ocean and that there is a constant rate of exchange or mixing with the fluid below; the deep water is presumed to have only dissolved N with a fixed value N_T. All unassimilated grazing and dead zooplankton are lost to the deep water. As an example, the NPZ model can then be written as

$$\begin{aligned}
\frac{\partial}{\partial t}N &= -\mu\frac{NP}{N+N_h} - k(N-N_t) \\
\frac{\partial}{\partial t}P &= \mu\frac{NP}{N+N_h} - g\frac{Z}{\nu}[1-\exp(-\nu P)] - kP \\
\frac{\partial}{\partial t}Z &= ag\frac{Z}{\nu}[1-\exp(-\nu P)] - d_z Z - kZ \quad .
\end{aligned}$$

If we specify the values of N, P, Z and N_t, we can write the steady-state equations as a linear system for μ/g, d_z/g, and k/g. We solve this and then choose g to give reasonable maximum uptake rates. This example underscores the freedom in specifying even this simple model: in addition to the degree of freedom in specifying g, the BATS data does not have values for Z, so we assumed the steady value is $0.64P$ based on Hurtt and Armstrong, 19xx.

When we vary the light level seasonally, using the formulae in Evans and Parslow (19xx), and multiply μ by the light level, we can generate seasonal cycles. The yearly cycles of P vs N in figure 4.27 show overall similarity, but significant differences in detail (e.g., the NPZD version has both a fall and spring bloom). The measured cycles show much stronger blooms, but with interannual variability such that one year did not have a bloom at all.

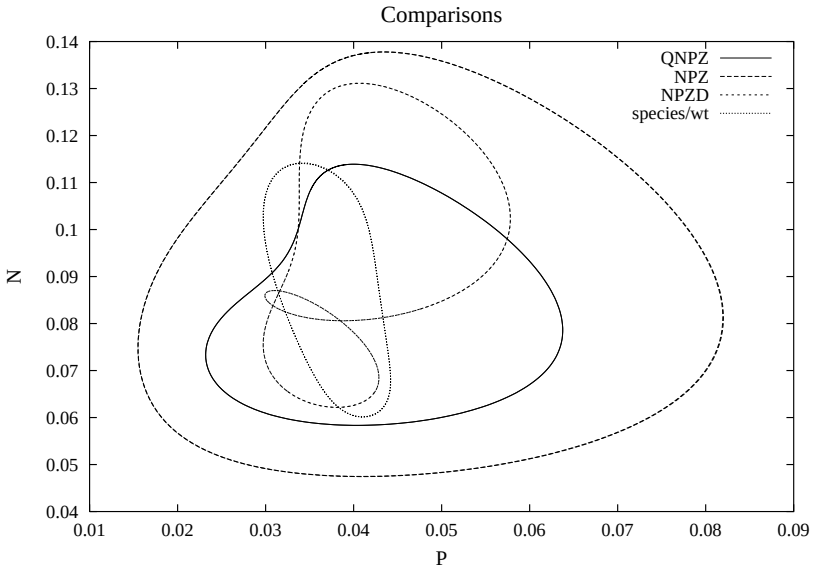

Figure 4.29a: NP cycles with seasonally-varying light for the QNPZ, NPZ, NPZD, and species-weight (section 4.3).

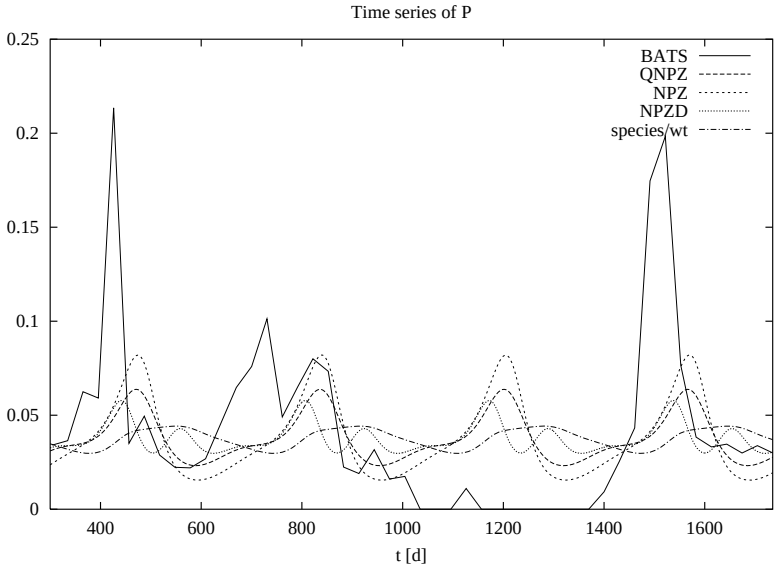

Figure 4.29b: measured P (from Chlorophyll-A/1.59) compared to the models.

To get some idea of the sensitivity, we vary parameters which are not well known (e.g., mean Z values, sinking rate for detritus) and compare the cycles. Some examples from the NPZD model are shown; we might expect that the model can fit the yearly cycle from the data. As figure 4.28 shows, the effort is not entirely successful: the spring bloom is weak, and the fall one is too strong. The model can make larger spring blooms, but puts them several months later in the summer.

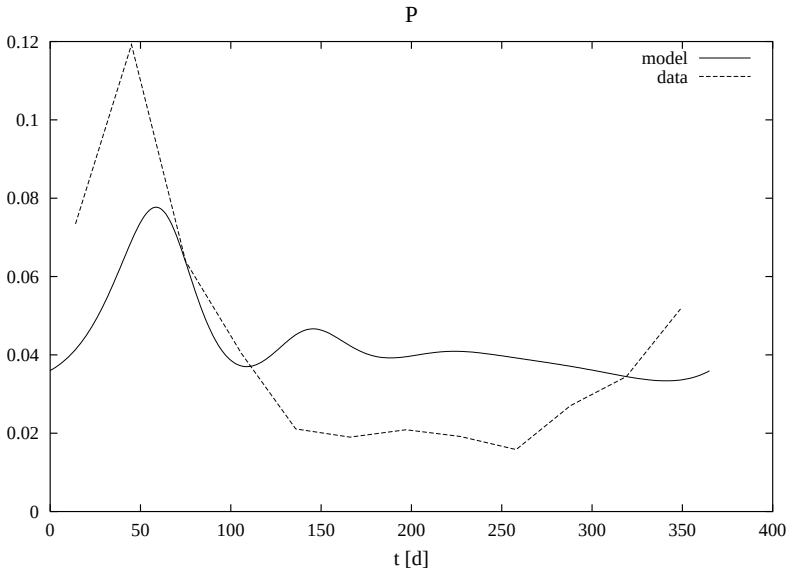

Figure 4.30a: measured 4-year average P (from Chlorophyll-A/1.59) compared to the model.

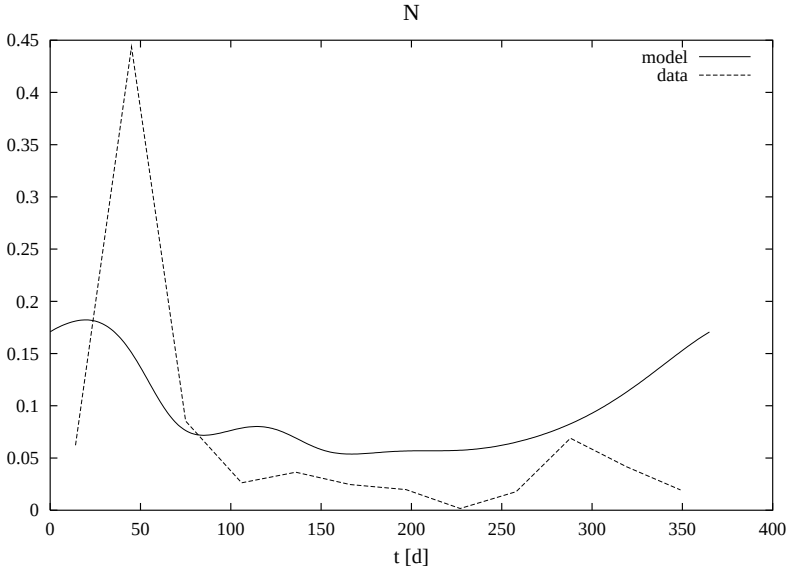

Figure 4.30b: measured 4-year average N compared to the model.

In a later chapter, we shall try to assess the effects of more complex physics (mixed-layer deepening and eddies), but note here that the temperature cycle (figure 4.xx) is much more regular. This result suggests either that the biology is more sensitve to the flows than the temperature or that the ecosystem dynamics is itself not smooth and regular. Thus, these chapters have pointed to the more complex processes which certainly occur in the ocean and discussed ways of incorporating them into models, while indicating that we will need to examine the structure and variability of the flows and environmental conditions in much more detail.

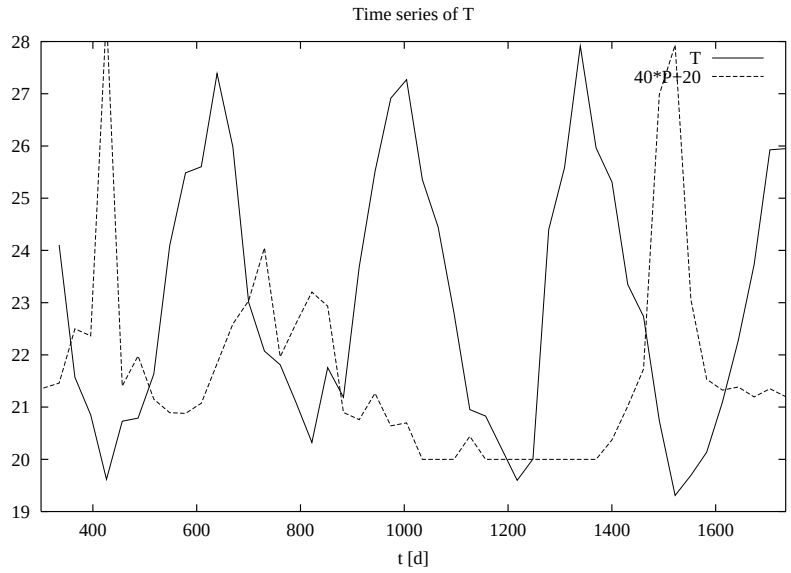

Figure 4.31: measured T and P